Charles University in Prague
Faculty of Science

BACHELOR THESIS

Tereza Uhlířová

Excitation Wavelength-Dependent Raman Spectra of Single-Layer Graphene-Phthalocyanine Hybrid Systems

Ramanova spektra hybridních systémů monovrstevný grafen-ftalocyanin v závislosti na vlnové délce excitace

Supervisor of the bachelor thesis: prof. RNDr. Blanka Vlčková, CSc.

Consultants of the bachelor thesis: doc. RNDr. Peter Mojzeš, CSc.
RNDr. Ivana Šloufová, Ph.D.

Study programme: Chemistry

Study branch: Chemistry

Prague 2016

Prohlašuji, že jsem tuto závěrečnou práci provedla samostatně a že jsem uvedla všechny použité informační zdroje a literaturu. Tato práce ani její podstatná část nebyly použity pro získání jiného nebo stejného akademického titulu

V Praze dne 25. 5. 2016 Podpis

Acknowledgment

First and foremost, I wish to thank my supervisor prof. RNDr. Blanka Vlčková, CSc. for her patient and devoted guidance, precious advice and always-available help throughout the entire process of research and writing. Also, I am deeply indebted to my consultant doc. RNDr. Peter Mojzeš, CSc. for his unflagging support and valuable advice, as well as for schooling in operating the Raman instrument, and for acquiring certified intensity standards and measuring their spectra. Likewise, I owe my gratitude to my consultant RNDr. Ivana Šloufová, Ph.D. for introducing me to Raman spectroscopy, giving me countless times invaluable help and creating a very friendly atmosphere in the laboratory. Also, I would like to thank Mgr. Veronika Sutrová who has given me much practical advice and whose enthusiastic support has been an integral part of the incentive environment.

This thesis would not have been possible without RNDr. Ing. Martin Kalbáč, Ph.D. who introduced members of our research group to the fundamental understanding of graphene, as well as prepared the starting graphene samples, and I would like to hereby express my gratitude. I also wish to thank prof. RNDr. Antonín Vlček, CSc. and professor George R. Rossman for measuring electronic absorption spectra of the studied systems with a very special micro-spectroscopic apparatus at the Californian Institute of Technology, Pasadena, USA.

I would also like to acknowledge GAČR 15-01953S for financing the research.

Last but not least, I am grateful to my family and friends for their unceasing encouragement, support and attention not only while writing this thesis.

Abstract

A systematic chemical and spectroscopic approach to evaluation of the effect of single-layer graphene (SLG) on Raman spectra of free-base phthalocyanine (H_2Pc) in glass/SLG/H_2Pc hybrid systems has been developed. By a combination of electronic absorption spectra, Raman spectra at five excitation wavelengths (532, 633, 647, 785 and 830 nm) and excitation profiles of H_2Pc Raman spectral bands, the constitution of the three prepared hybrid sysems has been established in the following manner: Hybrid system I comprises probably a bilayer of H_2Pc molecules, system VI approximately a monolayer of H_2Pc, and system X a slightly reorganized monolayer of H_2Pc molecules. Micro-Raman spectral mapping of all three hybrid systems yielded H_2Pc spectral bands (together with the SLG spectral bands) at all five excitation wavelengths. By contrast, for all three HOPG/H_2Pc reference systems (HOPG = highly oriented pyrolytic graphite), prepared by the same procedure as the corresponding samples, H_2Pc signal was detected only at 633 and 647 nm excitations. A selective increase of normalized Raman intensities of H_2Pc spectral bands for the glass/SLG/H_2Pc monolayer hybrid systems at 830 nm was revealed on the basis of a mutual comparison of Raman excitation profiles of all three samples of glass/SLG/H_2Pc hybrid systems. This excitation was found to mach the calculated difference between the Fermi level of SLG and lowest unoccupied molecular orbital (LUMO) of H_2Pc, and the intensity growth was attributed to the mechanism of GERS (graphene-enhanced Raman scattering) based on a photo-induced charge transfer. Operation of the second GERS enhancement mechanism at 647 and 633 nm excitations was revealed and attributed to favorable changes in electronic absorption spectra of H_2Pc caused probably by a weak interaction between Fermi level of SLG and highest occupied molecular orbital (HOMO) of H_2Pc. The latter mechanism was at least approximately quantitatively evaluated, yielding GERS enhancement factors 13-33 for 633 nm and 6-27 for 647 nm. Free-base phthalocyanine has proved to be a very well suited molecule for the study of GERS, namely due to its planar aromatic character and D_{2h} symmetry, as well as because of the positions of its HOMO and LUMO, that is, below and above the Fermi level of SLG, respectively.

Keywords: free-base phthalocyanine, single-layer graphene, Raman spectroscopy, graphene-enhanced Raman scattering, H_2Pc, SLG, GERS

Abstrakt

Efekt monovrstevného grafénu (SLG) na Ramanova spektra ftalocyaninu volné báze (H_2Pc) v hybridních systémech sklo/SLG/H_2Pc byl systematicky zkoumán z chemického a spektroskopického pohledu. Kombinací elektronových absorpčních spekter, Ramanových spekter na pěti excitačních vlnových délkách (532, 633, 647, 785 a 830 nm) a excitačních profilů Ramanových pásů H_2Pc bylo stanoveno pravděpodobné složení tří studovaných systémů: hybridní systém I sestává patrně z dvojvrstvy molekul H_2Pc, systém VI z monovrstvy a systém X z mírně přeuspořádané monovrstvy zmíněných molekul. Při micro-Ramanově spektrálním mapování všech tří vzorků byly pozorovány pásy H_2Pc (a SLG) na všech pěti excitačních vlnových délkách. V případě referenčních systémů HOPG/H_2Pc (HOPG = vysoce uspořádaný pyrolytický grafit), připravených shodným způsobem jako odpovídající vzorky SLG/H_2Pc, však byly pásy H_2Pc pozorovány pouze při excitacích 633 a 647 nm. Vzájemné porovnání Ramanových excitačních profilů všech tří vzorků SLG/H_2Pc vedlo k odhalení selektivního zesílení normalizovaných Ramanových intenzit v případě excitace monovrstevných systémů vlnovou délkou 830 nm. Bylo zjištěno, že tato excitační vlnová délka odpovídá vypočtenému energetickém rozdílu mezi Fermiho hladinou SLG a nejnižším neobsazeným molekulovým orbitalem (LUMO) H_2Pc. Intenzitní nárůst byl připsán jevu známému pod zkratkou GERS (grafénem zesílený Ramanův rozptyl), konkrétně mechanismu založeném na foto-indukovaném přenosu náboje. Druhý mechanismus GERS byl pozorován při excitacích 633 a 647 nm, kde taktéž docházelo k zesílení Ramanova signálu H_2Pc, což bylo přiřazeno příznivým změnám v elektronových absorpčních spektrech H_2Pc způsobených pravděpodobně slabou interakcí mezi Fermiho hladinou SLG a nejvýše obsazeným molekulovým orbitalem (HOMO) H_2Pc. Tento mechanismus se dále podařilo alespoň přibližně kvantifikovat: GERS faktory zesílení byly stanoveny na 13-33 v případě excitace 633 nm a 6-33 pro 647 nm. Ftalocyanin volná báze byl shledán jako velmi vhodná molekula pro studium GERS, a to především díky jeho planárnímu aromatickému charakteru, D_{2h} symetrii molekuly a vhodné poloze jeho HOMO a LUMO, které se nacházejí pod a nad Fermiho hladinou SLG.

Klíčová slova: ftalocyanin volná báze, monovrstevný grafén, Ramanova spektroskopie, grafénem zesílený Ramanův roztpyl, H_2Pc, SLG, GERS

Contents

Introduction

Relatively recently, a growth of Raman signal for molecules in the vicinity of graphene was observed, and firstly reported in 2010 by Dresselhaus et al. [1]. This effect has been dubbed graphene-enahnced Raman scattering (GERS) and studied widely since. However, this field of research has been almost entirely the domain of reasearch conducted by Dresselhaus et al. (e. g. [2, 3]), though other investigations may be also found [4, 5, 6]. Of those, challenges of the phenomenon of GERS have been reported in Ref. [6], since a decrease in Raman cross-section for Rhodamine 6G (Rh6G) was observed upon adsorption onto single-layer graphene (SLG). A GERS theory has been proposed by Barros and Dresselhaus and GERS enhancement conditions have been formulated [7]. The largest enhancement is to occur for planar aromatic molecules [3], thus free-base phthalocyanine (H_2Pc), chosen for the hereby presented work, stands as an ideal candidate for the study of GERS.

A great variety of molecules has already been investigated in relation to GERS and an extensive summary was presented in [3]. The enhancement factors (EFs) were determined to depend on several factors, such as molecule orientation and type, graphene-molecule distance, graphene thickness, and excitation wavelength characteristics [2], and they were found to range from 1 to 40. The highest EFs have been detected for copper(II) phthalocyanine, while the majority of the studied molecules exhibited rather lower values of their respective EFs [3].

Despite the fact that the EFs provided by GERS do not reach very impressive values in comparison e.g. to those achieved by surface-enhanced Raman scattering (SERS), the phenomenon of GERS appears to be worth a further detailed study. One of the reasons is that the theoretical treatment of this phenomenon has been proposed only recently, hence the previously published papers could not relate the observed GERS enhancement to one of the four theoretically suggested mechanisms. Another challenge for utilization of GERS may be its coupling to the electromagnetic mechanism of SERS in the plasmonic nanostructures/SLG/molecules hybrid systems.

1. Theoretical Background

1.1 Raman Spectroscopy

The explanation of Raman and resonance Raman spectroscopy in this chapter and its subchapters is based on Refs. [8] and [9].

Raman spectroscopy is a well-known and frequently used technique for experimental investigation of molecular vibrations. It is based on inelastic scattering of photons in ultraviolet (UV), visible (Vis) and near infrared (IR) spectral region; this phenomenon being called Raman scattering (RS). When electromagnetic radiation interacts with matter, molecules are excited from a ground into a virtual energy state, and a fraction of them relaxes into an excited vibrational mode (Stokes scattering). Inverse process, i.e. from an excited to the ground state, is also possible (anti-Stokes scattering). The energy difference between the incident and scattered photons in the Stokes process then corresponds to the amount of energy required to excite a molecule into a higher vibrational state of a particular oscillator, i. e. the normal vibration. Raman spectroscopy predominantly focuses on the Stokes process since the population of the individual states is given by Boltzmann distribution, and thus Stokes scattering is a markedly more probable process at ambient temperatures.

The incident radiation induces a dipole moment in the molecule:

$$\boldsymbol{P} = \alpha \boldsymbol{E}_0, \tag{1.1}$$

where $\boldsymbol{P}$ stands for the induced dipole moment, α for the polarizability tensor, and $\boldsymbol{E}_0$ for the electric field intensity. A selection rule for Raman activity of normal vibrations of a molecule applies: the polarizability tensor, α, must change at least one of its components in the course of the vibration. Otherwise, the vibration is Raman inactive.

In Raman spectra, individual bands represent normal vibrations, i. e. periodic changes of respective normal coordinates. These coordinates (and their changes) can be expressed as a linear combination of internal coordinates (or their changes, respectively), i.e. bond lengths and angles (usually determined by X-ray diffraction). The normal vibrations assignment may be achieved through comparison with known spectra and band assignments of related molecules (such as the one of free-base phthalocyanine molecule by Aroca [10]), or through the theoretical approaches using normal coordinate analysis (NCA, a semi-empirical method) or density functional theory (DFT).

Moreover, Raman spectra of randomly oriented molecules (in liquid phase or in a solution), measured in parallel and perpendicular polarization with respect to the incident light, allow for symmetry assignment of individual vibrations. Depolarization ratio, ρ_p, which characterizes symmetry properties of a particular mode, is defined as:

$$\rho_p = \frac{I_\perp}{I_\parallel}, \tag{1.2}$$

where $I_\perp$ and $I_\parallel$ represent intensity of a particular band in perpendicular and parallel, respectively, polarization. In case the depolarization ratio equals 0.75, the bands are depolarized (dp) and correspond to non-totally symmetric vibrations. If the depolarization ratio falls within the open interval $(0; 0.75)$, the bands are polarized (p) and belong to totally symmetric modes. These measurements are usually carried out at an off-resonance excitation to avoid anomalies.

1.1.1 Resonance Raman Spectroscopy

In case of normal (off-resonance) Raman spectroscopy, the energy of the exciting radiation is markedly lower than that of the first allowed electronic transition within a molecule. For resonance Raman scattering (RRS), the excitation energy must approach the energy of an allowed electronic transition, i.e. the intermediate state is located within the vibrational structure of an excited electronic state. The process of RRS occurs by about 3 orders of magnitude faster than absorption followed by emission. Fig. 1.1 schematically depicts the difference between RS and RRS.

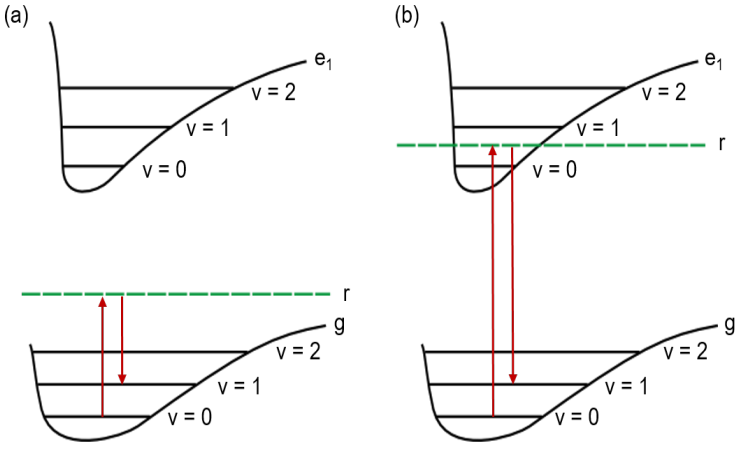

Figure 1.1: A schematic depiction (a) of Raman scattering and (b) resonance Raman scattering. The bottom curves represent electronic ground states with ground and first two excited vibrational states, the upper curves similarly show first excited electronic state with vibrational levels. Green dashed line denotes the intermediate state. Only Stokes processes are shown.

The "sum-over-state" model developed by Albrecht is outlined in Ref. [8] Molecular polarizability tensor, α, is considered as a function of the excitation wavelength. Each of the components of the molecular polarizability tensor represents a component of the transition moment ascribed to a two-photon process of excitation and depopulation of the intermediate state. The constituents of the molecular polarizability tensor are expressed in terms of eigenstates of the vibronic Hamiltonian of a molecule (for Stokes process and invoking Born-Oppenheimer approximation):

$$[\alpha_{\rho\sigma}]_{\mathrm{i,f}} = \frac{1}{hc} \sum_{v} \left(\frac{\langle \mathrm{f}|[\mu_\rho]_{\mathrm{ge}}|v\rangle\langle v|[\mu_\sigma]_{\mathrm{eg}}|\mathrm{i}\rangle}{\tilde{\nu}_{v\mathrm{i}} - \tilde{\nu}_0 - i\Gamma_v} + \frac{\langle \mathrm{f}|[\mu_\sigma]_{\mathrm{ge}}|v\rangle\langle v|[\mu_\rho]_{\mathrm{eg}}|\mathrm{i}\rangle}{\tilde{\nu}_{v\mathrm{f}} + \tilde{\nu}_0 - i\Gamma_v} \right) \tag{1.3}$$

where $[\alpha_{\rho\sigma}]_{\mathrm{if}}$ stands for one of the components of the transition moment between ground (i) and first excited (f) vibrational state of ground electronic state (g), v for any vibrational state of excited electronic state (e), $[\mu_\rho]$ and $[\mu_\sigma]$ for the respective components of transition moment between e and g, $\tilde{\nu_0}$ for the excitation wavenumber, $\tilde{\nu}_{\mathrm{vi}}$ and $\tilde{\nu}_{\mathrm{vf}}$ for wavenumbers of the corresponding transitions, Γ_{v} for the damping factor (which is inversely proportional to the lifetime of the intermediate state) and finally h and c for Planck constant and speed of light, respectively.

Upon expansion of the transition moment into Taylor series and consideration of only the first two terms, two contributors to the molecular polarizibility may be recognized: A-term (Eq. 1.4) and B-term (Eq. 1.5). Enhancement via the former is based on Franck-Condon mechanism, hence it is an imperative the overlap integrals to be nonzero. The latter describes enhancement via Herzberg-Teller mechanism, which originates from the vibronic coupling of two close-lying excited states. However, the B-term contribution is usually much smaller in comparison to the A-term.

$$A = \frac{1}{hc} [\mu_\rho]^0_{\mathrm{ge}} [\mu_\sigma]^0_{\mathrm{eg}} \sum_{v} \frac{\langle \mathrm{f}|v\rangle\langle v|\mathrm{i}\rangle}{\tilde{\nu}_{v\mathrm{i}} - \tilde{\nu}_0 - i\Gamma_v}, \tag{1.4}$$

$$\begin{aligned} B = &\frac{1}{hc} \sum_{s\neq \mathrm{v}} [\mu_\rho]^0_{\mathrm{gs}} [\mu_\sigma]^0_{\mathrm{eg}} \frac{h^k_{\mathrm{se}}}{\Delta\tilde{\nu}_{\mathrm{se}}} + \sum_{v} \frac{\langle \mathrm{f}|\mathrm{Q_k}|v\rangle\langle v|\mathrm{i}\rangle}{\tilde{\nu}_{v\mathrm{i}} - \tilde{\nu}_0 - i\Gamma_v} \\ &+ \frac{1}{hc} \sum_{s\neq \mathrm{v}} [\mu_\rho]^0_{\mathrm{ge}} [\mu_\sigma]^0_{sg} \frac{h^k_{\mathrm{se}}}{\Delta\tilde{\nu}_{\mathrm{se}}} + \sum_{v} \frac{\langle \mathrm{f}|v\rangle\langle v|\mathrm{Q_k}|\mathrm{i}\rangle}{\tilde{\nu}_{v\mathrm{i}} - \tilde{\nu}_0 - i\Gamma_v} \end{aligned} \tag{1.5}$$

where $[\mu_\rho]^0$ represents one of the components of the purely electronic transition moment, s a close-lying excited state to the excited state e, $\Delta\tilde{\nu}_{\mathrm{se}}$ energy difference between the two excited states, and $h^{\mathrm{k}}_{\mathrm{se}}$ the change of hamiltonian with respect to normal coordinate $\mathrm{Q_k}$ upon e-s coupling.

1.2 Graphene and Raman Spectroscopy

1.2.1 Raman Spectra of Graphene

This section was written based on Refs. [11] and [12].

Raman spectroscopy is one of the principal tools used in the study of graphene and other sp^2 carbon materials, e. g. single-wall carbon nanotubes. It is a fast and non-destructive method providing us with considerable amount of structural and electronic information. For example, the positions, intensities and shapes of the peaks are highly sensitive to the strain, doping, number of layers and the presence of any defects, and thus can easily reveal any of those.

Raman spectrum of single-layer graphene comprises several distinct bands, as shown in Fig. 1.2 (adopted from [12]). There are two always-present principal modes: G and 2D [1], two defect modes: D and D', and a few other modes: D+D', D+D" and 2D'.

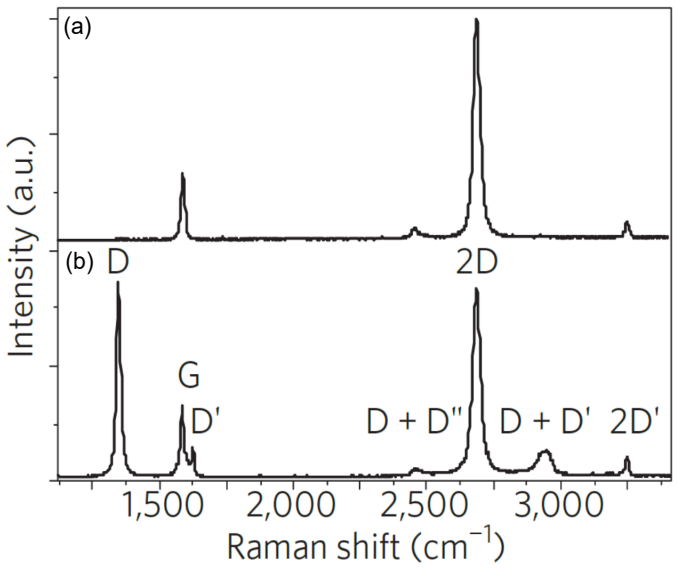

Figure 1.2: Raman spectra of graphene. Spectrum (a) corresponds to pristine graphene, spectrum (b) to graphene with disorder. Bands labeled as described in the text. Adopted from [12].

The G-band appears at around 1585 cm^{-1} and arises from in-plane C-C bond stretching. This band is sensitive to doping and especially to strain, the former causing shifts (blue-shifts in case of weak doping, blue(red)-shifts for $p(n)$ doping). Under uniaxial stretching, the G peak splits into G^- and G^+, and both of them are also red-shifted when the stretching is increased.

[1] Note that the 2D mode is sometimes called G' in literature in order to stress that it is not a defect mode and to avoid possible misreading as "two-dimensional".

The D-band is observed as a peak in the range $1250 - 1400$ cm^{-1}, with strong dispersion with the excitation energy ($\simeq 50$ cm^{-1}/eV), and corresponds to the breathing of the six-atom rings. A defect is required for its activation, hence the presence of the D-band in a spectrum is indicative of disorder and its intensity can be used to quantify the disorder.

The D'-band serves as another indicator of the presence of a defect, since it is necessary for its activation. This mode appears at around 1620 cm^{-1}.

The 2D- and 2D'-band are overtones of the D- and D'-mode, respectively. The former appears in the range $2500 - 2800$ cm^{-1}, the latter at around 3240 cm^{-1}, and no defects are required for their activation. The position of the 2D-mode is strongly dependent on the excitation energy ($\simeq 100$ cm^{-1}/eV) as well as on the number of graphene layers and the stacking order in case of few-layer graphene or graphite.

The D+D" and D+D' bands, visible at $\simeq 2450$ cm^{-1} and $\simeq 2970$ cm^{-1}, respectively, are combination bands of the respective modes. The name D" has been assigned to a mode seen at $\simeq 1100$ cm^{-1} when a defected graphene sample is measured with visible light.

1.2.2 Graphene-Enhanced Raman Spectroscopy

Graphene-enhanced Raman scattering is only a relatively recently observed phenomenon, first reported in 2010 by Ling et al. [1]. It has been widely studied in the past few years [2, 3] and a theory has been developed by Barros and Dresselhaus [7]. The subsequent explanation of this effect is based on the above mentioned references, i.e. [1, 2, 3, 7].

Graphene possesses the ability to enhance the resonance (and, in some cases, also the normal) Raman scattering of molecules located in the vicinity of the graphene surface. The extent to which the scattering is amplified depends on several factors, such as the type of the molecule, molecular concentration and orientation, molecule-graphene distance, graphene thickness, graphene Fermi level energy, and laser wavelength and polarization. About 30 different molecules have already been studied in relation to GERS with variable results. The best enhancement factors, calculated as the ratio of the GERS signal to a reference signal, were observed for planar aromatic molecules, namely EF equal to 40 was obtained for copper(II) phthalocyanine. However, EFs for other molecules were substantially lower (below 10).

These findings corroborate the model proposed by Barros and Dresselhaus [7], which puts the origin of GERS down to the charge transfer (CT) between the Fermi level of graphene and the ground and/or excited electronic state of

the molecule. According to this approach, the larger enhancements occur for the following conditions:

$$\hbar\omega_0 = E_L - E_H \quad \text{or} \quad \hbar\omega_0 = E_L - E_H + \hbar\omega_q \tag{1.6a}$$

$$E_F = E_H \pm \hbar\omega_q \quad \text{or} \quad E_F = E_L \pm \hbar\omega_q \tag{1.6b}$$

$$\hbar\omega_0 = E_F - E_H \quad \text{or} \quad \hbar\omega_0 = E_F - E_H + \hbar\omega_q \tag{1.6c}$$

$$\hbar\omega_0 = E_L - E_F \quad \text{or} \quad \hbar\omega_0 = E_L - E_F - \hbar\omega_q \tag{1.6d}$$

where $\hbar\omega_0$ is the excitation energy, E_L and E_H the energies of the lowest unoccupied molecular orbital (LUMO) and highest occupied molecular orbital (HOMO) states of the molecule, respectively, E_F the energy of Fermi level of graphene, and $\hbar\omega_q$ the phonon energy.

Two molecular selectivity rules for GERS have been formed: Energy Level Rule and Structure Rule. The former states that strong enhancement occurs when the HOMO or LUMO energy differs from the Fermi level of graphene by the phonon energy or when the excitation laser energy is close to the HOMO or LUMO energy separation, or the excitation energy approaches the difference between the Fermi level of graphene and HOMO or LUMO of the molecule. According to the latter rule, D_{nh} symmetry is favored since it shows better compatibility with the honey-comb structure of graphene.

However, as mentioned in the beginning of this section, GERS has been discovered only a few years ago, and therefore it is yet to be generally accepted (or disproved). Hence works challenging the idea of GERS exist, such as the report on rhodamine 6G by Brus et al [6].

1.3 Free-Base Phthalocyanine: Raman Spectra and Electronic Structure

Free-base phthalocyanine, a member of the group of porphyrin analagues, consists of four isoindol groups interconnected with nitrogen atoms. The two hydrogen atoms are located in the center of the structure on diagonally opposite nitrogen atoms (Fig. 1.3). As an aromatic planar centrosymmetric molecule (D_{2h} symmetry group), H_2Pc stands as an ideal candidate for the study of GERS.

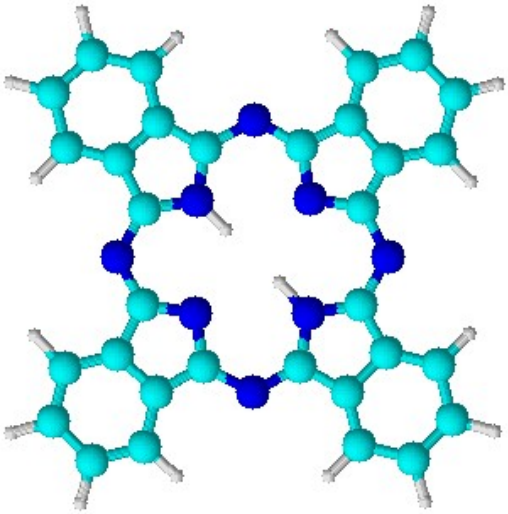

Figure 1.3: H_2Pc molecule composed of 16 carbon and nitrogen atoms building up the inner macrocycle and of four benzene rings linked to the macrocycle via carbon atoms.

Phthalocyanines find applications in a variety of fields, e.g. they were tested as photosensitizers in photodynamic terapy [13], incorporated into a polysiloxane sol-gel materials which leads to promising utilization in optics and photonics [14], used to functionalize single-walled nanotubes for ammonia vapor detection [15].

1.3.1 Electronic Absorption Spectra

The first few excitations of phthalocyanines involve π-π^* transitions, and in a simple model featuring the construction of molecular orbitals as a linear combination of atomic orbitals (MO LCAO) for porphyrines and considering only p_z atomic orbitals of carbons and nitrogens, the lowest lying singlet states are fourfold degenerate. However, configuration interaction decreases this degeneracy to two doubly degenerate states. H_2Pc, Fig. 1.3, compared to metal phthalocyanines with D_{4h} symmetry (a single metal atom is bonded to the all four nitrogen atoms in the center of the molecule), has a reduced symmetry, which breaks the equiva-

lence of x and y directions. This results in a further removal of the degeneracy of both the first (Q, transition in the visible range) and second (B or Soret, transition in the ultraviolet range) excited states, and Q splits into Q_x and Q_y. [16] It has been also ascertained that the electron density involved in the Q-band transition is localized on the macrocycle, whereas B-band affects the benzene rings. [17]

The nature of H_2Pc and its physical state significantly influence its respective absorption spectra, namely the position of the Q-band and even how many peaks are visible. As an isolated molecule, H_2Pc shows two absorption maxima at 661 and 632 nm corresponding to Q_x and Q_y, respectively. [16] When dissolved in 1-chloronaphtalene, two distinct sharp and intense bands appear at 697 and 662 nm for Q_x and Q_y [2] , respectively, accompanied with lower bands at 596 nm and 631 nm with a shoulder to 638 nm, as depicted in Fig. 1.5. [14] In a 61μm-thick phthalocyanine-doped polyphenylsiloxane film, absorption maxima shift red to 702 nm (Q_x) and 666 nm (Q_y) and additional broad bands appear at 610 and 637 nm, Fig. 1.6. [14] Absorption spectrum of a 60-nm α-H_2Pc film consists of a broad band with a maximum at roughly 620 nm and a shoulder at around 720 nm, Fig. 1.4. [17] This observation is in agreement with two absorption maxima at ca. 350 nm and 620 nm for a 100-nm-thick film of α-H_2Pc mentioned in Ref. [10].

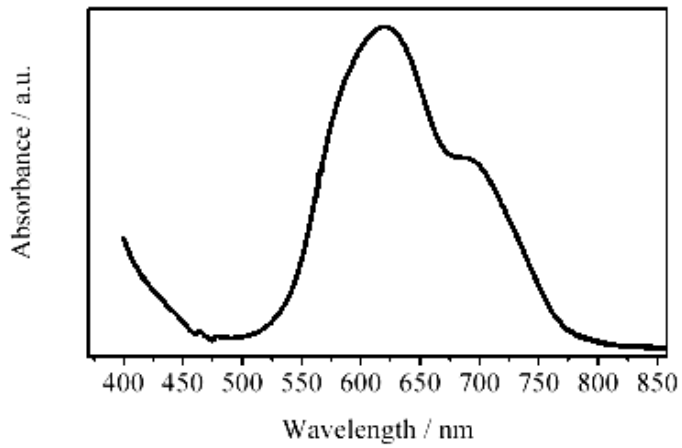

Figure 1.4: Absorption spectra of a 60-nm α-H_2Pc film on glass substrate. Adapted from [17].

[2] In Ref. [16], the Q_x and Q_y bands were observed at 700 and 663 nm, respectively.

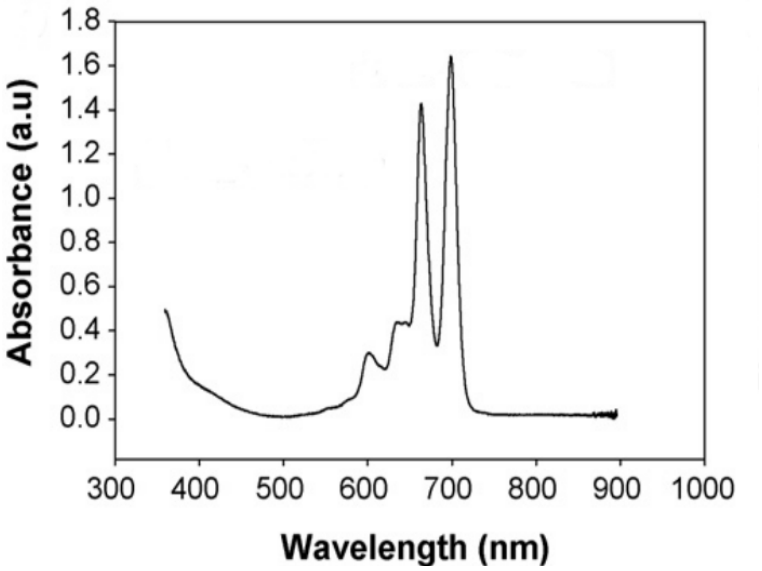

Figure 1.5: Absorption spectra of H_2Pc in chloronaphtalene. Adapted from [14].

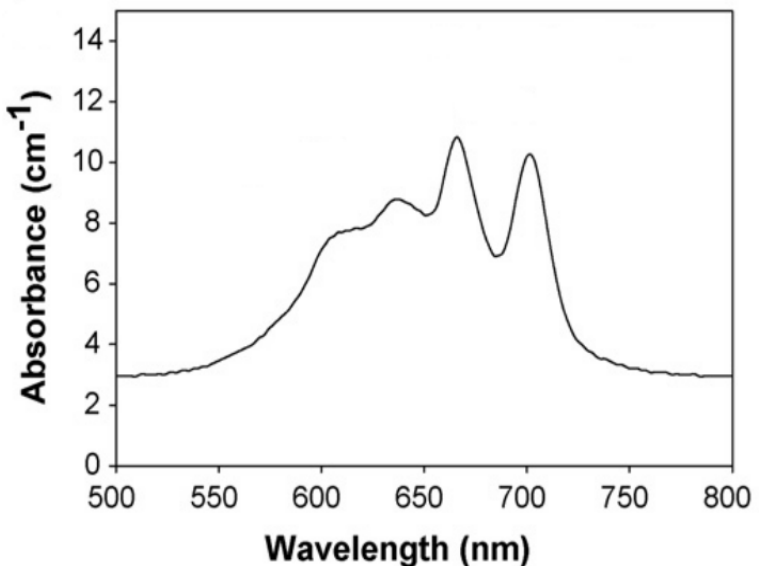

Figure 1.6: Absorption spectra of H_2Pc-doped polyphenylsiloxane film. Adapted from [14].

1.3.2 Fluorescence

H_2Pc shows strong fluorescence, thus Raman spectra cannot be obtained at resonance wavelengths unless the photoluminiscence is suppressed. In a chloronaphtalene solution, fluorescence spectrum exhibits one intense emission band at 702 nm (Fig. 1.7). In a polyphenylsiloxane phthalocyanine-doped film, the fluorescence maximum appears at 707 nm (Fig. 1.8). [14] Furthermore, strong fluorescence background was reported for measurements of H_2Pc in KBr discs at 633 nm excitation. [18] However, no fluorescence has been mentioned when examining thin phthalocyanine films. [10, 17, 19]

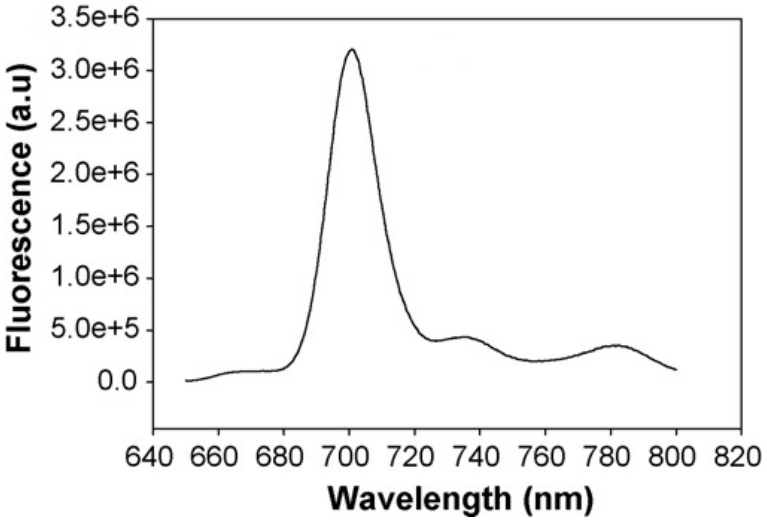

Figure 1.7: Fluorescence spectra of H_2Pc in chloronaphtalene. Adapted from [14].

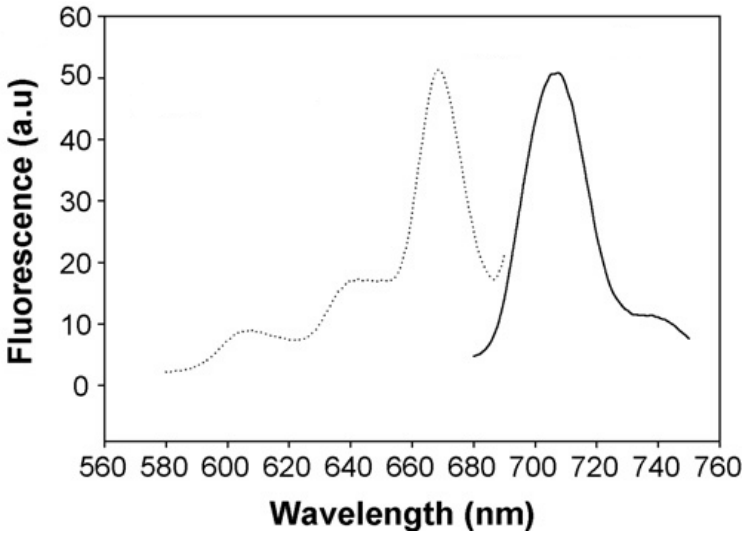

Figure 1.8: Fluorescence spectra of H_2Pc-doped polyphenylsiloxane film (solid line). The dotted line corresponds to excitation spectrum in the original in Ref. [14], from which it was adapted.

1.3.3 Raman Spectra

Raman spectra of H_2Pc have been investigated several times in order to assign vibrational frequencies by comparison with porphyrins, metallophthalocyanines and other related structures [10, 17, 19, 20], and to ascertain the symmetry of the particular vibrations [10, 17, 18]. A brief summary is presented in this chapter.

Vibrations of H_2Pc may be divided into two main groups: those of the inner macrocycle and those of the isoindole parts. The former includes chiefly macrocycle breathing at 682 cm^{-1}, macrocycle deformation at 796 cm^{-1} and 720 cm^{-1}, and in-phase motion of four isoindole groups at 182 cm^{-1}. The latter comprises mainly isoindole and pyrrole stretching and breathing at 1450 cm^{-1} and 1428 cm^{-1}, and 1534 cm^{-1}, 1513 cm^{-1}, 1337 cm^{-1} and 1140 cm^{-1}, respectively. Furthermore, benzene ring stretches have been assigned to 1618 cm^{-1} and isoindole ring deformation to 480 cm^{-1}. [10, 20] [3]

A detailed list of H_2Pc both observed and calculated peaks is presented in Tab. 1.1 and complemented with respective spectra in Fig. 1.9 [18]. The measured positions of the H_2Pc peaks match those DFT calculated [18] and agree within quoted literature. However, that is not the case of symmetry assignments [10, 17, 18]. Those based on theoretical approach in Ref. [18] differ from those proposed on the basis of the analogy between the porphyrin and the phthalocyanine spectral bands [10].

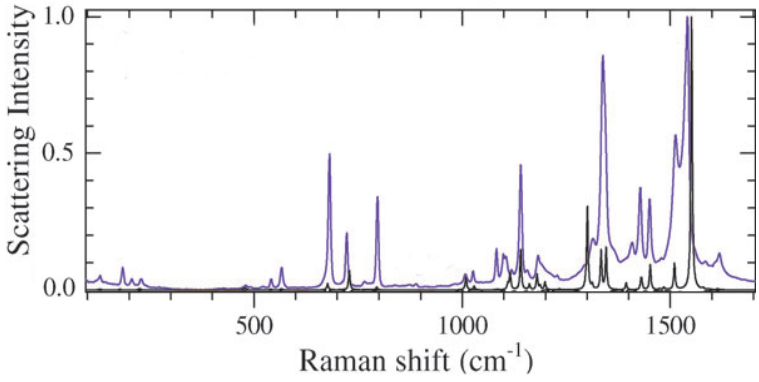

Figure 1.9: Calculated (in black) and observed (in blue) spectra of H_2Pc. Adapted from [18].

H_2Pc exists in several forms, namely as α-H_2Pc, β-H_2Pc and x-H_2Pc, however, Raman spectra of thin films of the respective polymorphs show only minor variations. [10] Raman spectra of α-H_2Pc thin films have been further studied at different excitation wavelengths, Fig. 1.10. [10, 17, 19]

Three different types of intensity dependence on excitation wavelength may

[3] The given wavenumbers were adopted from Ref. [10], respective figures in Ref. [20] may slightly differ.

Obs.	Calc. scaled	Calc. unscaled	Sym.
129.9 (w)	130.2 (0.0017)	132.9	A_g
182.9 (m)	177.6 (0.0015)	181.2	B_{1g}
204.7 (w)	207.7 (0.0000)	211.9	B_{1g}
228.3 (w)	225.4 (0.004)	229.7	A_g
—			
479.9 (w)	477.9 (0.007)	487.6	B_{1g}
541.3 (w)	540.3 (0.002)	551.3	A_g
565.7 (m)	566.0 (0.002)	577.5	A_g
679.9 (s)	676.6 (0.02)	690.4	A_g
722.8 (m)	728.6 (0.06)	743.5	A_g
764.7 (vw)	763.7 (0.001)	779.3	A_g
796.1 (s)	794.5 (0.01)	810.7	A_g
888.9 (w)	889.3 (0.0000)	907.4	B_{1g}
1007.3 (w)	1008.4 (0.012)	1029.0	A_g
1026.3 (w)	1028.7 (0.012)	1049.7	B_{1g}
1081.4 (m)	1084.8 (0.002)	1107.0	B_{1g}
1099.1 (m)	1099 (0.0000)	1121.7	B_{1g}
1104.4 (m)	1109.9 (0.02)	1132.5	B_{1g}
1117.4 (w)	1116.0 (0.05)	1138.3	A_g
1140.3 (s)	1140.7 (0.13)	1164.0	A_g
1154.9 (vw)	1161.3 (0.18)	1185.2	A_g
1180.9 (w)	1179.9 (0.06)	1211.4	A_g
1190.0 (vw)	1191.1 (0.006)	1223.6	B_{1g}
1227.8 (w)	1233.5 (0.14)	1258.7	B_{1g}
1293.7 (sh)	1300.4 (0.30)	1327.0	A_g
1312.8 (w)	1312.5 (0.01)	1339.3	B_{1g}
1336.7 (vs)	1333.7 (0.13)	1360.9	A_g
	1345.8 (0.14)	1373.3	A_g
1406.5 (w)	1393.9 (0.025)	1422.4	A_g
1426.9 (m)	1430.8 (0.05)	1459.0	B_{1g}
	1431.6 (0.148)	1460.9	
1450.5 (m)	1452.0 (0.09)	1481.6	A_g
—	—	—	—
1511.5 (s)	1510.3 (0.09)	1541.1	A_g
1539.5 (vs)	1551.2 (1.0)	1582.9	A_g
1584.4 (w)	1579.1 (0.006)	1611.4	A_g
1616.8 (w)	1613.9 (0.004)	1646.8	B_{1g}

Table 1.1: Comparison of observed and DFT calculated peaks for H_2Pc, and vibrational symmetry assignment. Relative intensities are indicated in parenthesis. Scaling of the calculated values is by factor of 0.98. Adopted from [18].

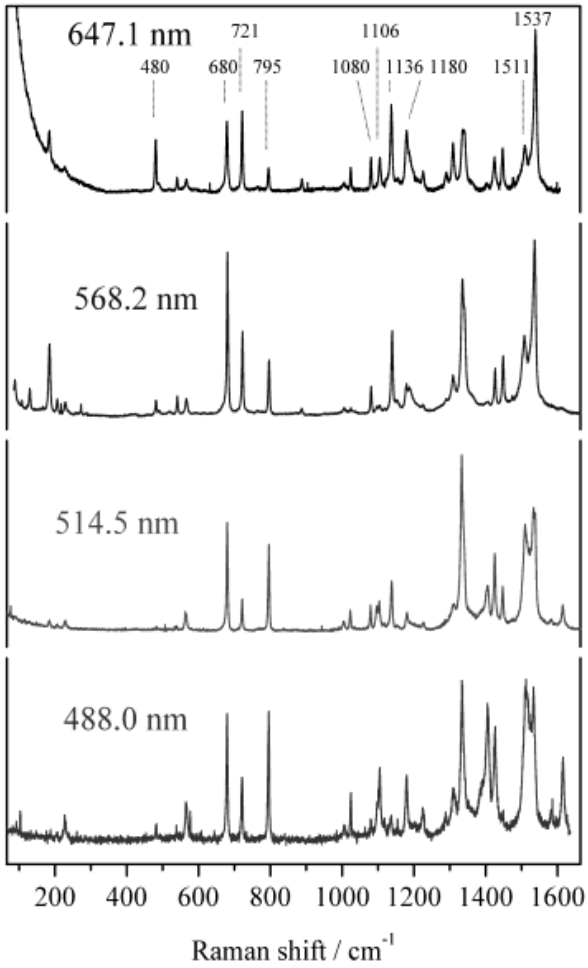

Figure 1.10: Spectra of 60-nm α-H_2Pc film measured at four excitation wavelengths (488.0, 514.5, 568.2 and 647.1 nm). Adopted from [17].

be distinguished [10, 17], as illustrated by Fig. 1.11: [4]

(i) Relative intensity profile exhibits a minimum at roughly 500 nm and climbs steeply towards both higher and lower frequencies. These vibrations are expected to be enhanced by both the B and Q-band, and include vibrations at 480, 682, 720, 1104, 1181 and 1534 cm^{-1}.

(ii) Relative intensity decreases as laser excitation wavelength increases, and thus resonance with the B-band is the prevailing mechanism, such as for 230, 571, 796, 1406, 1513 and 1618 cm^{-1}.

(iii) Relative intensity increases with the laser wavelength, and resonance with the Q-band is predominant, e. g. for 182, 1080 and 1140 cm^{-1}.

Aroca et al. [10], in an analogy to porphyrins, concluded that the types (i) and (ii) correspond to the totally symmetric vibrations which derive their intensity

[4]The subsequently given wavenumbers were adopted from Ref. [10], respective figures in Ref. [17] may slightly differ.

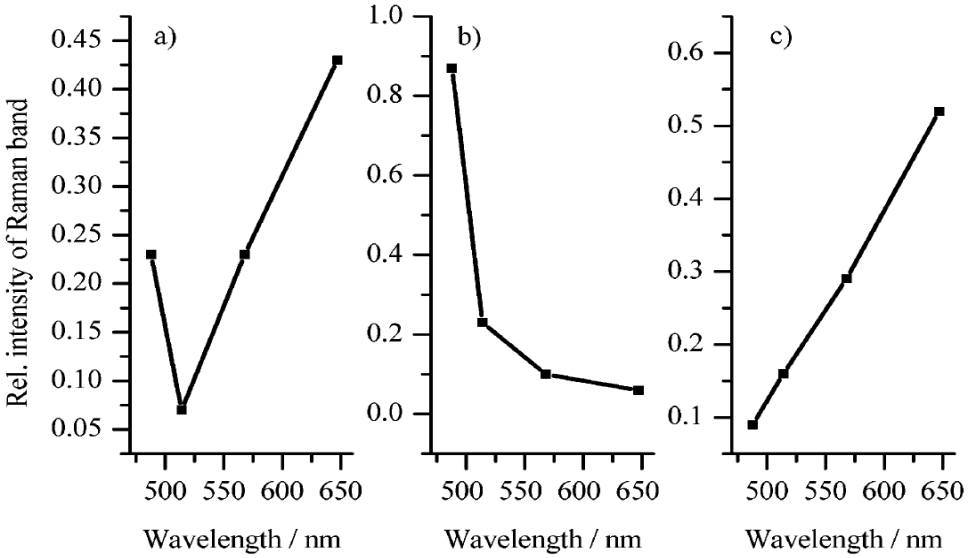

Figure 1.11: Relative intensity of Raman bands for 60-nm α-H_2Pc films as a function of laser wavelength (488.0, 514.5, 568.2 and 647.1 nm). Three different trends are observed, represented by the vibrations at (a) 721 cm^{-1}, (b) 1406 cm^{-1} and (c) 1140 cm^{-1}. Adopted from [17].

from the B-band. The last type, on the other hand, would belong to non-totally symmetric vibrations which may decrease and finally become negligible upon the approach of the B-band.

However, Heutz et al. [17] argued that enhancement of non-totally symmetric modes seems also possible via the B-term resonance. While totally symmetric vibrations are amplified by the A-term (due to Franc-Condon overlap), the B-term (and the consequent enhancement of non-totally symmetric modes) grows in importance because of the close-lying electronic levels of the Q- or B-band and the possibility of their coupling. Considering the transition symmetries, a conclusion has been drawn that either A_g or B_{3g} modes can be enhanced by excitation into the Soret band, while both A_g and B_{1g} modes are intensified through resonance with the Q-band.

Murray et at. [18] conducted an extensive study of the H_2Pc molecule, focusing on both DFT calculated and experimental data. The ascertained vibrational symmetries are summarized in Tab. 1.1.

H_2Pc was also investigated in relation to GERS [1], namely on Si/SiO_2 substrate with H_2Pc molecules deposited thereon by vacuum evaporation in two thicknesses (1 and 2 Å). Raman spectra were obtained with the excitation wavelengths 458, 514.5 and 633 nm, and bands of H_2Pc were found to reach significantly higher values for graphene-containing systems. EFs were ascertained to range from 2 to 17, and overtones were observed for H_2Pc on SLG upon 633 nm excitation.

2. Objectives

1. Preparation of SLG/H_2Pc hybrid systems and their characterization by UV-Vis electronic absorption microspectroscopy.

2. Micro-Raman spectral measurements of the SLG/H_2Pc hybrid systems at 5 excitation wavelengths and assignment of SLG and H_2Pc spectral bands.

3. Preparation and micro-Raman spectral measurements of a suitable selected H_2Pc-containing reference hybrid system at 5 excitation wavelengths.

4. Raman spectral measurements of H_2Pc in solution and in the microcrystalline state as well as of pristine SLG at 5 excitation wavelengths, complemented by UV-Vis electronic absorption measurements of H_2Pc in solution and by Raman depolarization measurements of H_2Pc in solution at a selected, off-resonance excitation wavelength.

5. Evaluation of changes in the Raman spectra of H_2Pc and of SLG upon the SLG/H_2Pc hybrid system formation, and determination of graphene-enhancement of Raman scattering of H_2Pc in the particular SLG/H_2Pc hybrid system.

3. Experimental Section

3.1 Materials

- 29,31H-Phthalocyanine, H_2Pc (Sigma-Aldrich, β-form, 98%)
- 29,31H-Phthalocyanine-C,C,C,C-tetrasulfonate hydrate, H_2PcTS (Sigma-Aldrich)
- Toluene for spectroscopy (Merck, Uvasol)
- Single-layer graphene on glass, SLG
- Highly-ordered pyrolytic graphite, HOPG

Graphene samples (glass/SLG) were obtain from J. Heyrovský Institute of Physical Chemistry, Academy of Sciences of the Czech Republic, where they had been prepared by Dr. Martin Kalbáč according to a previously reported chemical vapor deposition procedure [21].

3.2 Preparation of Samples

3.2.1 Preparation of H_2Pc Solution

A saturated ($< 10^{-5}$ M) phthalocyanine solution was prepared by dissolving 1.1 mg of H_2Pc in 41 mL of toluene in 100mL Erlenmeyer flask. After thorough manual shaking and dissolving in ultrasonic bath, the mixture was left standing for a day. Afterwards, it was filtered through a 1-μm-filter into a new clean 100mL Erlenmeyer flask.

3.2.2 Preparation of Glass/SLG/H_2Pc Systems

Three types of glass/SLG/H_2Pc samples were prepared. Since they differ solely in the extent of final toluene rinse, only one description follows with the difference and sample notation presented at its end.

Toluene was poured into a weighting bottle so as its bottom side was covered with approximately 5mm-thick layer of toluene. An 1-cm-long inverted cut-off bottom of a vial was placed into the center of the weighting bottle with toluene, and graphene on glass was then carefully laid onto a cover slip which had been placed on the vial bottom. The weighting bottle was closed and left standing for approximately 10 minutes. Then, the beforehand prepared solution of H_2Pc in

toluene was carefully poured using a pipette onto the sample until the sample was covered with a layer of this solution. The weighting bottle was closed and sealed with parafilm, and left standing for 24 hours. Then the sample was removed from the weighting bottle and dried using a slip of filter paper. Similar procedure as described above was carried out again, except for covering the sample with pure (spectroscopic) toluene for 10 minutes instead of H_2Pc/toluene solution for 24 hours. In case of the system denoted as glass/SLG/H_2Pc-I, the final step was performed only once (i. e. only one 10-minute toluene rinse). For systems labeled as glass/SLG/H_2Pc-VI and glass/SLG/H_2Pc-X, the final step was done six times (6x10 minutes), and ten times (10x10 minutes), respectively.

3.2.3 Preparation of HOPG/H_2Pc Systems

Top layers of HOPG were removed using a scotch tape. The tape was gently laid on one of the sides (top) of the HOPG and slightly pushed towards the surface of the HOPG. Then the tape, with a few carbon layers stuck on its bottom side, was carefully removed, creating a clean and relatively smooth surface. These steps were repeated one more time on the same side. Same procedure was applied to the opposite (bottom) side of the HOPG.

Immediately after the above described procedure had been finished, the HOPG was placed into a clean small weighting bottle and covered with solution of H_2Pc in toluene. The weighting bottle was closed and sealed with parafilm, and left standing for 24 hours. Afterwards, the HOPG was removed from the solution and dried with a slip of filter paper. Next, the HOPG was placed into another weighting bottle partially filled with toluene and left there for 10 minutes. Finally, the HOPG was removed from the weighting bottle and again dried with a slip of filter paper, this sample being labeled as HOPG/H_2Pc-I. The glass/SLG/H_2Pc samples alike, HOPG/H_2Pc-VI was washed six times with toluene (6x10 minutes) and HOPG/H_2Pc-X ten times (10x10 minutes) in total.

3.2.4 Preparation of H_2PcTS Solution

A $1.0 \cdot 10^{-2}$ M solution of H_2PcTS in water was prepared in a small vial by dissolving 1.3 mg of H_2PcTS in 160 μL of deionized water. To ensure complete dissolution, the mixture was shaken for an hour.

This $1.0 \cdot 10^{-2}$ M solution was used for polarized Raman measurements. For UV-Vis absorption spectra, it was diluted by adding 990 μL of deionized water to 10.0 μL of the original solution, hence the new concentration was $1.0 \cdot 10^{-4}$ mol $\cdot$ dm^{-3}.

3.3 Instrumentation

3.3.1 Raman Spectroscopy

Raman spectra as well as optical images were obtain using WITec alpha300 Raman microspectrometer. An objective (Zeiss) with 100x magnification was used for all measurements of solid samples. A long-working-distance (LWD) objective (Zeiss) with 50x magnification was used for measurements of solutions in 1mm-thick quartz cuvettes. Laser types, wavelengths and laser powers are listed in Tab. 3.1 (laser powers measured at the sample). Parameters for all area scans were 25μm-by-25μm with 50-by-50 points and integration time was set to 0.4 s. In case of H_2Pc in crystalline form, the laser power was set to 0.3 mW.

Table 3.1: Laser types, excitation wavelengths, and laser powers used for measuring Raman spectra.

Laser type	Excitation wavelength (nm)	Power (mW)
SHG Nd:YVO_4	531.994	2.3
He-Ne	632.847	2.5
Kr^+	647.125	5.0
Diode	784.793	50.0
Diode	830.042	11.0

Raman polarization measurements were carried out on LabRAM (Horiba) Raman microspectrometer using a LWD objective with 50x magnification. Argon laser was used, namely excitation wavelengths 488 and 514.5 nm. Spectra collected at the former excitation are presented in the following chapter, while those acquired at the latter excitation wavelength may be found in the Supplement.

3.3.2 Absorption Spectroscopy in UV-Vis

UV-Vis electronic absorption spectra of H_2Pc in toluene and H_2PcTS in water solutions were obtained with Shimadzu UV-2401 PC UV-VIS (Shimadzu corporation) recording spectrometer. Quartz cuvettes with optical paths 1 cm (H_2Pc in toluene) and 1 mm (H_2PcTS in water) were used.

UV-Vis absorption spectra of glass/SLG/H_2Pc-I hybrid system were acquired by professor George R. Rossman and professor Antonín Vlček at the Californian Institute of Technology, Division of Geological and Planetary Sciences. The spectra were measured at a home-assembled microspectrometer system consisting of a 20-watt Oriel tungsten-halogen lamp coupled to a modified Nicolet Nicplan microscope which in turn passes through an Acton spectrograph (resolution of approximately 1.7 nm) and the light is finally detected by a Princeton Instruments Si diode-array detector [22]. The measured area was 350-by-260 μm.

3.4 Data Processing and Analysis

Program WITec Project FOUR was used first for spectra processing. Further treatment of Raman spectra was carried out in a set of Matlab-based programs, Origin and Omnic. Excitation profiles were constructed in Microsoft Excel, as well as this software served for some calculations, e. g. of intensity correction functions, enhancement factors and excitation profiles.

UV-Vis electronic absorption spectra were processed in UV Probe and Origin.

Optical images and schemes were processed in programs GIMP and Inkscape.

3.4.1 Wavenumber Calibration

Spectrographs of the WITec alpha300 apparatus were calibrated via a standardized step sequence prescribed by the manufacturer (namely an automatic procedure employing a built-in Hg-Ar lamp) prior to the series of measurements. Furthermore, an additional calibration was carried out in order to establish more precise wavenumbers and to ensure accuracy of the Raman spectra measured at different excitation wavelengths and on different days. The method is based on complementing each acquired Raman spectrum with an emission spectrum of the built-in Hg-Ar lamp. Emission lines of these two elements are well-known, and therefore could be used for the purpose of relatively precise wavenumber calibration.

The wavenumbers of the mercury and argon transitions of interest were taken from [23] and their precise positions (Raman shifts) in the spectra for each excitation wavelength were calculated, Tab. 3.3. Each pair comprising a Hg-Ar calibration spectrum and a spectrum of interest (e.g. a spectrum of glass/SLG/H_2Pc system) was then horizontally shifted so as the measured and standardized Hg-Ar emission lines matched each other. This horizontal shift usually did not exceed 1 cm^{-1}.

3.4.2 Intensity Calibration

For measurements on WITec alpha300, two different spectrographs equipped with charge-coupled device (CCD) detectors optimized for blue-green and red-NIR (near infra-red) spectral ranges have been used, the first one for collection of spectra at 532 nm excitation and the second one for the other four excitation wavelengths, i.e. 633, 647, 785 and 830 nm. Especially in the case of the latter, the sensitivity of the detector decreases rapidly for longer excitation wavelengths. For reliable comparison of relative intensities of Raman spectra obtained with different excitations throughout broader wavenumber ranges, intensity correction

functions have been determined.

Two approaches to the spectrograph response calibration were considered. The first one employed measurements of a substance whose spectra are independent of excitation wavelength. For this purpose, a mixture of water, deuterated water, ethanol and acetone was chosen since the compounds contribute by Raman bands which cover sufficiently densely the wavenumber range from 400 up to 3700 cm^{-1}. An equal amount (volume) of H_2O and D_2O was pipetted into a 1-mm-quartz cuvette and 50 μL of ethanol and acetone were subsequently added, and finally the mixture was thoroughly shaken to ensure uniform composition throughout the cuvette. Spectra of this mixture were then obtained at all five excitations and under similar experimental conditions as the previously carried out measurements. Spectrum acquired at 633 nm excitation was then selected as a reference and correction functions for the other four excitations with respect to the mentioned spectrum were calculated. Ratios of corresponding bands in the spectrum at 633 nm excitation and in a spectrum of interest were determined (Raman shifts of selected points are listed in Tab. 3.2), and the ascertained values were subsequently fitted in the appropriate range with a suitable function (a second order polynomial in case of 830 nm excitation, and forth-order polynomials for 532, 647 and 785 nm). Graphs featuring the chosen points as well as the fitting functions may be found in the Supplement, Fig. S5. The accuracy of the calculated correction functions was tested on the spectra of the above mentioned mixture as well as on spectra of polystyrene and toluene (all acquired under the same conditions).

Table 3.2: Raman shifts of selected points in the spectra of the calibration mixture for construction of correction functions.

Raman shift (cm^{-1})			
532 nm	647 nm	785 nm	830 nm
547	546	547	547
801	801	801	801
879	879	879	879
1051	1052	1051	1051
1243	1243	1243	1243
	1305	1365	
1430	1430	1430	1430
1457	1457	1457	1457
	1485		
1701	1701	1701	1701
2510	2510	2500	
2934	2934	2696	
	2981		
3418	3418		

The other method for calculation of correction functions used certified spectroscopic standards which emit broadband fluorescence spectra when excited with a specified laser wavelength. The fluorescence spectra of the standards have been calibrated by National Institute of Standards and Technology (NIST) through the use absolutely calibrated white-light source and described by mathematical expressions [24, 25]. Spectra of the appropriate reference sample were repeatedly measured (under same experimental conditions as in the case of the studied systems), and a correction function was calculated as a ratio of the acquired spectrum and the certified defined curve. However, only official standards for spectral corrections for the excitation wavelengths 532, 633, 785 and 830 nm were available from NIST at present, of which only the first two were obtained at the time of experiments. Therefore, corrections for the remaining excitations, i. e. 647, 785 and 830 nm, were carried out by employing the firstly outlined procedure based on a mixture of water, deuterated water, ethanol and acetone. That is, the spectra were firstly corrected to the 633 nm excitation, and then correction to the certified standard for 633 nm was applied.

Original and corrected spectra of the calibration mixture of water, deuterated water, ethanol and aceton are shown in Figs. 3.1 and 3.2, respectively. Final correction factors for all excitation wavelengths may be found in the Supplement, Fig. S6, as well as spectra of the certified fluorescence standards, Fig. S2, and measured and corrected spectra of polystyrene, Figs. S9 and S10.

In addition, it shall be noted that the two remaining certified fluorescence standards, i. e. those for excitation wavelengths 785 and 830 nm, were obtained after the collection, treatment and interpretation of acquired data. Nevertheless, their both measured and certified spectra (from Refs. [26] and [27]) are included in the Supplement (Fig. S2), as well as graphs of the calculated correction functions, Fig. S3. Corrected spectra of the calibration mixture of water, deuterated water, ethanol and acetone are also included for comparison, Figs. S4, S7 and S8. However, since calibration of the apparatus, though crucial for appropriate interpretation of collected data, is not among the principal objectives of the hereby presented study, this subject is not discussed here further.

Raman spectra acquired using WITec alpha300 presented hereafter were corrected in terms of both wavenumber and intensity calibrations unless explicitly stated otherwise.

Table 3.3: Wavenumbers of Hg and Ar emission lines from [23], $\tilde{\nu}$(NIST), and their position in spectra measured at 531.994 nm, $\Delta\tilde{\nu}(532)$, 632.847 nm, $\Delta\tilde{\nu}(633)$, 647.125 nm, $\Delta\tilde{\nu}(647)$, 784.793 nm, $\Delta\tilde{\nu}(785)$, and 830.042 nm excitation, $\Delta\tilde{\nu}(830)$.

$\tilde{\nu}$(NIST) (cm^{-1})	$\Delta\tilde{\nu}(532)$ (cm^{-1})	$\Delta\tilde{\nu}(633)$ (cm^{-1})	$\Delta\tilde{\nu}(647)$ (cm^{-1})	$\Delta\tilde{\nu}(785)$ (cm^{-1})	$\Delta\tilde{\nu}(830)$ (cm^{-1})
18307.4	489.8	-	-	-	-
17327.3	1469.8	-	-	-	-
17264.3	1532.8	-	-	-	-
16909.8	1887.4	-	-	-	-
16573.3	2223.9	-	-	-	-
16348.9	2448.3	-	-	-	-
14804.5	-	997.1	648.5	-	-
14473.1	-	1328.5	979.9	-	-
14352.7	-	1449.0	1100.3	-	-
14220.3	-	1581.3	1232.6	-	-
14145.9	-	1655.7	1307.0	-	-
13987.9	-	1813.7	1465.0	-	-
13745.8	-	2055.8	1707.1	-	-
13560.9	-	2240.7	1892.1	-	-
13539.1	-	2262.5	1913.9	-	-
13322.8	-	2478.8	2130.2	-	-
13303.7	-	2497.9	2149.3	-	-
13093.8	-	2707.8	2359.2	-	-
12942.8	-	2858.9	2510.2	-	-
12578.0	-	3223.6	2874.9	-	-
12487.0	-	3314.7	2966.0	-	-
12473.5	-	3328.1	2979.5	-	-
12336.7	-	3464.9	3116.3	405.6	-
12319.0	-	3482.6	3134.0	423.2	-
12096.6	-	3705.0	3356.4	645.6	-
11889.9	-	3911.7	3563.1	852.3	-
11866.7	-	3934.9	3586.3	875.5	-
11731.9	-	-	3721.1	1010.3	-
11533.6	-	-	3919.4	1208.6	514.0
10958.3	-	-	-	1783.9	1089.2
10837.7	-	-	-	1904.5	1209.9
10687.4	-	-	-	2054.8	1360.2
10351.5	-	-	-	2390.7	1696.1
10217.4	-	-	-	2524.8	1830.1

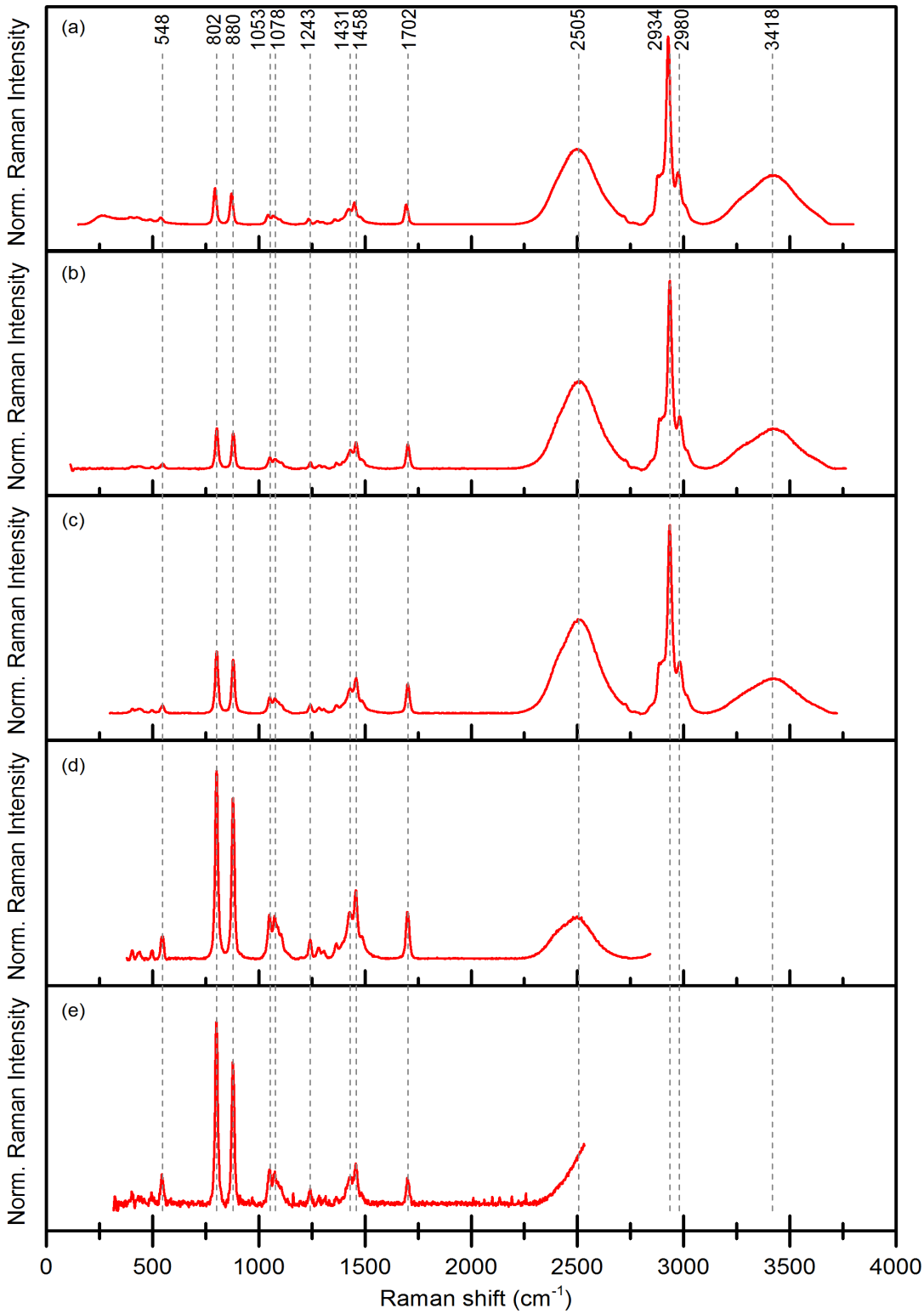

Figure 3.1: Raman spectra of the calibration mixture at five excitation wavelengths prior to intensity correction. Normalized to unity at maximum and baseline corrected. (a) 532 nm, (b) 633 nm, (c) 647 nm, (d) 785 nm, and (e) 830 nm.

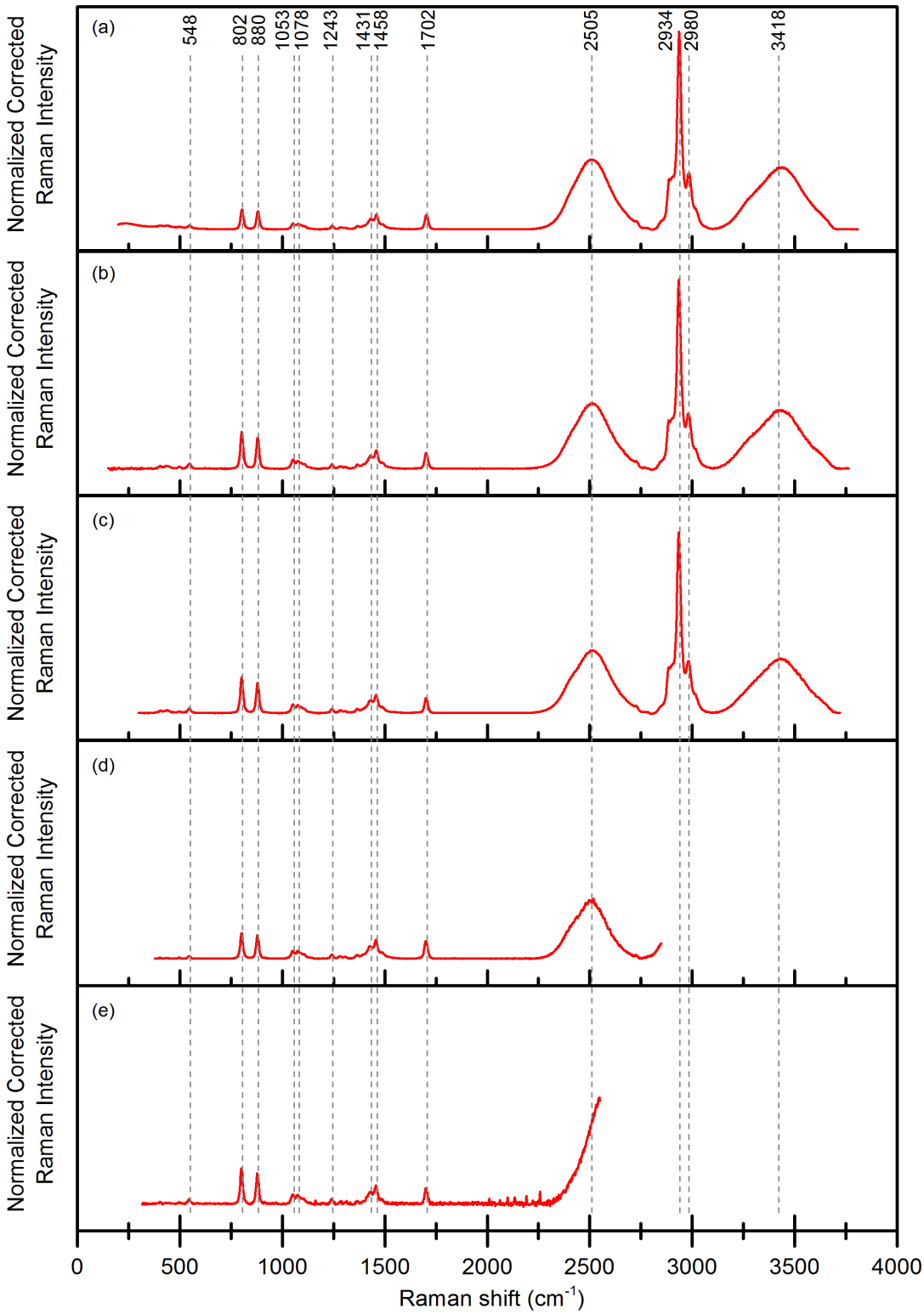

Figure 3.2: Raman spectra of the calibration mixture at five excitation wavelengths after intensity correction. Normalized to 1458 cm^{-1} and baseline corrected. (a) 532 nm, (b) 633 nm, (c) 647 nm, (d) 785 nm, and (e) 830 nm.

4. Results and Discussion

4.1 Electronic Absorption Spectra of H_2Pc and of Glass/SLG/H_2Pc Hybrid System

Electronic absorption spectra in UV-Vis region were obtained for saturated solution of H_2Pc in toluene and for glass/SLG/H_2Pc-I hybrid system, and are presented in Figs. 4.1 and 4.2, respectively. The former exhibits two maxima at 693 (Q_x) and 656 nm (Q_y) accompanied with two lower bands at 594 and 639 nm with shoulder to 627 nm. In case of glass/SLG/H_2Pc-I hybrid system, the two maxima appear at 718 (Q_x) and 693 nm (Q_y) with a vibronic sideband at about 630 nm. The absorption spectrum is red-shifted for both Q-bands when compared to those of isolated molecules in toluene (by 25 and 37 nm for the respective Q-bands), in chloronaphthalene (by 21 and 31 nm) [14], in a-supersonic free jet (by 57 and 94 nm) [28], in isolation matrices (by 48 and 66 nm, and 687 and 646 nm for neon and xenon matrices, respectively) [29], and also to that of a H_2Pc-doped polyphenylsiloxane film (by 16 and 27 nm) [14]. In addition, it does not match any of the electronic absorption spectra of various H_2Pc crystalline forms which are discussed in Ref. [30]. Furthermore, the width of the Q_x and Q_y splitting decreases to only 25 nm in comparison to the splitting of the above mentioned systems. On the other hand, Ref. [16] presents Raman scattering-excitation profile spectra of H_2Pc molecule adsorbed on silver surface, and the maxima appear at 692 and 674 nm with only 18 nm splitting.

It was also attempted to collect electronic absorption spectra of glass/H_2Pc (as a part of the glass/SLG/H_2Pc-I hybrid system). However, no bands were observed, therefore it is reasonable to assume that no or too few H_2Pc molecules adsorbed directly on the glass substrate. Due to these reasons, the spectra are not shown in this study.

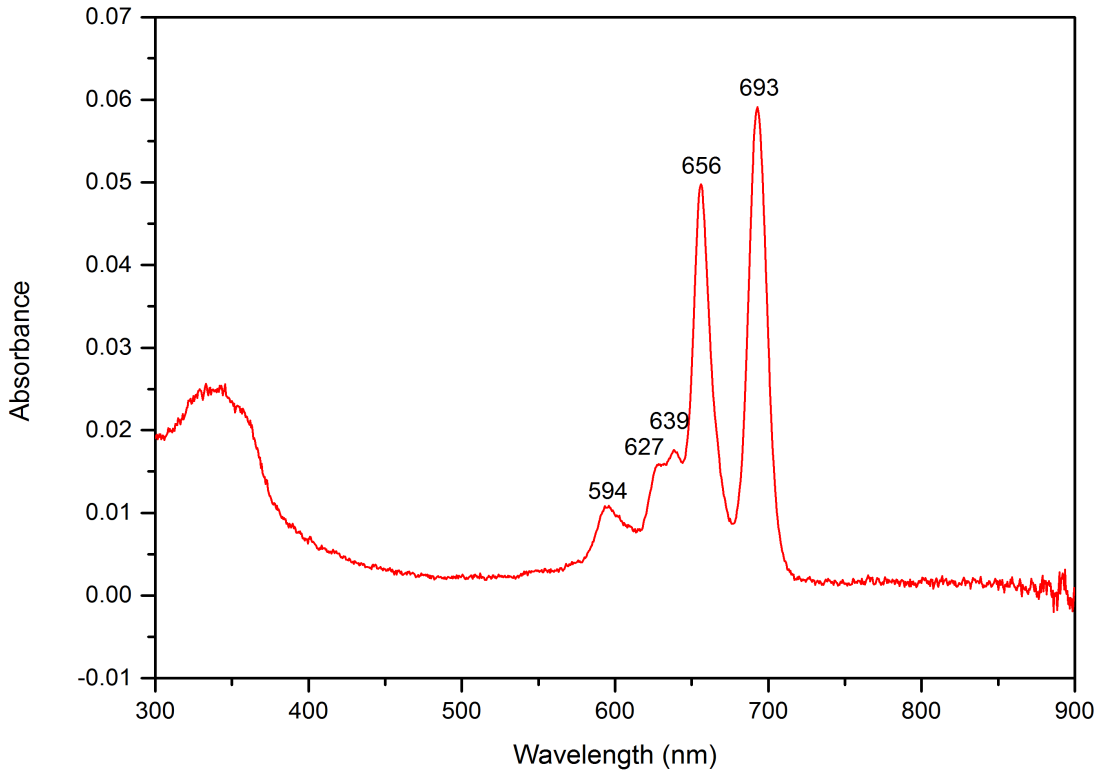

Figure 4.1: Electronic absorption spectrum of saturated solution of H_2Pc in toluene.

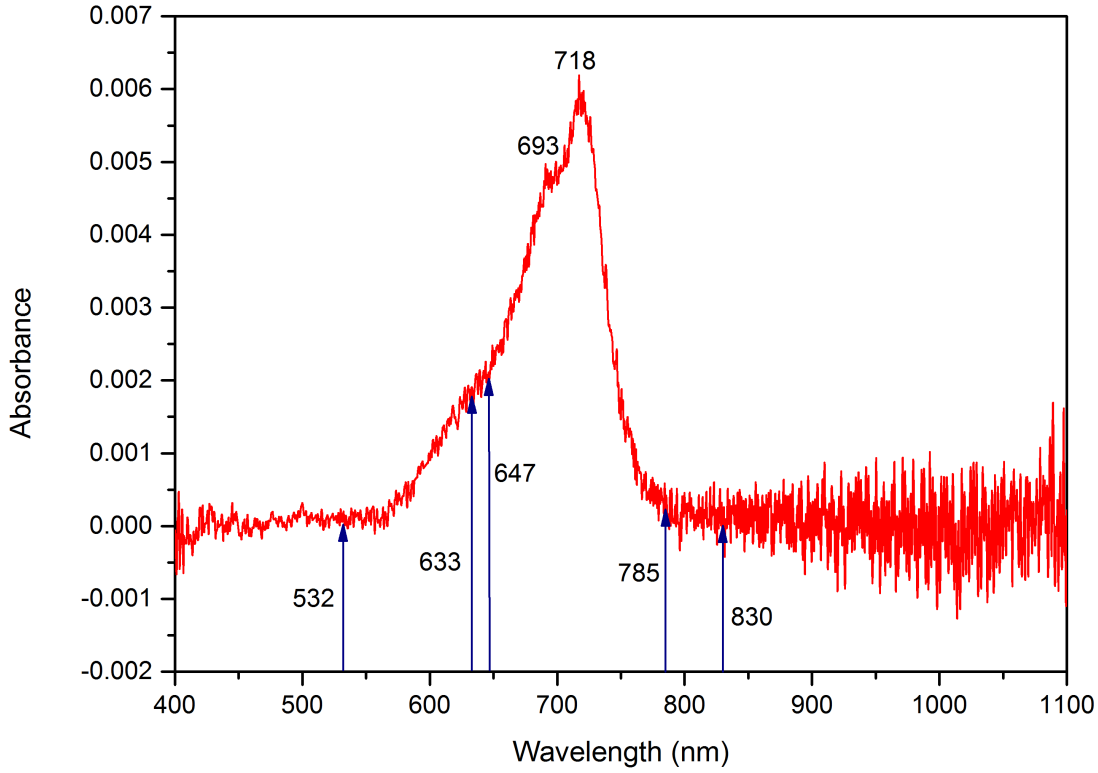

Figure 4.2: Electronic absorption spectrum of glass/SLG/H_2Pc hybrid system (baseline corrected), and projections of the excitation wavelengths for Raman measurements.

4.2 Acquisition, Evaluation and Interpretation of Excitation Wavelength-Dependent Raman Spectra of Glass/SLG/H_2Pc Hybrid Systems and of Selected Reference Systems

4.2.1 Micro-Raman Spectral Mapping of Selected 2D Systems

Systems investigated in this study require special care due to their extraordinary thinness. Especially in the case of SLG, the sample is as thick as one-carbon-atom layer. Therefore, measurements were carried out in a micro-Raman setup and areas of 25μm-by-25μm in size were mapped to acquire spectra with a better signal-to-noise ratio, as described in the preceding chapter in detail. In addition, scanning of an area allowed for inspecting the homogeneity of the samples.

Two sets of measurements of glass/SLG/H_2Pc-I hybrid system will be presented shortly to underline the significance and illustrate the process of collecting Raman spectra over a region, namely of those acquired at 633 and 830 nm excitations. A map of a defected SLG on glass will follow to demonstrate the application of spectral scanning, especially as a tool for scrutinizing the sample structure.

The 830 nm excitation wavelength was considered first, and its characteristics apply also to other off-resonance spectra of glass/SLG/H_2Pc systems (i. e. 532 and 785 nm), and resonance spectra of HOPG/H_2Pc (i. e. 633 and 647 nm), as well as to glass/SLG measurements. Fig. 4.3 shows a single spectrum from a randomly selected point in the scanned area, a spectrum obtained as an average of 9 single spectra, and eventually an average spectrum from the entire region. These spectra clearly illustrate the rapidly increasing signal-to-noise ratio with the increasing number of spectra. Figures displaying intensity distribution of selected bands over the scanned area are not presented in case of this excitation wavelength for little illustrativeness due to high noise.

In the case of 633 nm excitation wavelength, resonant for H_2Pc, the summation of spectra was not as crucial as in the aforementioned instance since the Raman signal reached intensity of about two orders of magnitude higher. Nevertheless, mapping ensures enables elimination of some possible inhomogeneity effects within the sample, and establishes identical conditions for analysis and comparison of acquired spectra among each other. Fig. 4.5, as in the previous paragraph, shows a random single spectrum, a spectrum created as an average of 9 spectra, and an overall average. Fig. 4.4 illustrates the intensity distribution for selected bands. The overall increasing intensity from upper left corner to the

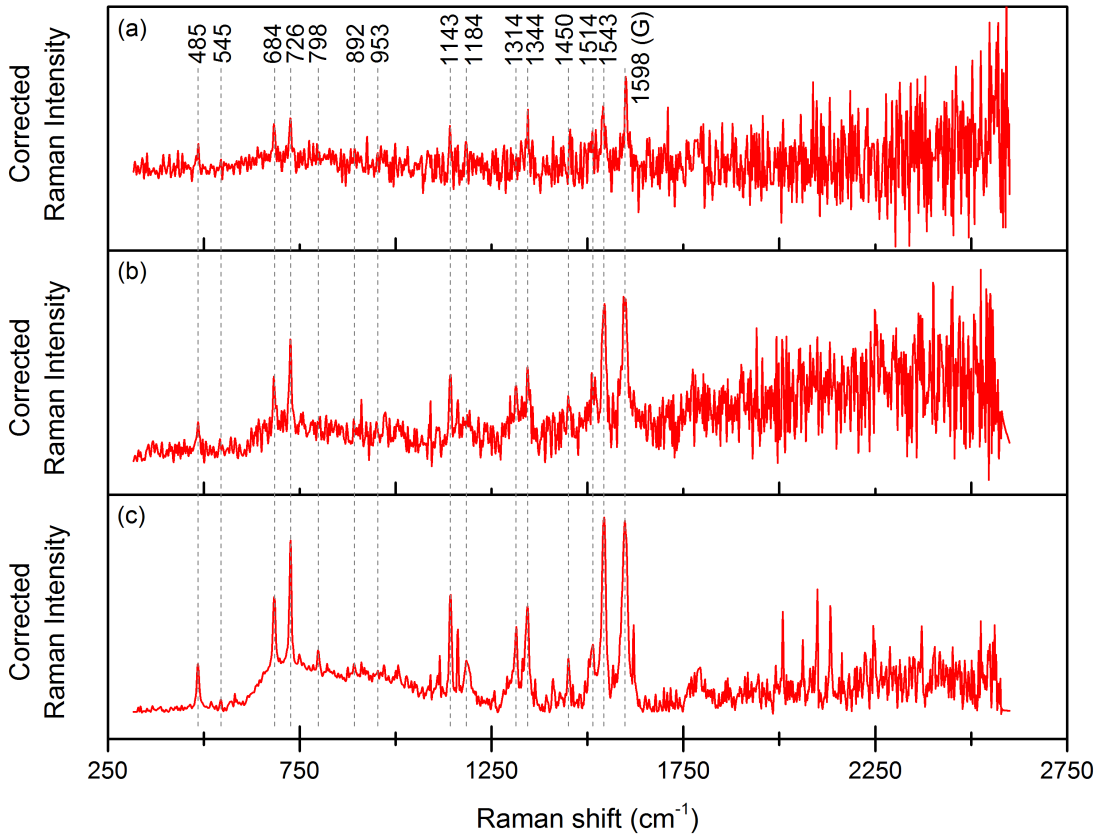

Figure 4.3: Raman spectra of glass/SLG/H_2Pc hybrid system at 830 nm excitation. Spectrum (a) represents a single spectrum from the map, (b) shows an average of 9 spectra, and (c) displays a total average spectrum from the entire scanned area.

bottom right is given by the sample being slightly slanted with respect to the scanning plane. Aside from few defects in graphene which project themselves into H_2Pc spectra, the sample appears to be homogeneous.

Finally, a map of glass/SLG system at the excitation wavelength 647 nm is explored. This area features four different regions: a pristine single-layer graphene, a graphene fold, a graphene multilayer and a region with no graphene. Fig. 4.7 presents Raman spectra from the respective areas, and Fig. 4.6 captures intensity distribution of the G (1597 cm^{-1}) and 2D (2647 cm^{-1}) graphene modes as well as a microscopic picture of the scanned area. It is worth noting that the displayed maps superbly match the optical image of the scrutinized area. Therefore, it was possible to employ the optical images for selection of areas with minimum defects for the actual Raman mapping of the samples.

The above introduced measurement strategy was applied to glass/SLG/H_2Pc-VI and glass/SLG/H_2Pc-X hybrid systems, as well as to HOPG/H_2Pc reference system and glass/SLG system at all excitation wavelengths. The further analyzed spectra of the enumerated systems were obtained as an average from the respective entire mapped area unless otherwise stated.

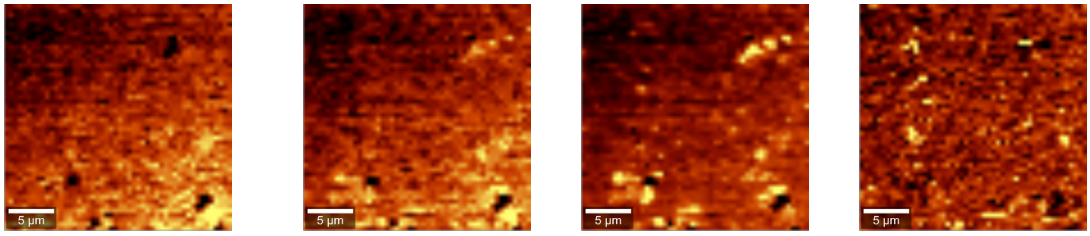

(a) (b) (c) (d)

Figure 4.4: Map of Raman intensity distribution of H_2Pc modes at (a) 726 cm^{-1}, (b) 1143 cm^{-1} and (c) 1544 cm^{-1}, and of (d) graphene G mode (1595 cm^{-1}) at the excitation wavelength 633 nm. The brighter parts indicated stronger signal, however, the overall increasing intensity from the left upper corner towards the opposite results from the sample being slanted with respect to the scanning plane.

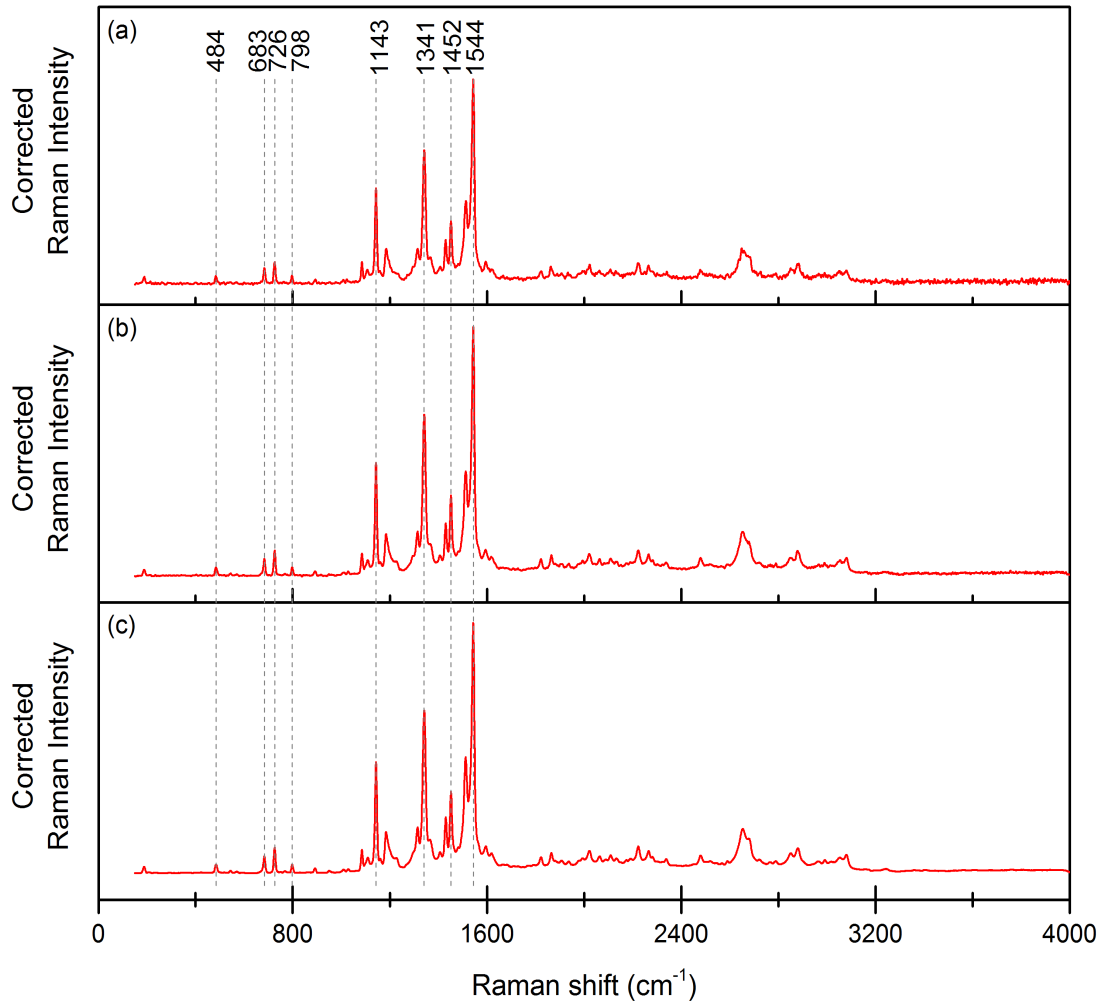

Figure 4.5: Raman spectra of glass/SLG/H_2Pc hybrid system at 633 nm excitation. Spectrum (a) represents a single spectrum from the map, (b) shows an average of 9 spectra, and (c) displays a total average spectrum from the entire scanned area. (baseline corrected)

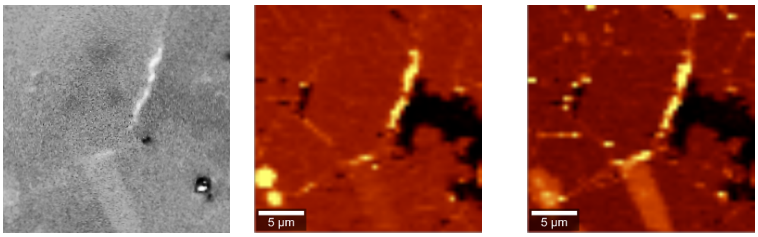

(a) (b) (c)

Figure 4.6: A microscopic image of the scanned area (contrast has been modified to highlight the different regions). Maps of Raman intensity distribution of (b) G (1597 cm^{-1}) and (c) 2D (2647 cm^{-1}) graphene modes at the excitation wavelength 647 nm. The brighter areas correspond to multiple layers and folds of graphene, while no graphene is present where black.

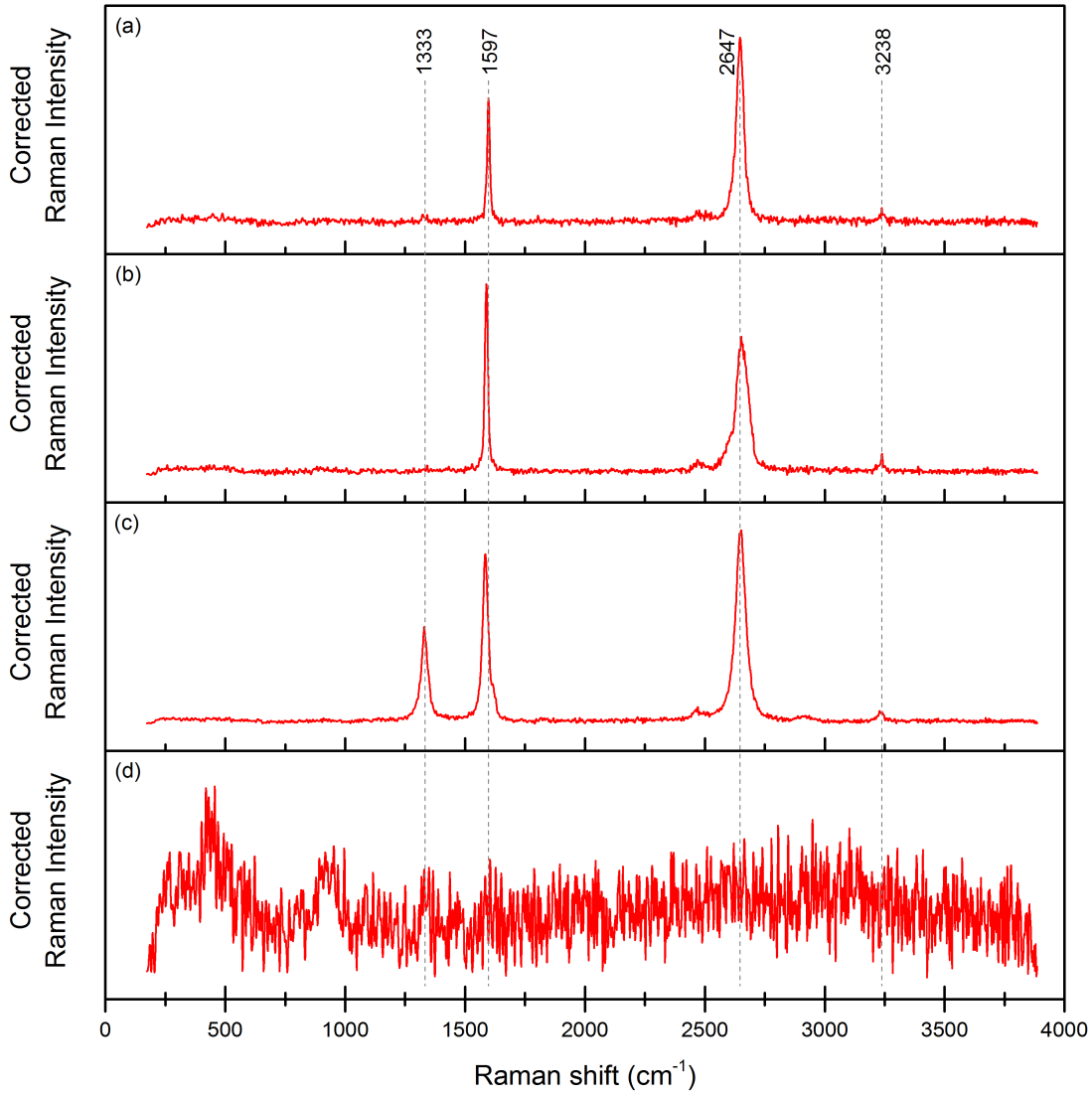

Figure 4.7: Raman spectra from a mapped area of (a) pristine SLG, (b) multilayer graphene, (c) a graphene fold, and (d) an area with no graphene. (single spectra, baseline corrected)

4.2.2 Selected Reference Systems

HOPG/H_2Pc Systems

HOPG was selected as a reference for calculations of GERS enhancement factors owing to its similarity to SLG. It is constituted of an immense number of stacked graphene layers which ensures same adsorption characteristics as SLG and simultaneously, it takes advantage of the fact that the enhancement caused by graphene diminishes with increasing number of graphene layers [1]. However, the surface of HOPG is more flat than that of the glass substrate, features of which SLG copies, and therefore a correction is essential prior to calculations of GERS enhancement factors. This coefficient has been ascertained to equal 1.34 [31]. The preparation of HOPG/H_2Pc systems and measurements of Raman spectra were carried out the other samples alike, as described in the Experimental Chapter. Acquired spectra are presented later in Chapter 4.2.8, Figs. 4.33 and 4.34, and in the Supplement, Figs. S11 and S12.

Polystyrene

Raman spectrum of polystyrene features numerous distinct bands, intensity and position of which are independent of the excitation wavelength (except for the ν^4-dependence of scattered radiation intensity common to all Raman spectra). On that account, it was chosen as an external standard for intensity normalization of phthalocyanine bands. Spectra of polystyrene measured at the five excitation wavelengths of interest, i. e. 532, 633, 647, 785 and 830 nm, may be found in the Supplement, Figs. S9 and S10.

Glass/SLG System

Apart from the above described reference systems, Raman spectra of glass/SLG system were also obtained for evaluation of changes upon formation of the hybrid systems, and are presented in Fig. 4.21 (Chapter 4.2.4).

Glass/H_2Pc System

Glass/H_2Pc system, as a part of the glass/SLG/H_2Pc samples and hence undergoing the very same procedure as the main system of interest, was also considered as a reference. However, neither Raman nor electronic absorption spectra indicated the presence of a detectable amount of H_2Pc on glass.

H_2Pc in Crystalline Form

Raman spectra of crystalline H_2Pc (β-form) were attempted to be acquired at all five excitation wavelengths. However, due to the strong fluorescence of H_2Pc at 633, 647, 785, and 830 nm excitations, spectrum was collected only at the off-resonance 532 nm excitation. Fig. 4.8 presents the Raman spectrum which, however, rather resembles that of the α-polymorph than that of the β-form presented in Ref. [32], although β-H_2Pc had been purchased. Gradual conversion of the original β- to the α-form may have occurred due to higher stability of the latter [33].

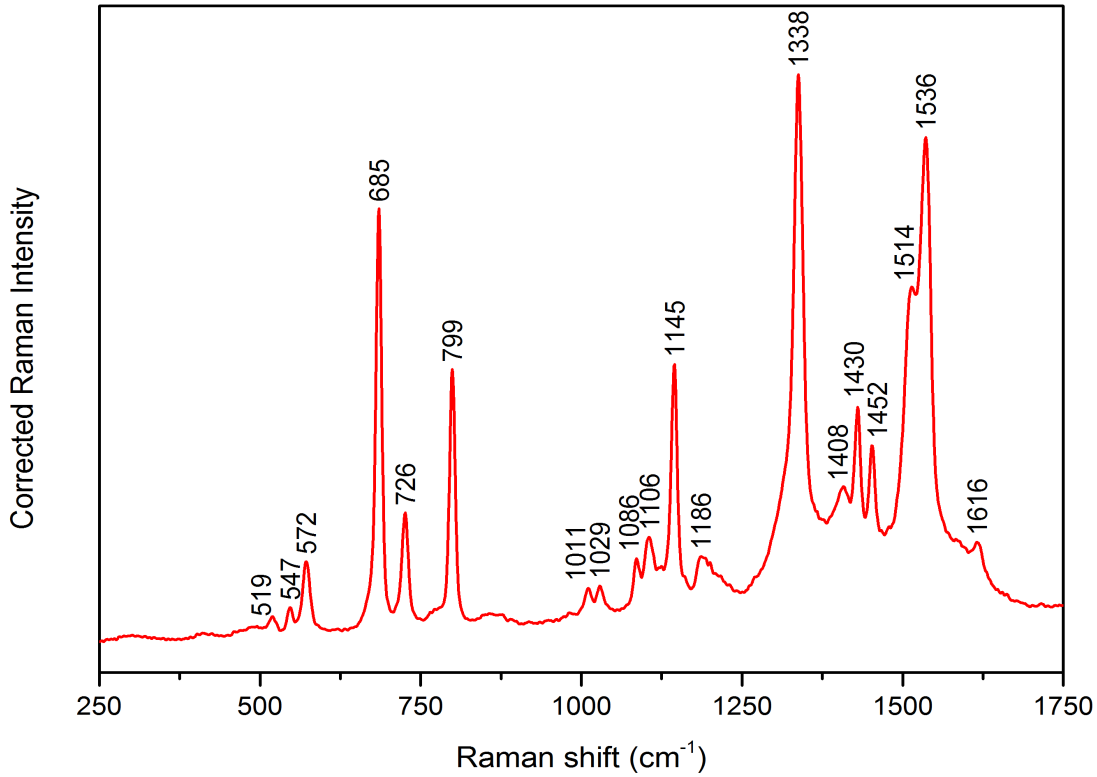

Figure 4.8: Raman spectrum of H_2Pc in crystalline form at 532 nm excitation.

4.2.3 Excitation-Wavelength Dependence and Mutual Comparison of Raman Spectra of Glass/SLG/H_2Pc Hybrid Systems

Raman spectra of all three glass/SLG/H_2Pc hybrid systems were obtained under identical experimental conditions as stated earlier, and are presented in Figs. 4.10-4.20. Figs. 4.10-4.14 show entire spectra of the three discussed systems at individual excitation wavelengths, while Figs. 4.15-4.20 offer closer views of the relevant regions at lower wavenumbers of each system, as well as contain a more detailed labeling of observed bands.

According electronic absorption spectra of both H_2Pc and glass/SLG/H_2Pc (Fig. 4.2), the excitation wavelength 532 nm is non-resonant, and hence could serve for determination of the ratios of the number of H_2Pc molecules in the respective systems. Selected H_2Pc Raman spectral bands for comparison are presented in Tab. 4.1, as well as the corresponding intensity ratios. [1] Both Raman spectra (Fig. 4.10) and numerical data (Tab. 4.1) indicate that the system glass/SLG/H_2Pc comprises rather a multilayer (probably a bilayer) of H_2Pc molecules on SLG, and its electronic absorption spectrum (Fig. 4.2) supports this idea. Formation of a partial bilayer of H_2Pc molecules on HOPG was observed by scanning tunneling microscopy [34], and the possibility of formation of slightly slipped H_2Pc molecules (Fig. 4.9, in case of porhyrins, this ordering is known as J-type dimers and exhibits a red shift in their electronic absorption bands with respect to those of monomers) was considered. The slipped dimer geometry was found to be the most stable one in Ref. [35], and the red-shift of the Q absorption band was observed also upon aggregation of zinc-phthalocyanine molecules during argon matrix preparation [36].

Table 4.1: Intensity ratios of selected H_2Pc bands of glass/SLG/H_2Pc hybrid systems at the excitation wavelength 532 nm. Intensity ratios, R, of the glass/SLG/H_2Pc-VI and glass/SLG/H_2Pc-X to the glass/SLG/H_2Pc-I bands are distinguished with the appropriate roman numeral in parenthesis.

Raman shift (cm^{-1})	R(VI)	R(X)
685	3.0	2.0
727	2.4	2.4
800	2.6	2.9
1145	1.8	1.3
1453	1.9	1.9

[1] Unfortunately, the mode at around 1344 cm^{-1}, though of relatively high intensity, could not be chosen for numerical evaluation due to the contribution of the close-lying dispersive SLG G-mode.

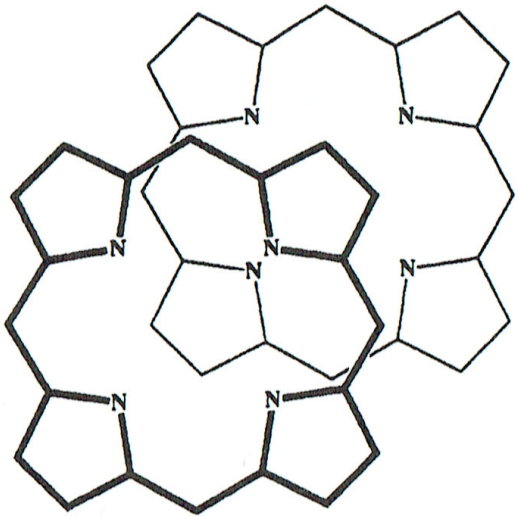

Figure 4.9: A scheme illustrating the mutual position of two porphyrin molecules upon creation of a J-type dimer. Adopted from Ref. [35]

On the other hand, the samples glass/SLG/H_2Pc-VI and glass/SLG/H_2Pc-X appear to be constituted by a monolayer of H_2Pc as the respective Raman intensities are lower in comparison to those of the glass/SLG/H_2Pc-I hybrid system but do not differ significantly when contrasted with each other. Furthermore, individual bands vary in their relative intensities and some of them are visible much more distinctively particularly in comparison to the glass/SLG/H_2Pc-I hybrid system, especially those at 752, 958, 1219 and 1534 cm^{-1}. These new bands were compared to those of toluene, benzylalcohol (which may arise via a reaction occuring upon prolonged exposure of graphene to toluene [37]), and polymethylmetacrylate (used for transferring of graphene during the SLG preparation), however, none yielded a positive result. The observation could be explained by reorganization of the H_2Pc molecules on the SLG surface upon extended washing with toluene so as the individual molecules adopt more favorable positions and intensify their interaction with SLG. Especially the two bands at 1534 and 1545 cm^{-1} appear to be highly sensitive to the form of H_2Pc and to its surrounding environment, and are yet to be fully understood. As of now, their origin in the glass/SLG/H_2Pc hybrid systems may be only ascribed to the probable interaction with graphene.

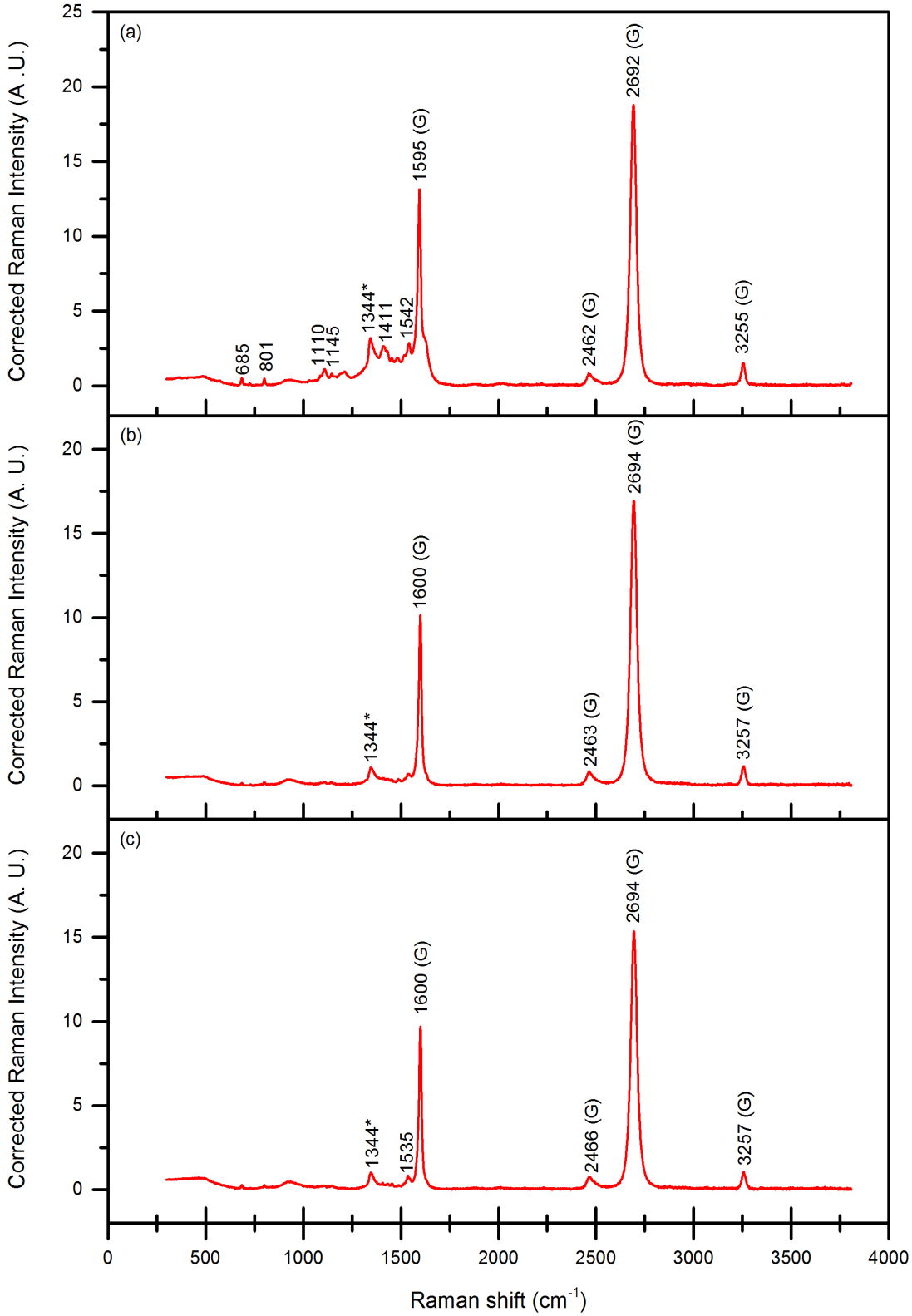

Figure 4.10: Raman spectra glass/SLG/H_2Pc hybrid systems at excitation wavelength 532 nm (baseline corrected): (a) glass/SLG/H_2Pc-I, (b) glass/SLG/H_2Pc-VI, and (c) glass/SLG/H_2Pc-X. Graphene bands are marked (G).
*The band at 1344 cm^{-1} is an overlap of H_2Pc and graphene bands.

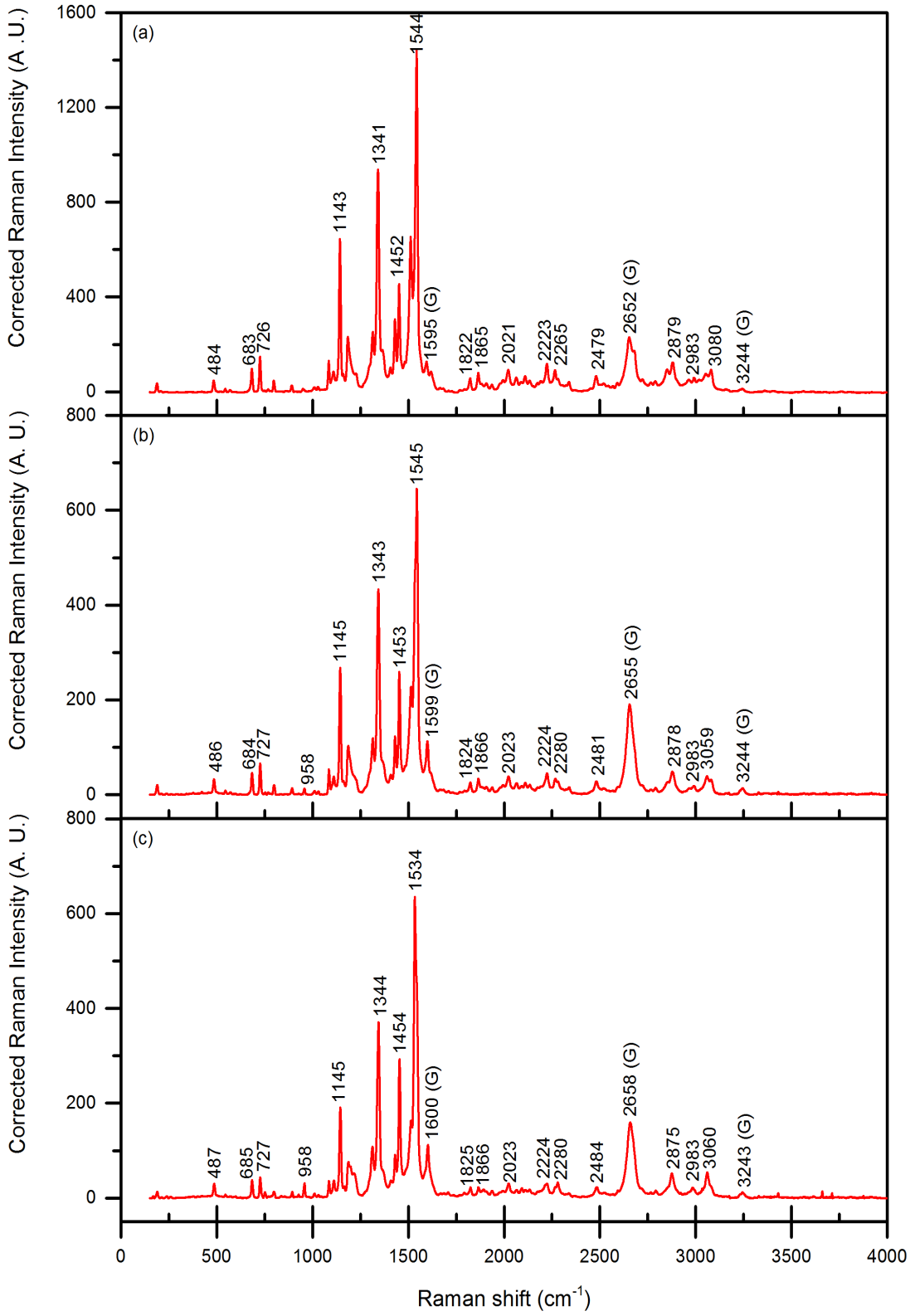

Figure 4.11: Raman spectra glass/SLG/H_2Pc hybrid systems at excitation wavelength 633 nm (baseline corrected): (a) glass/SLG/H_2Pc-I, (b) glass/SLG/H_2Pc-VI, and (c) glass/SLG/H_2Pc-X. Graphene bands are marked (G).

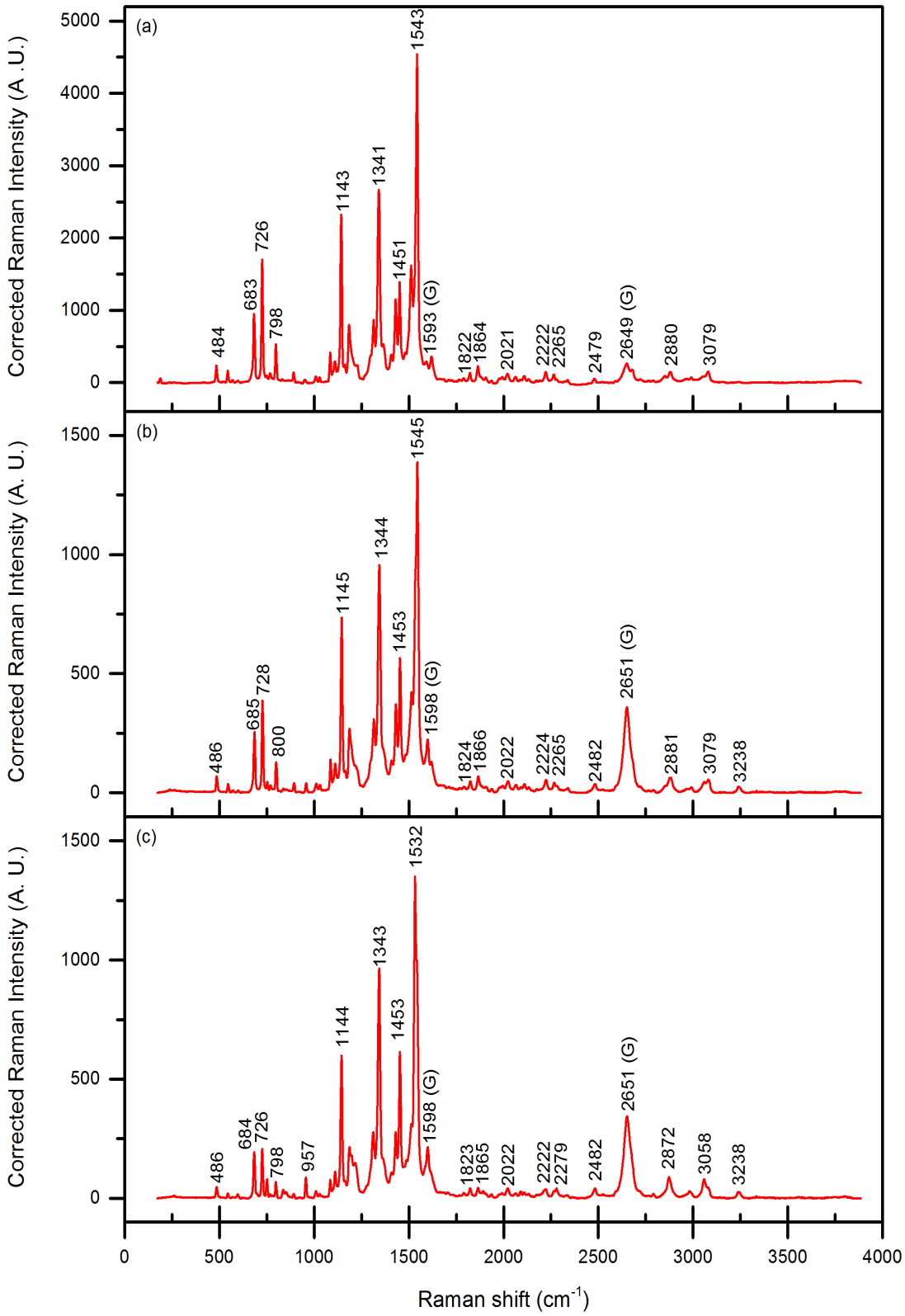

Figure 4.12: Raman spectra glass/SLG/H_2Pc hybrid systems at excitation wavelength 647 nm (baseline corrected): (a) glass/SLG/H_2Pc-I, (b) glass/SLG/H_2Pc-VI, and (c) glass/SLG/H_2Pc-X. Graphene bands are marked (G).

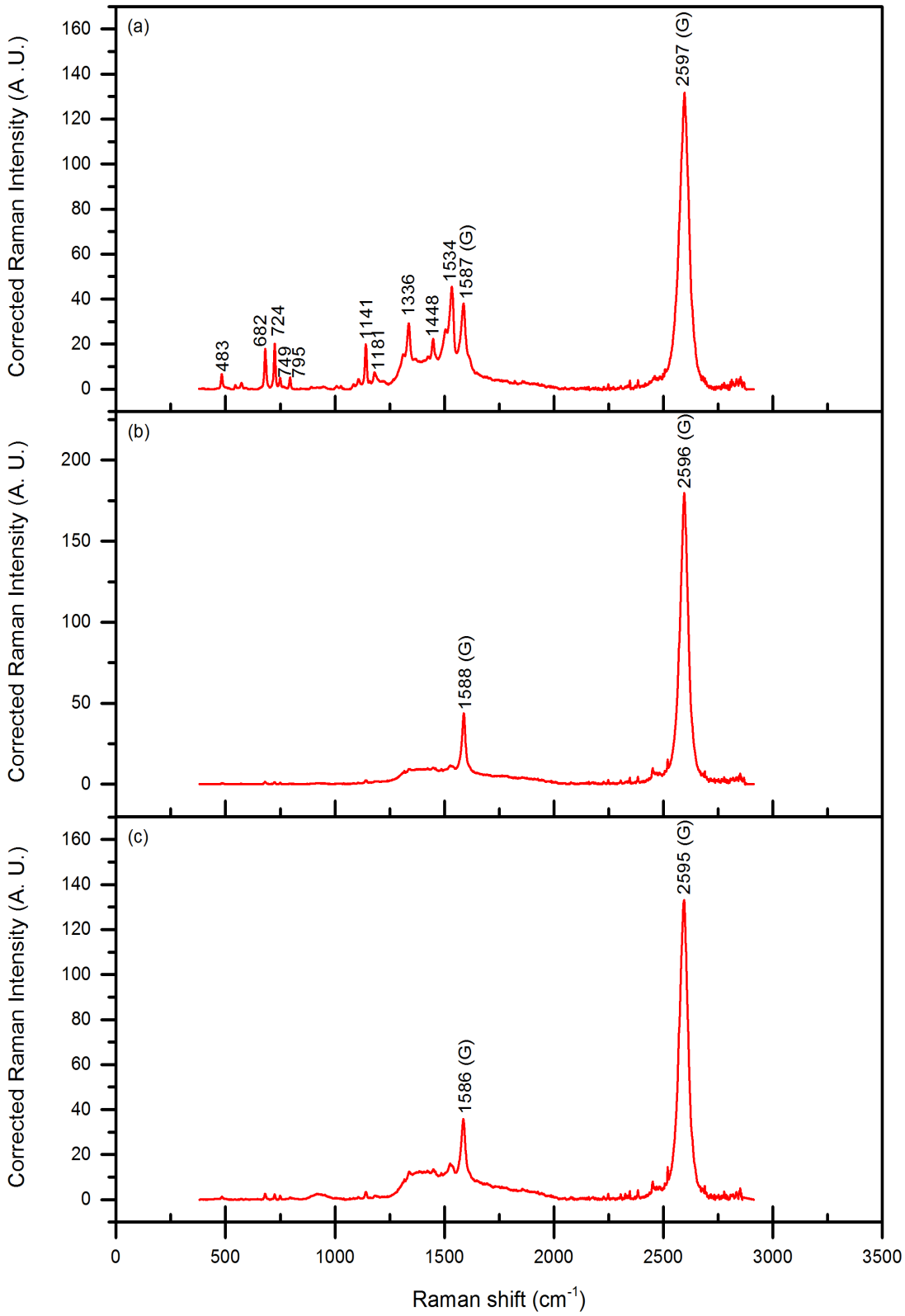

Figure 4.13: Raman spectra glass/SLG/H_2Pc hybrid systems at excitation wavelength 785 nm (baseline corrected): (a) glass/SLG/H_2Pc-I, (b) glass/SLG/H_2Pc-VI, and (c) glass/SLG/H_2Pc-X. Graphene bands are marked (G).

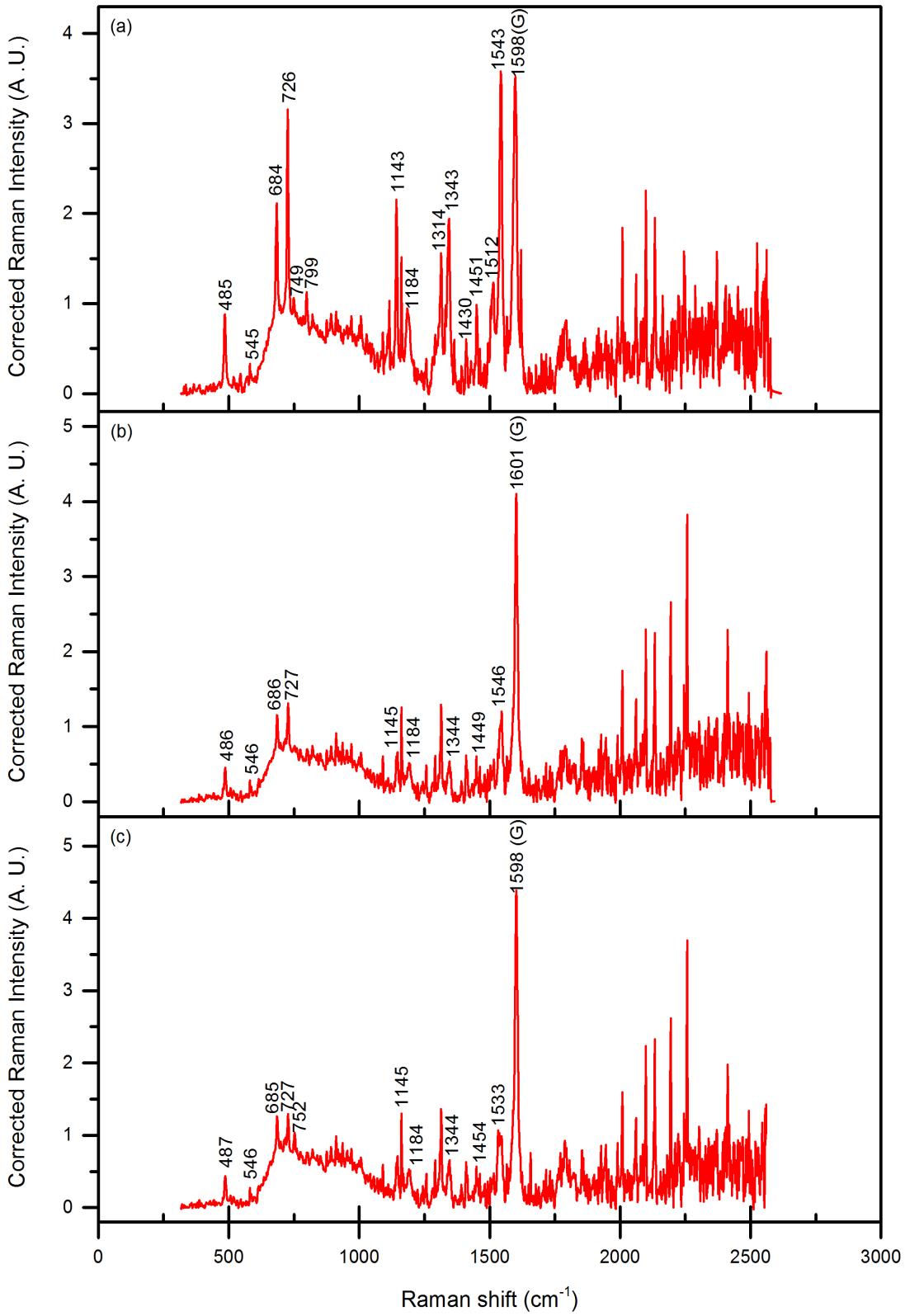

Figure 4.14: Raman spectra glass/SLG/H_2Pc hybrid systems at excitation wavelength 830 nm (baseline corrected): (a) glass/SLG/H_2Pc-I, (b) glass/SLG/H_2Pc-VI, and (c) glass/SLG/H_2Pc-X. Graphene bands are marked (G).

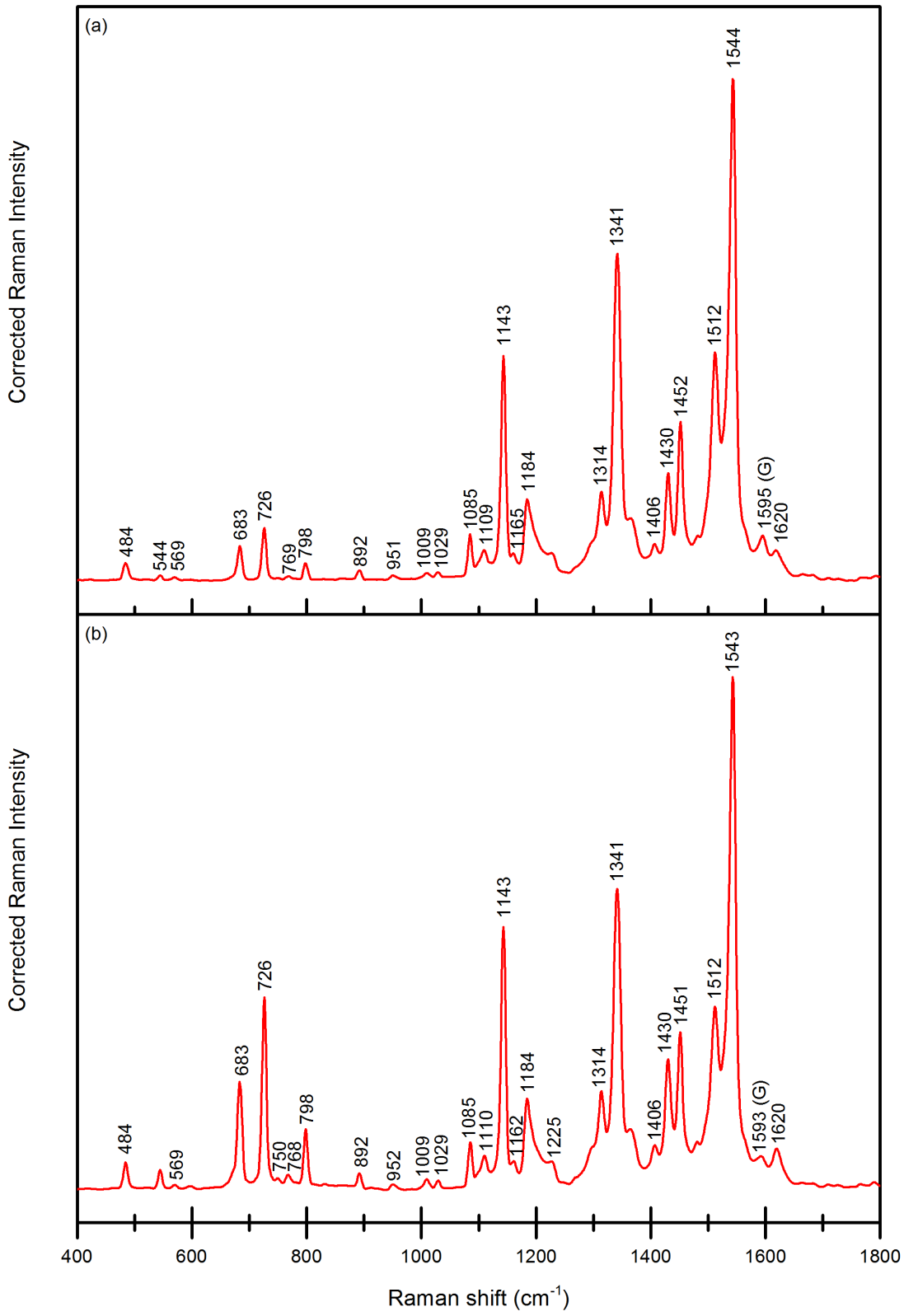

Figure 4.15: Enlarged regions of Raman spectra of glass/SLG/H_2Pc-I hybrid system at excitation wavelengths (a) 633 and (b) 647 nm (baseline corrected). Graphene bands are marked (G).

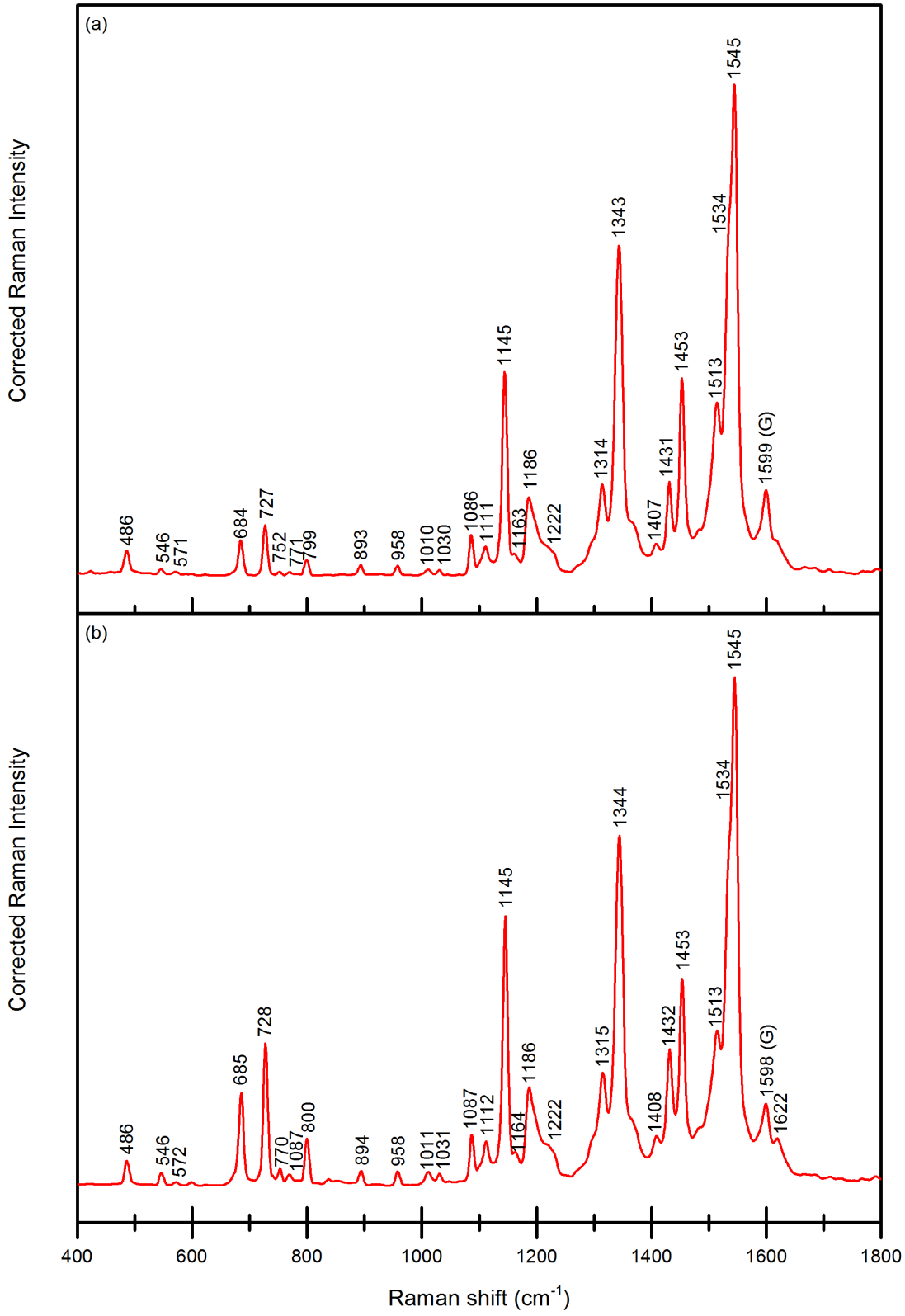

Figure 4.16: Enlarged regions of Raman spectra of glass/SLG/H_2Pc-VI hybrid system at excitation wavelengths (a) 633 and (b) 647 nm (baseline corrected). Graphene bands are marked (G).

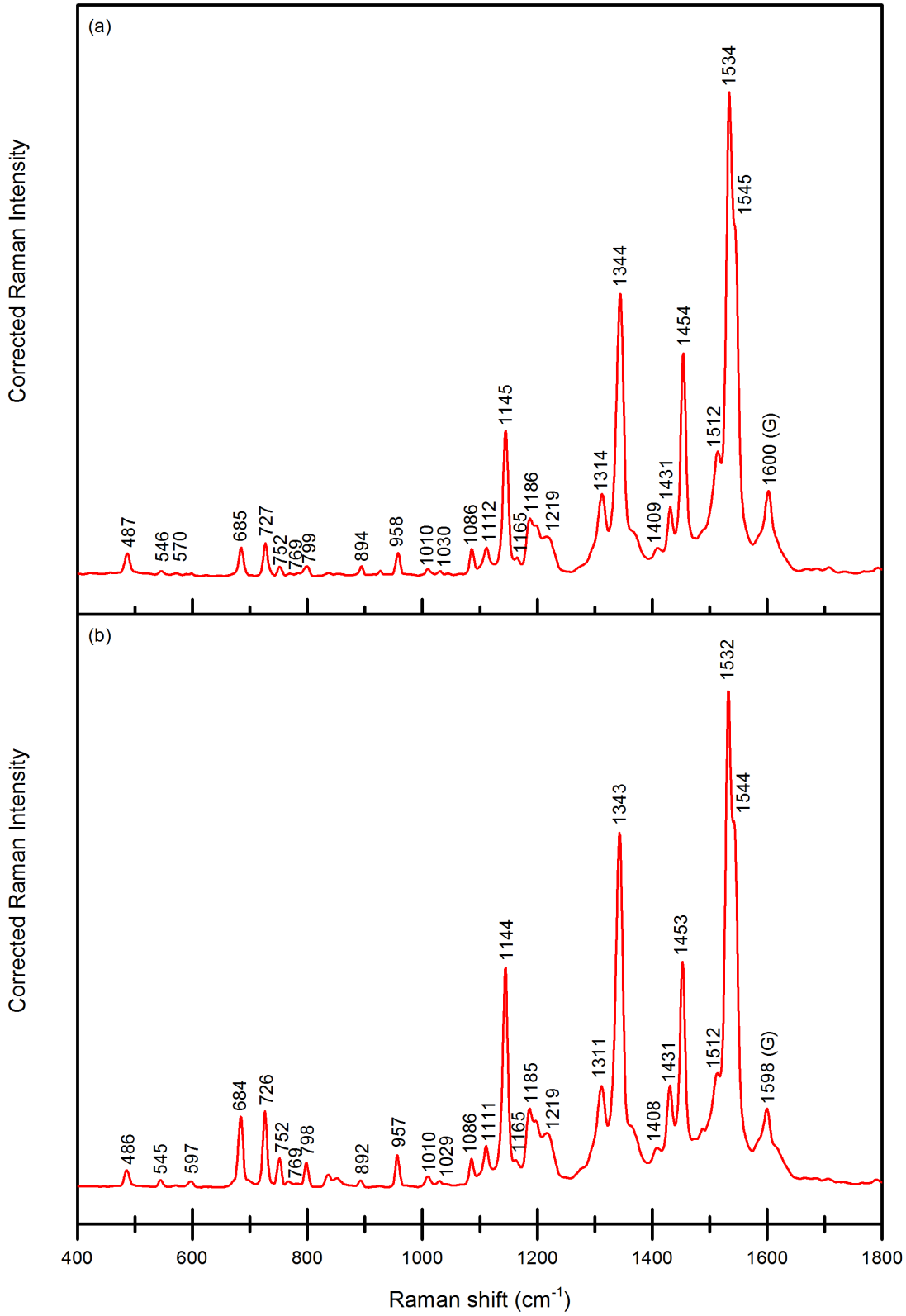

Figure 4.17: Enlarged regions of Raman spectra of glass/SLG/H_2Pc-X hybrid system at excitation wavelengths (a) 633 and (b) 647 nm (baseline corrected). Graphene bands are marked (G).

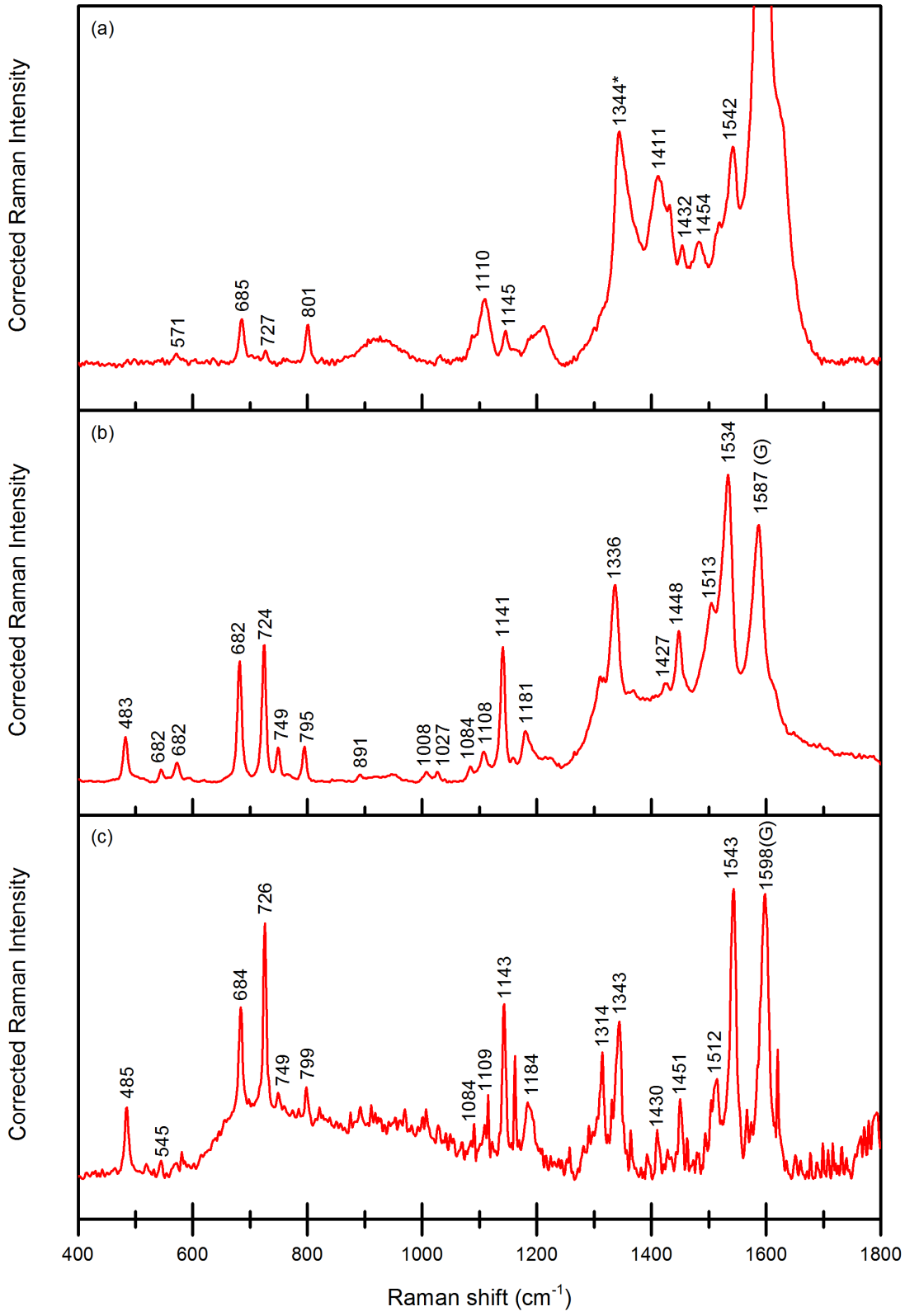

Figure 4.18: Enlarged regions of Raman spectra of glass/SLG/H_2Pc-I hybrid system at excitation wavelengths (a) 532, (b) 785 and (c) 830 nm (baseline corrected). Graphene bands are marked (G).
*The H_2Pc and graphene bands coincide.

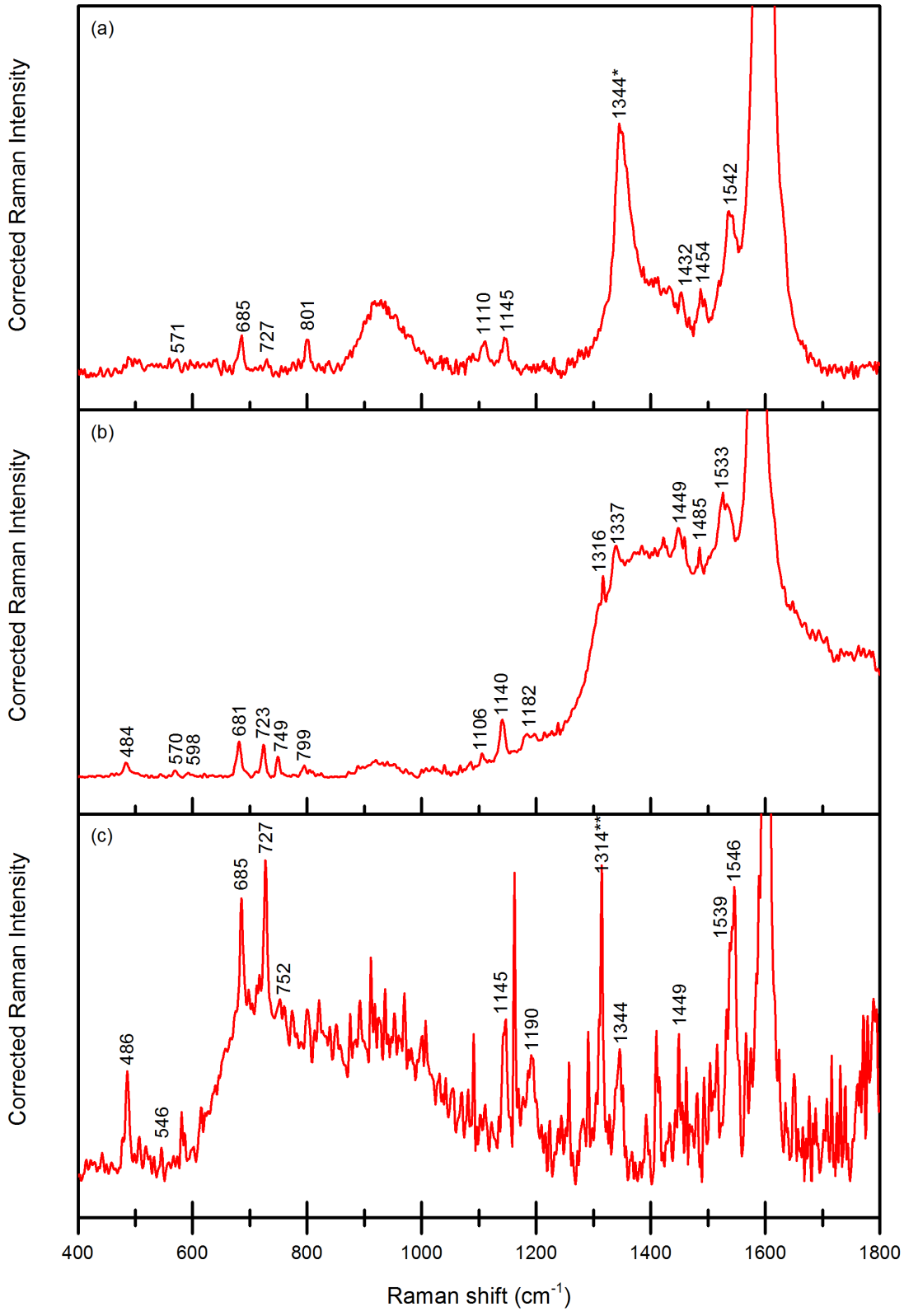

Figure 4.19: Enlarged regions of Raman spectra of glass/SLG/H_2Pc-VI hybrid system at excitation wavelengths (a) 532, (b) 785 and (c) 830 nm (baseline corrected). Graphene bands are marked (G).
*The H_2Pc and graphene bands coincide.

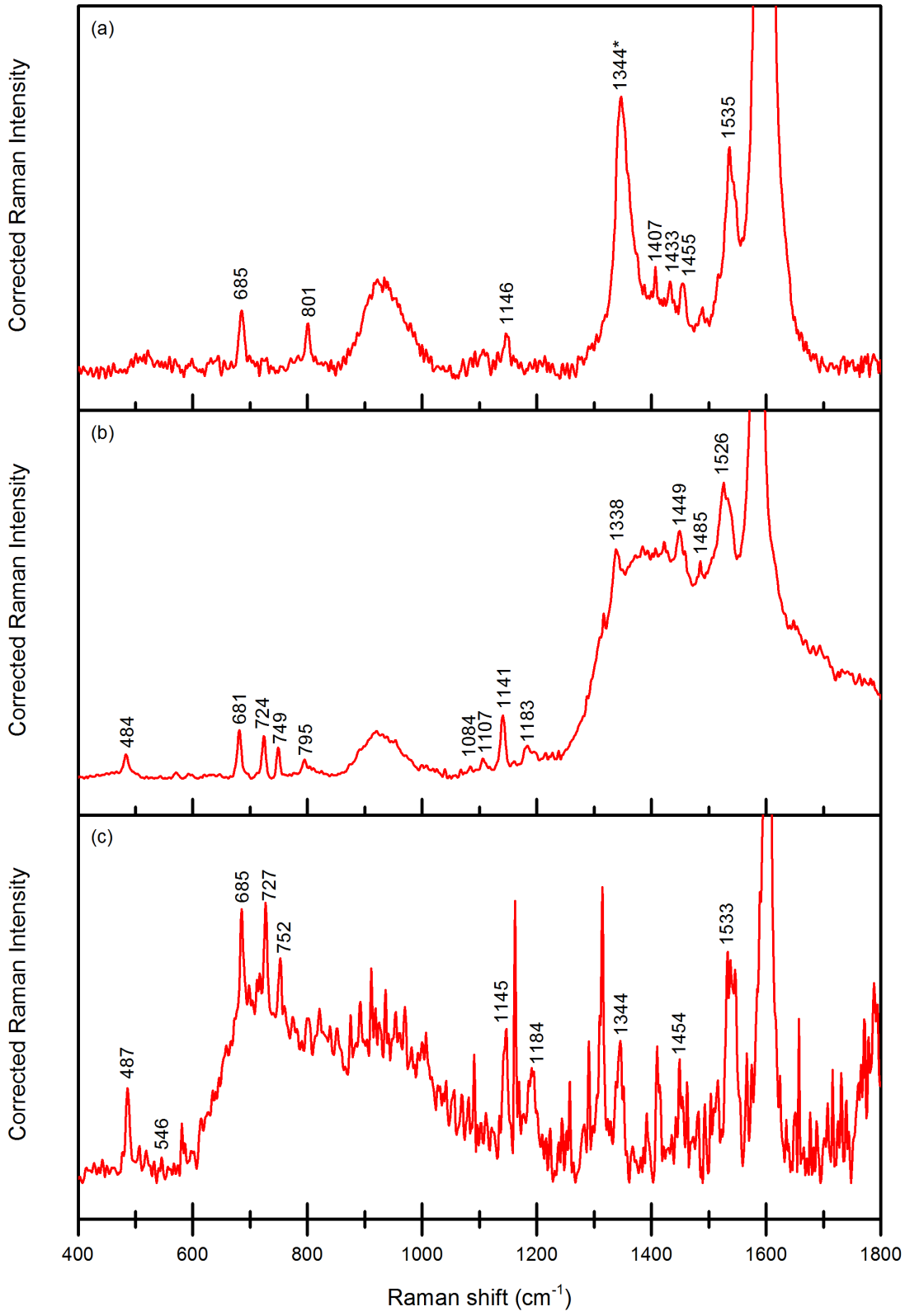

Figure 4.20: Enlarged regions of Raman spectra of glass/SLG/H_2Pc-X hybrid system at excitation wavelengths (a) 532, (b) 785 and (c) 830 nm (baseline corrected). Graphene bands are marked (G).
*The H_2Pc and graphene bands coincide.

4.2.4 Comparison of Raman Spectra of SLG in Glass/SLG and Glass/SLG/H_2Pc Hybrid Systems

Graphene is very sensitive towards its surrounding environment, and doping of graphene may easily take place. Specifically in this study, doping by toluene and glass is of concern. The former may occur upon prolonged exposure to toluene (more than 1 hour) via a reaction yielding benzylalcohol [37], however, bands of neither toluene nor benzylalcohol were observed in any of the spectra. Doping by glass, on the other hand, appears more probable and would explain the relatively high wavenumbers of graphene G-band at 1598-1602 cm^{-1} [38]. Raman spectra of glass/SLG acquired prior to any manipulation with the same are shown in Fig. 4.21.

Tabs. 4.2 and 4.3 summarize Raman shifts of graphene bands in glass/SLG and glass/SLG/H_2Pc systems, respectively. Especially the positions of the G and 2D modes moved to slightly higher values in the latter, though it is questionable whether this minor shift results from interaction between SLG and H_2Pc or falls within experimental error. Tab. 4.4 presents calculated and observed Raman shifts of the dispersive D and 2D modes in glass/SLG system The starting theoretical values were adopted from Refs. [11] and [12], namely Raman shift 1350 cm^{-1} at 2.4 eV (514.5 nm) excitation with dispersion $\simeq$ 50 cm^{-1}/eV for D mode, and Raman shift 2700 cm^{-1} at 2.4 eV (514.5 nm) excitation with dispersion $\simeq$ 100 cm^{-1}/eV for 2D mode. The calculated and observed values differ by 7-8 cm^{-1} for D mode while relatively match for the 2D mode.

Table 4.2: Positions of graphene modes in glass/SLG system at each excitation wavelength.
* G mode was observed at lower values due to glass reflection.

Excitation	Raman shifts of modes (cm^{-1})				
Wavelength (nm)	D	G	D+D"	2D	2D'
532	1354	1598	2462	2692	3255
633	1336	1599	2470	2655	3245
647	1333	1597	2469	2647	3238
785	1317	*		2600	
830	1314	1598			

Table 4.3: Positions of graphene modes in glass/SLG/H_2Pc system at each excitation wavelength.
* G mode was observed at lower values due to glass reflection.
** D mode coincides with H_2Pc bands.

Excitation	Raman shifts of modes (cm^{-1})				
Wavelength (nm)	D	G	D+D"	2D	2D'
532	**	1600	2466	2694	3257
633	**	1600	2484	2658	3243
647	**	1598	2482	2651	3238
785	**	*		2595	
830	**	1598			

Table 4.4: Positions of graphene D and 2D modes in glass/SLG system at each excitation wavelength, calculated and observed values as described in the text.

Excitation		Raman shift (cm^{-1})			
Wavelength (nm)	Energy (eV)	D(calc.)	D(obs.)	2D(calc.)	2D(obs.)
532	2.33	1347	1354	2693	2692
633	1.96	1328	1336	2656	2655
647	1.92	1326	1333	2652	2647
785	1.58	1309	1317	2618	
830	1.49	1305	1313	2609	

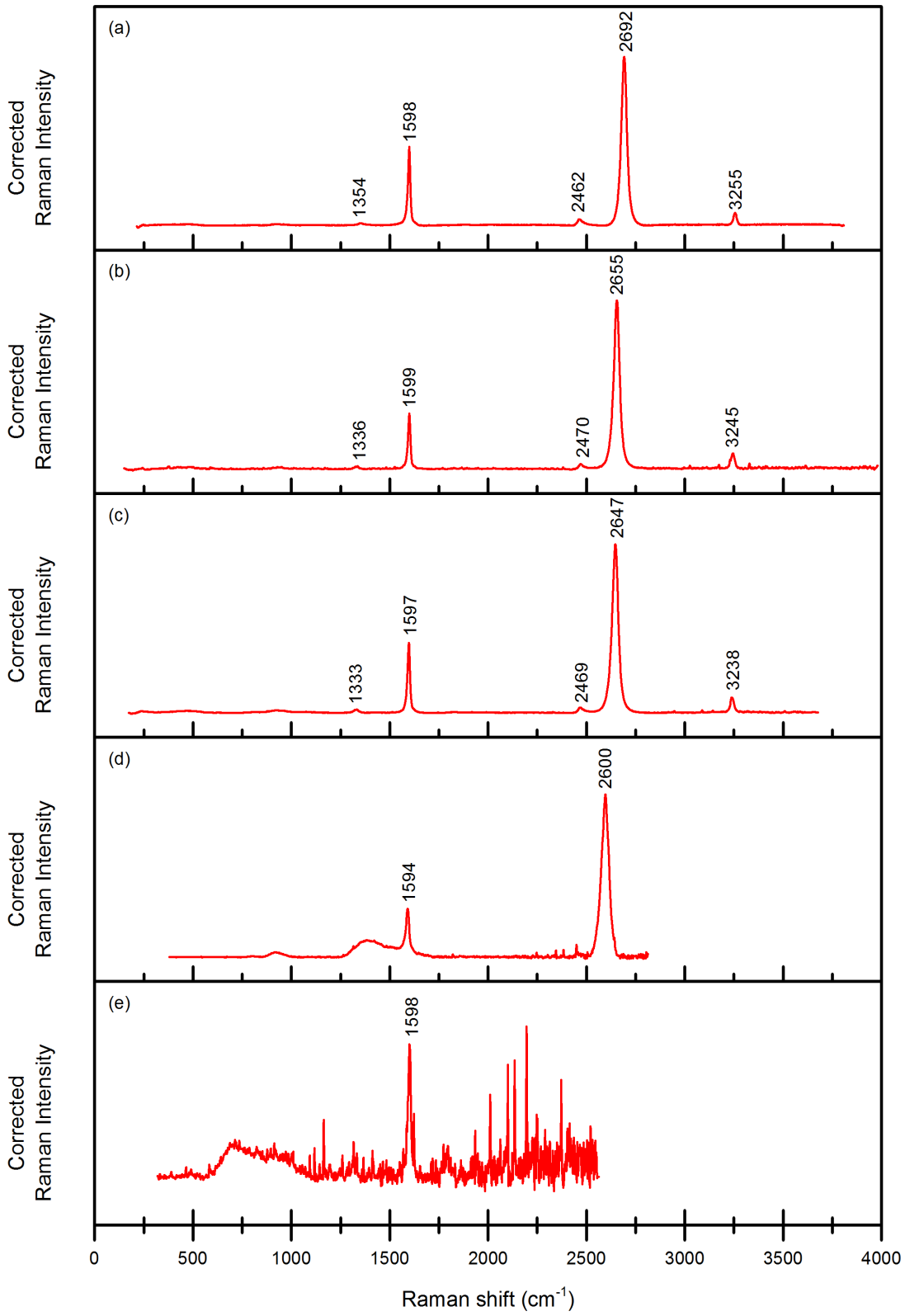

Figure 4.21: Raman spectra glass/SLG system at five excitation wavelengths: (a) 532 nm, (b) 633 nm, (c) 647 nm, (d) 785 nm, and (e) 830 nm.

4.2.5 Symmetry of Selected H_2Pc Vibrations: Raman Depolarization Ratios of H_2PcTS Spectral Bands in Aqueous Solution

As discussed in the Theoretical Chapter, symmetry assignment of free-base phthalocyanine normal vibrations varies within literature [10, 17, 18]. To address this problem, an attempt was made to ascertain depolarization ratios of H_2Pc bands of interest. Unfortunately, H_2Pc shows little (if any at all) solubility in the majority of common solvents, namely toluene and 1-chloronaphthalene [2] were considered for these measurements. However, neither of the concentrations was sufficient for Raman spectra at an off-resonance excitation.

A sulfonated derivative of H_2Pc, namely 29,31H-phthalocyanine-C,C,C,C-tetrasulfonate hydrate (H_2PcTS), was opted for instead. This substance dissolves easily in polar solvents due to the four polar HSO_3-substituents, therefore a $1.0 \cdot 10^{-2}$ M water solution was prepared for the further-described measurements.

A UV-Vis electronic absorption spectrum of a $1.0 \cdot 10^{-4}$ M water solution of H_2PcTS (Fig. 4.22) was measured to determine an appropriate off-resonance excitation wavelength to avoid anomalies present when at resonance. Specifically, wavelength 488 was selected since it falls within the minimum of the two absorption bands, as illustrated in the figure. Polarized spectra were also acquired for 514.5 nm excitation, and may be found in the Supplement, Fig. S1.

Fig. 4.23 presents Raman spectra of a $1.0 \cdot 10^{-2}$ M solution of H_2PcTS in water acquired at the excitation wavelength 488 nm. Tab. 4.5 summarizes observed Raman shifts of the H_2PcTS bands and whether they are polarized (p) or depolarized (dp), as well as the positions of the corresponding H_2Pc bands (specifically those of glass/SLG/H_2Pc-X hybrid system observed at 647 excitation) and their DFT calculated symmetries in Ref. [18]. The table has been completed with the help of polarized spectra collected at 514.5 nm excitation which may be found in the Supplement, Fig. S1. An excellent match has been achieved between in assignment of both totally symmetric A_g and non-totally symmetric B_{1g} modes of H_2Pc by (a) determination based on Raman depolarization ratios for H_2PcTS in aqueous solution, and (b) on the basis of DFT calculations [18]. Of the total of 22 bands, for which the comparison has been carried out, discrepancy has been observed in only three instances, namely at 1010, 1145, 1532/1544 cm^{-1} for H_2Pc.

[2] Ref. [14] claims to have prepared a H_2Pc solution in chloronaphthalene of concentration equal to 10^{-2} $mol \cdot dm^{-3}$. However, even after lengthy shaking and heating, the suspension did not turn into a solution.

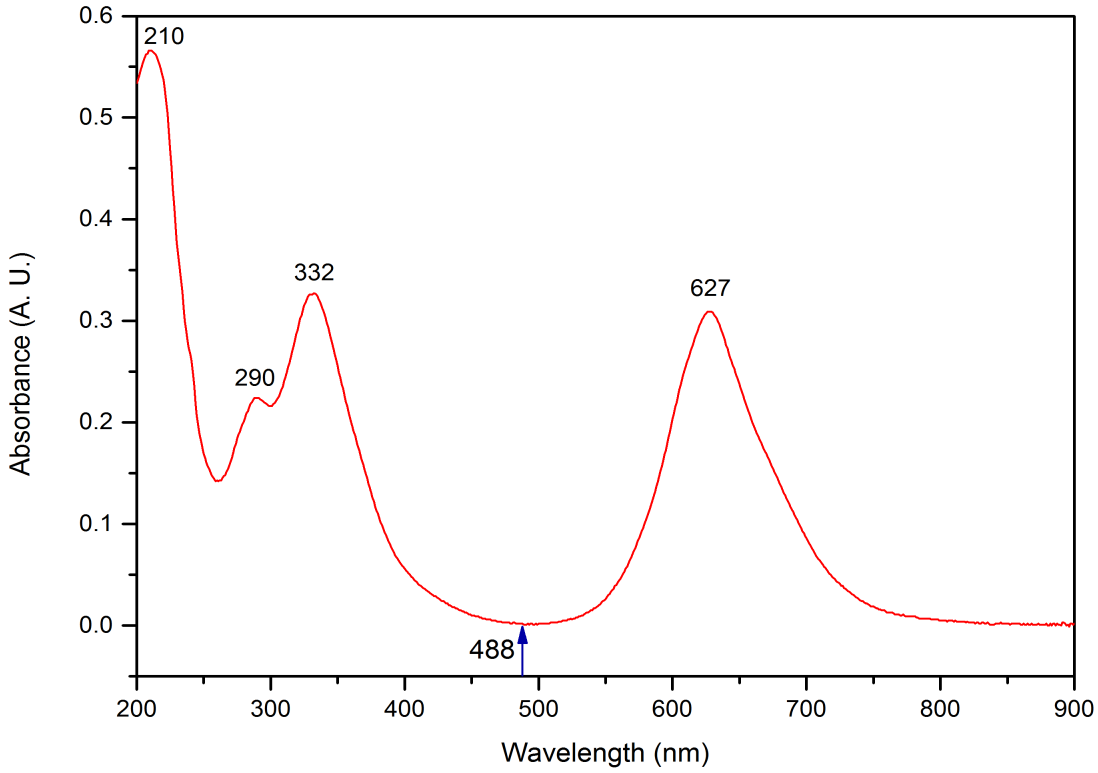

Figure 4.22: Electronic absorption spectrum of a $1.0 \cdot 10^{-4}$ M H_2PcTS in water.

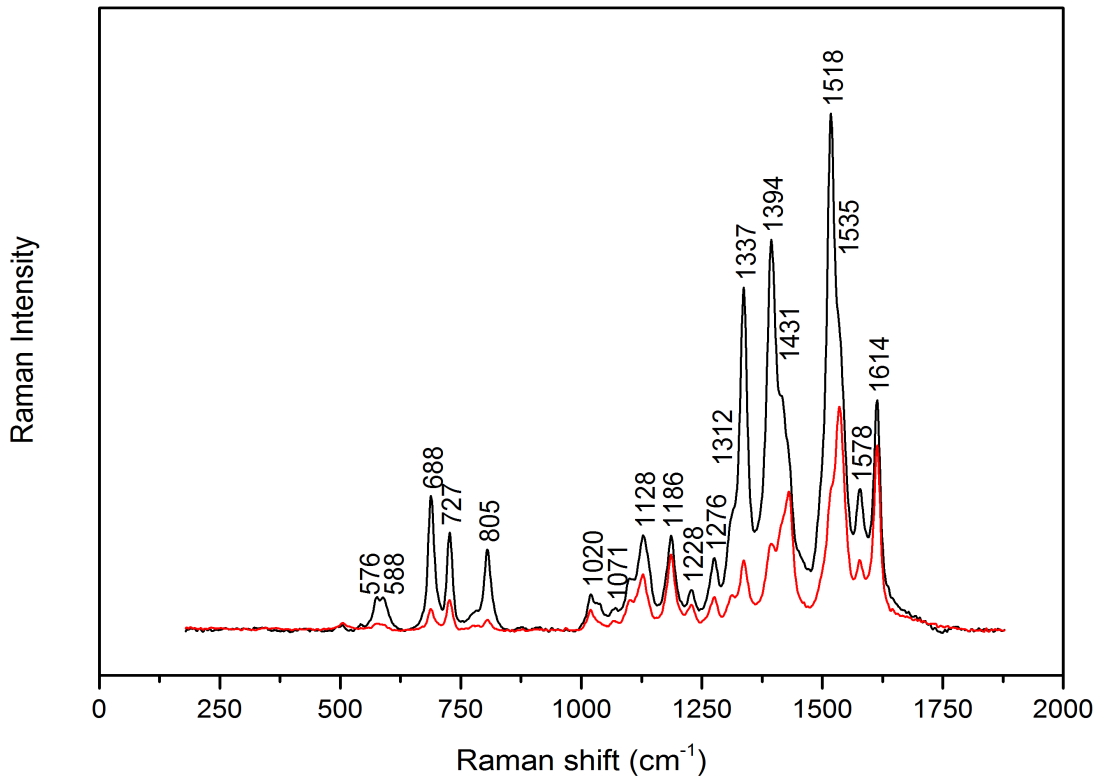

Figure 4.23: Raman spectra of $1.0 \cdot 10^{-4}$ M H_2PcTS in water at 488 nm excitation with parallel (black) and perpendicular (red) polarization with respect to the incident radiation. (baseline corrected)

Table 4.5: H_2PcTS bands and their symmetries (p = polarized, dp = depolarized), and H_2Pc vibrations in glass/SLG/H_2Pc-X hybrid system and symmetry assignment from DFT calculations by Murray et al. [18]. Similar experimental analogy has been drawn between iron phthalocynine and its sulfonated analogue [39], where the band observed at 1276 cm^{-1} (marked *) was ascribed to the sulfonate group.

Raman shift of H_2PcTS (cm^{-1})	Polarization	Raman shift of H_2Pc (cm^{-1})	Symmetry
576	p	545	A_g
588	p	597	A_g
688	p	684	A_g
727	p	726	A_g
805	p	798	A_g
1020	dp	1010	A_g
1035	dp	1029	B_{1g}
1071	dp	1085	B_{1g}
1103	dp	1111	B_{1g}
1128	dp	1145	A_g
1180	p	1185	A_g
1190	dp	1197	B_{1g}
1228	dp	1219	B_{1g}
1276	*	–	
1312	dp	1311	B_{1g}
1337	p	1343	A_g
1394	p	1408	A_g
1431	dp	1431	B_{1g}
1463	p	1453	A_g
1518	p	1512	A_g
1535	dp	1532	-
		1544	A_g
1578	p	–	A_g
1614	dp	1620	B_{1g}

4.2.6 Assignment of H_2Pc Raman Spectral Bands in Hybrid Systems to Normal Vibrations and of Those to the Symmetry Species of D_{2h} Point Group

Tabs. 4.7, 4.8 and 4.9 summarize observed Raman shifts for individual H_2Pc normal vibrations in glass/SLG/H_2Pc-I and glass/SLG/H_2Pc-X hybrid systems at the five excitation wavelengths. Furthermore, these tables present assignment of the observed modes to normal vibrations and of those to the symmetry species of D_{2h} point group based on thorough examination of available literature [10, 16, 18, 29, 39, 40, 41, 42]. Normal coordinate analysis of iron phthalocyanine (FePc) performed by Melendres and Maroai [39] indicates that vibrations of the phthalocyanine molecule are strongly coupled and changes of many internal coordinates are involved in a particular vibration. This, in turn, hampers the band assignment for H_2Pc molecule for which NCA has not been performed. Hence the approach of Aroca et al. [10] who assumed selectivity of individual H_2Pc vibrations and compared the observed modes bands to those of related molecules (e. g. benzene and pyrrole) appears not to be as accurate as may have originally seemed. Therefore, the assignment was mostly based on Ref. [29], Tabs. 4.7-4.9.

It shall be noted that both A_g and B_{1g} vibrations were observed, which points to the participation of both Franck-Condon and Herzberg-Teller mechanism, where the latter results from Q_x and Q_y coupling, as concluded in Ref. [17]. The weak spectral bands stepping out in the Raman spectra of glass/SLG/H_2Pc-VI and glass/SLG/H_2Pc-X hybrid systems were observed also in the above enumerated studies, and some of them are found to belong to the infra-red active modes which become Raman activated in the hybrid systems, as reported previously in Ref. [1] for 633 nm excitation. In addition, overtones and combination bands were observed at excitation wavelengths 633 and 647 nm, and are listed in Tab. 4.6. Observation of overtones at 633 nm was also reported in Ref. [1].

Table 4.6: Observed overtones and combination bands of H_2Pc and their assignment to fundamental modes.

Raman shift (cm^{-1})	Assignment
1824	combination band of 684 and 1144
1866	combination band of 727 and 1144
2023	combination band of 684 and 1343
2224	combination band of 684 and 1544
2267	overtone of 1144
2481	combination band of 1144 and 1343
2878	combination band of 1343 and 1544
2990	combination band of 1453 and 1544
3080	overtone of 1544

Table 4.7: Wavenumbers of H_2Pc Raman spectral bands observed for glass/SLG/H_2Pc-I and glass/SLG/H_2Pc-X hybrid systems (denoted as $\tilde{\nu}$(I) and $\tilde{\nu}$(X), respectively) for each excitation wavelength, assignment of the bands to normal vibrations and symmetry species. (Part I - wavenumbers below 850 cn^{-1})

532 nm		633 nm		647 nm		785 nm		830 nm		Assignment	Symmetry
$\tilde{\nu}$(X) (cm^{-1})	$\tilde{\nu}$(I) (cm^{-1})	$\tilde{\nu}$(X) (cm^{-1})	$\tilde{\nu}$(I) (cm^{-1})	$\tilde{\nu}$(X) (cm^{-1})	$\tilde{\nu}$(I) (cm^{-1})	$\tilde{\nu}$(X) (cm^{-1})	$\tilde{\nu}$(I) (cm^{-1})	$\tilde{\nu}$(X) (cm^{-1})	$\tilde{\nu}$(I) (cm^{-1})		
		487	484	486	484	484	483	487	485	isoindole deformation	B_{1g}
		546	544	545	544	543	545	546	545	isoindole (mostly benzene) ring deformation	A_g
		571	570	571	570	571	572		570	benzene ring deformation	A_g
685	685	685	683	684	683	681	682	685	684	macrocycle breathing (C-N-C and benzene ring deformation)	A_g
726	727	727	726	726	726	724	724	727	726	pyrrole deformation (C-N-C deformation)	A_g
		752	750	752	750	749	749	752	749	N-H out-of-plane bending ***	-
771		770	769	769	768	768	767			*****	A_g
801	801	799	798	798	798	795	795	800	799	macrocycle deformation (pyrrole and aryl C=C stretching)	A_g

*** IR active modes [42]
***** Not assigned in [29]

Table 4.8: Wavenumbers of H_2Pc Raman spectral bands observed for glass/SLG/H_2Pc-I and glass/SLG/H_2Pc-X hybrid systems (denoted as $\tilde{\nu}$(I) and $\tilde{\nu}$(X), respectively) for each excitation wavelength, assignment of the bands to normal vibrations and symmetry species. (Part II - wavenumbers $850 - 1300$ cn^{-1})

532 nm		633 nm		647 nm		785 nm		830 nm		Assignment	Symmetry
$\tilde{\nu}$(X) (cm^{-1})	$\tilde{\nu}$(I) (cm^{-1})	$\tilde{\nu}$(X) (cm^{-1})	$\tilde{\nu}$(I) (cm^{-1})	$\tilde{\nu}$(X) (cm^{-1})	$\tilde{\nu}$(I) (cm^{-1})	$\tilde{\nu}$(X) (cm^{-1})	$\tilde{\nu}$(I) (cm^{-1})	$\tilde{\nu}$(X) (cm^{-1})	$\tilde{\nu}$(I) (cm^{-1})		
		894	892	892	892		891				B_{1g}
		958	951	957	952		949			C-H deformation	B_{1g}
		1010	1009	1010	1009		1008			symmetric benzene ring C-H deformation	A_g (B_{1g}*)
		1030	1029	1029	1029		1027			C-N and C-H deformation	B_{1g}
	1087	1086	1085	1086	1085	1084	1084		1084	N-H in-plane bending	B_{1g}
1112	1110	1112	1109	1111	1110	1107	1108	1111	1109	*****	B_{1g}
1146	1145	1145	1143	1144	1143	1141	1141	1145	1143	pyrrole breathing (benzene C-C stretching and C-H deformation)	A_g (B_{1g}*)
	1162	1165	1161	1164	1162	1160	1159			*****	A_g
	1187	1186	1184	1185	1184	1183	1181	1184	1184	benzene C-H deformation	A_g
	1197	1197	1197	1197	1197	1195	1195	1193	1193	*****	A_g and/ /or B_{1g}
	1212	1219	1225	1219	1225	1216	1219			benzene deformation and N-H in-plane bending	B_{1g}

* Raman depolarization measurements of H_2PcTS

***** Not assigned in [29]

Table 4.9: Wavenumbers of H_2Pc Raman spectral bands observed for glass/SLG/H_2Pc-I and glass/SLG/H_2Pc-X hybrid systems (denoted as $\tilde{\nu}$(I) and $\tilde{\nu}$(X), respectively) for each excitation wavelength, assignment of the bands to normal vibrations and symmetry species. (Part III - wavenumbers above 1300 cn^{-1})

532 nm		633 nm		647 nm		785 nm		830 nm		Assignment	Symmetry
$\tilde{\nu}$(X) (cm^{-1})	$\tilde{\nu}$(I) (cm^{-1})	$\tilde{\nu}$(X) (cm^{-1})	$\tilde{\nu}$(I) (cm^{-1})	$\tilde{\nu}$(X) (cm^{-1})	$\tilde{\nu}$(I) (cm^{-1})	$\tilde{\nu}$(X) (cm^{-1})	$\tilde{\nu}$(I) (cm^{-1})	$\tilde{\nu}$(X) (cm^{-1})	$\tilde{\nu}$(I) (cm^{-1})		
		1312	1314	1311	1314	1308#	1311#	1314	1314	C=C benzene and pyrrole stretching	B_{1g}
		1344	1341	1343	1341	1338#	1336#	1344	1343	benzene and pyrrole C-C stretching	A_g
1407	1411	1409	1406	1408	1406	1407#		1410	1410	C-H deformation (isoindole stretching**)	A_g
1433	1432	1431	1430	1431	1430				1430	isoindole stretching	B_{1g}
1455	1454	1454	1452	1453	1451	1449#	1448#	1454	1451	C-H deformation	A_g
	1512	1512	1512	1512	1512		1507#	1513	1512	*****	A_g
1535		1534		1532				1533		N-H in-plane bending***	-
1546	1542	1545	1544	1544	1543	1538#	1534#	1546	1543	C-N_m-C asymmetric stretching and C-N_H-C symmetric stretching****	A_g
1619	1620	1620	1620	1619	1620	1613#	1616#			benzene ring deformation	B_{1g}

** NCA of FePc [39]
*** IR active modes [42]
**** The subscripts m and H denote the bridge and H-carrying nitrogen atoms, respectively.
***** Not assigned in [29]
# The H_2Pc Raman bands appear at lower values due to glass reflection.

4.2.7 Excitation Profiles of Selected Raman Spectral Bands of Glass/SLG/H_2Pc Hybrid Systems

Excitation profiles (EP) of H_2Pc Raman spectral bands were constructed from Raman spectra of glass/SLG/H_2Pc-I, glass/SLG/H_2Pc-VI and glass/SLG/H_2Pc-X hybrid systems collected at the five excitation wavelengths. Raman spectra of polystyrene acquired under the very same experimental conditions were employed as external standards, and may be found in the Supplement, Fig. S10. At each excitation wavelength, intensity of the particular H_2Pc band was normalized to the intensity of the polystyrene mode observed at 1005 cm^{-1}. The EPs are presented in Figs. 4.24-4.32, of which Figs. 4.24, 4.27 and 4.29 show an overview of EPs of all selected H_2Pc spectral bands, Figs. 4.25, 4.28 and 4.30 display the detail of the close-lying less enhanced bands, and finally Figs. 4.26, 4.31 and 4.32 offer a closer view on the EPs at higher excitation wavelengths (785 and 830 nm).

In case of all three samples, the EPs of the selected spectral bands exhibit a maximum for the excitation wavelength 647 nm. In addition, while the EP of glass/SLG/H_2Pc-I appears rather flat for higher excitation wavelengths (with some of the bands slightly declining and some slowly increasing, Fig. 4.26), the EPs of glass/SLG/H_2Pc-VI and glass/SLG/H_2Pc-X hybrid systems show a pronounced growth from 785 to 830 nm for at least half of the spectral bands (Figs. 4.31 and 4.32). Furthermore, the EP of the glass/SLG/H_2Pc-I hybrid system (Fig. 4.24) may be related to its electronic absorption spectrum (Fig. 4.2, with projections of the five excitation wavelengths). Unfortunately, the EP of the three hybrid systems could not be compared with that of H_2Pc in solution or in crystalline state due to strong fluorescence which prevents acquisition of Raman spectra. On the other hand, this observation demonstrates the significance of the fluorescence quenching upon formation of glass/SLG/H_2Pc hybrid system which in turn allows for collecting Raman spectra of a decent quality and for constructing appropriate EPs. Similar advantage of fluorescence quenching was also exploited in a SERRS (surface-enahnced resonance Raman scattering) spectral study of H_2Pc adsorbed on silver islands, which presents very detailed EPs in the $660 - 700$ nm region of low wavenumber bands (namely of those observed at $545 - 797$ cm^{-1}) [16].

A more detailed analysis of the H_2Pc Raman bands EPs follows hereafter. In particular, sequences of relative band intensities for individual bands (from highest to lowest) were determined for all three hybrid systems at the excitation wavelengths 633 and 647 nm, and for glass/SLG/H_2Pc-VI and glass/SLG/H_2Pc-X also at the excitation 830 nm. The series were analyzed in terms of the symmetries of the corresponding normal vibrations (indicated in parenthesis after the

respective band Raman shift given in cm^{-1}) and localization within the H_2Pc molecule (where appropriate). This approach was based on a previously reported method in Ref. [43] which was applied to analysis of SERRS EP.

Excitation Profiles of Glass/SLG/H_2Pc-I

The sequence at the excitation wavelength 647 nm (Fig. 4.24, spectrum (b) in Fig. 4.15) was ascertained as follows: 1543 (A_g) > 1341 (A_g) > 1143 (A_g) > 726 (A_g) > 1451 (A_g) > 683 (A_g) ≈ 1184 (A_g) ≈ 1314 (B_{1g}) > 1367 > 798 (A_g) > 1110 (B_{1g}) > 1085 (B_{1g}) > 484 (B_{1g}) > 544 (A_g) > 768 (A_g) > 1009 (B_{1g}) ≈ 1162 (A_g) > 1029 (B_{1g}) > 750. The mostly enhanced modes belong to A_g symmetry and comprise both stretching and bending (deformation) vibrations of the macrocycle (or its parts). The B_{1g} modes, the A_g vibrations localized also (or preferentially) on the benzene, as well as C-H deformation modes are to be found among the less enhanced ones. This enhancement pattern is consistent with the expected behavior upon excitation into Q_x (or Q_y) purely electronic (0-0) transition which is localized predominantly on the tetrapyrrole macrocycle [10, 16, 29].

The series at 633 nm excitation (Fig. 4.24, spectrum (a) in Fig. 4.15) was found to be: 1543 (A_g) > 1341 (A_g) > 1143 (A_g) > 1451 (A_g) > 1314 (B_{1g}) > 1184 (A_g) ≈ 1367 > 726 (A_g) > 1110 (B_{1g}) > 1085 (B_{1g}) > 683 (A_g) > 484 (B_{1g}) > 798 (A_g) > 1162 (A_g) ≈ 1009 (B_{1g}) ≈ 1029 (B_{1g}) ≈ 768 (A_g) > 544 (A_g) > 750. Although the relative intensities of the three most enhanced bands (1543, 1344 and 1144 cm^{-1}) are comparable at the excitation wavelengths 633 and 647 nm, there is a substantial difference in case of the macrocycle deformation (685 cm^{-1}) and breathing (726 cm^{-1}) modes. While they are to be found among the more enhanced bands at 647 nm, they fall into the category of weakly enhanced for the 633 nm excitation. It may be overall stated that stronger enhancement occurs for higher frequency bands only.

This rather minor though significant difference may be tentatively explained by consideration of the electronic absorption spectrum of glass/SLG/H_2Pc-I hybrid system (Fig. 4.2). The excitation wavelength 647 nm appears to fall within the main electronic transition belonging to Q_x, which shows to be consistent with the observed relative intensities of the individual bands at 647 nm and their Raman activation by excitation into this Q(0-0) band. The excitation wavelength 633 nm, on the other hand, seems to coincide with the shoulder located at about the same position. This shoulder may be tentatively attributed to the vibronic sideband of the split Q-band arising from the coupling of the Q and B electronic states by vibrations of both A_g and B_{1g} symmetry [29]. Its wavenumber position equals approximately 1368 cm^{-1} (ascertained as the difference between the Q-band maximum at 693 nm and the shoulder at ≈ 633 nm), i. e. it falls within the

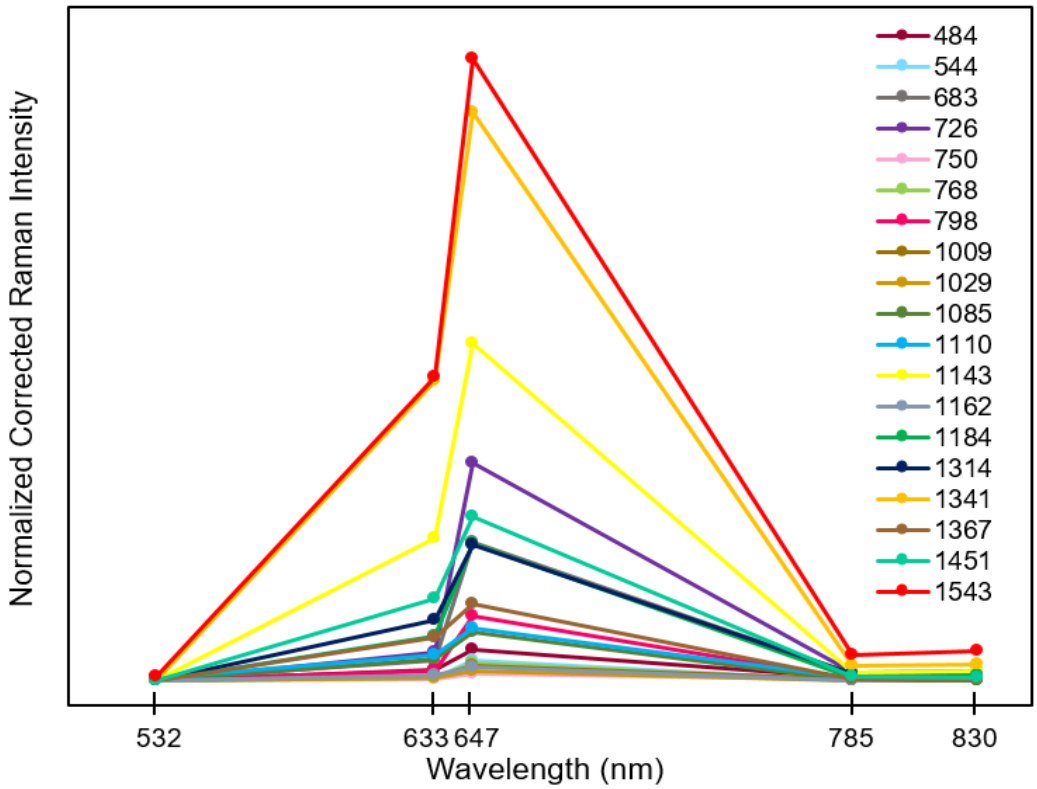

Figure 4.24: Excitation profile of glass/SLG/H_2Pc-I Raman spectral bands.

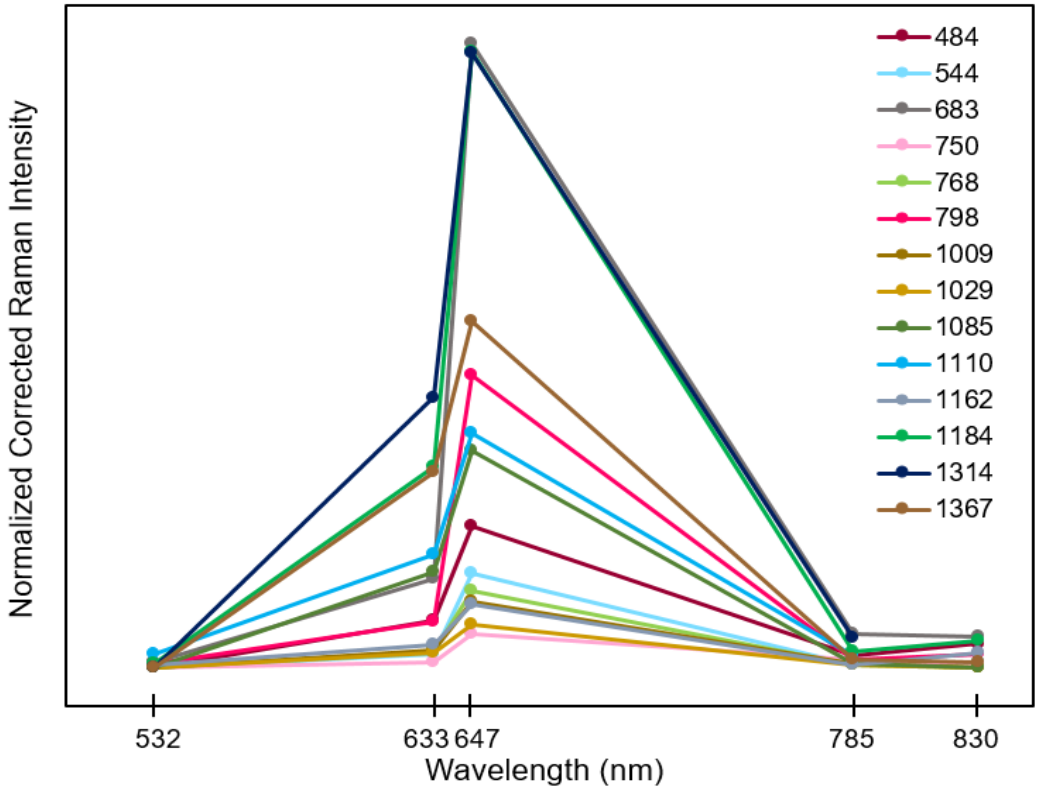

Figure 4.25: Excitation profile of glass/SLG/H_2Pc-I Raman spectral bands - detail of less enhanced bands.

higher wavenumber region. This reasoning, once again, agrees with the preferential enhancement of higher wavenumber modes of both A_g and B_{1g} symmetries at the excitation wavelength 633 nm.

The previously outlined explanation of the difference between the sequences at 647 and 633 nm, specifically the excitation into the main Q_y band at 647 nm, is further corroborated by evaluation of the sequence of the most enhanced bands at 785 nm for this system. Fig. 4.2 shows that this particular excitation wavelength falls into the very onset of the Q_x band with its maximum appearing at 718 nm. This implies that the enhancement of Raman spectral bands at the mentioned excitation wavelength may originate in the resonance with the Q_x (0-0) electronic transition. The series was ascertained to follow (Fig. 4.26, spectrum (b) in Fig. 4.18): 1543 (A_g) > 1341 (A_g) > 1143 (A_g) ≈ 726 (A_g) > 683 (A_g) > 1314 (B_{1g}) > 1451 (A_g) > 1184 (A_g) > 484 (B_{1g}) ≈ 1110 (B_{1g}) > 798 (A_g) ≈ 750 ≈ 1367 > 1009 (B_{1g}) ≈ 1085 (B_{1g}) ≈ 544 (A_g) ≈ 1162 (A_g) ≈≈ 1029 (B_{1g}) ≈ 768 (A_g). The sequence of the most enhanced bands bears resemblance to that at 647 nm, and in particular the macrocycle deformation and breathing modes at 684 and 726 cm^{-1} appear among the most enhanced bands.

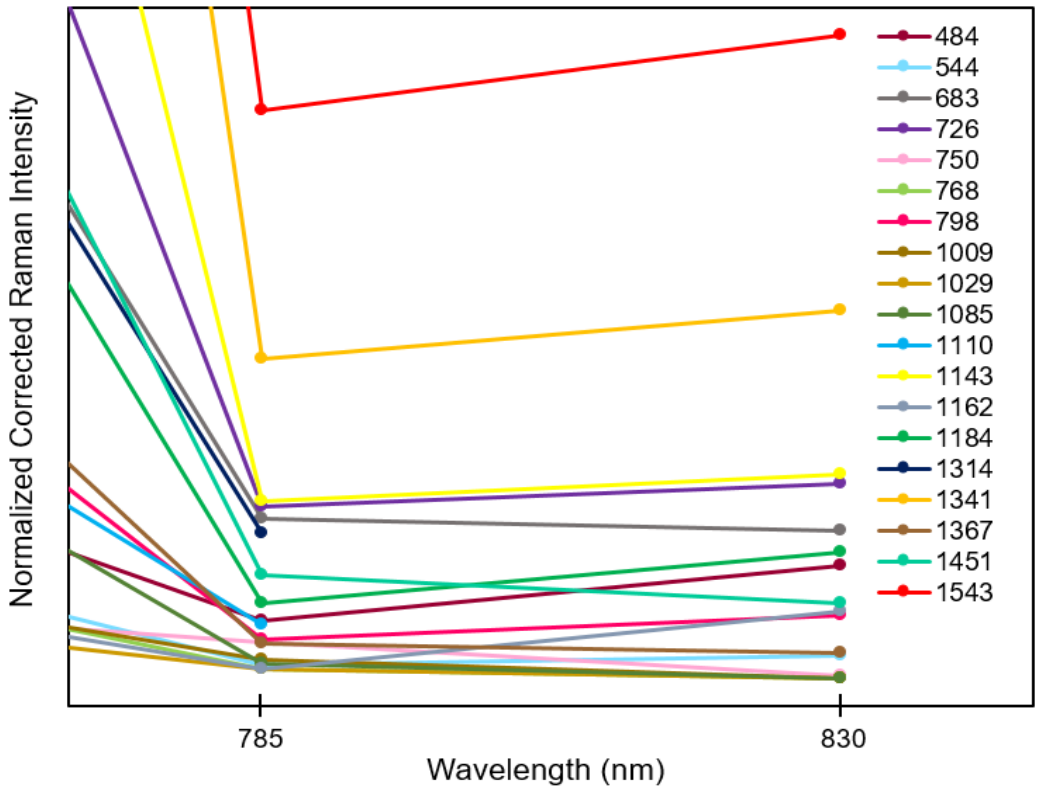

Figure 4.26: Excitation profile of glass/SLG/H_2Pc-I Raman spectral bands - detail at 785 and 830 nm.

Excitation Profiles of Glass/SLG/H_2Pc-VI

The sequence for the glass/SLG/H_2Pc-VI at 647-nm excitation (Fig. 4.27, spectrum (b) in Fig. 4.16) was found to be: 1545 (A_g) > 1343 (A_g) > 1534 ≈ 1144 (A_g) > 1453 (A_g) > 1314 (B_{1g}) > 727 (A_g) > 684 (A_g) > 1186 (A_g) > 1111 (B_{1g}) > 1369 > 799 (A_g) > 1086 (B_{1g}) > 486 (B_{1g}) > 1163 (A_g) > 546 (A_g).

For the excitation 633 nm, the band order is following (Fig. 4.27, spectrum (a) in Fig. 4.16): 1545 (A_g) > 1343 (A_g) > 1534 ≈ 1144 (A_g) > 1453 (A_g) > 1314 (B_{1g}) > 1186 (A_g) > 727 (A_g) ≈ 1369 > 1111 (B_{1g}) ≈ 684 (A_g) > 1086 (B_{1g}) > 486 (B_{1g}) > 799 (A_g) > 1163 (A_g) > 546 (A_g).

These two sequences match each other well, as in both cases, the most enhanced are higher wavenumber modes of A_g symmetry while the non-totally symmetric vibrations appear rather at the end of the respective series. The EP of glass/SLG/H_2Pc-I alike, the macrocycle deformation (684 cm^{-1}) and breathing (727 cm^{-1}) modes differ in the extent to which they are enhanced at the two discussed excitations, though the difference is not as remarkable as in case of the former sample.

Excitation Profiles of Glass/SLG/H_2Pc-X

The relative intensity sequence for glass/SLG/H_2Pc-X at 647 nm was ascertained to be (Fig. 4.29, spectrum (b) in Fig. 4.17): 1343 (A_g) ≈ 1533 > 1544 (A_g) > 1144 (A_g) > 1453 (A_g) > 1311 (B_{1g}) > 685 (A_g) > 727 (A_g) > 1185 (A_g) > 1112 (B_{1g}) > 752 ≈ 799 (A_g) > 1086 (B_{1g}) > 486 (B_{1g}) > 1164 (A_g) > 546 (A_g). This order follows similar pattern as in the case of glass/SLG/H_2Pc-VI at 647 and 633 nm, i. e. the highest enhancement occurs for totally symmetric high wavenumber bands. The difference, as observed before, lies in the macrocycle deformation (685 cm^{-1}) and breathing (727 cm^{-1}) modes. For the glass/SLG/H_2Pc-X hybrid system, the relative intensity of the two mentioned bands interchanges in comparison to the sequences of the two other samples. This observation holds also for the relative intensity sequence at 633 nm excitation, which was determined as (Fig. 4.29, spectrum (a) in Fig. 4.17): 1533 > 1343 (A_g) > 1544 (A_g) > 1453 (A_g) > 1144 (A_g) > 1311 (B_{1g}) > 1185 (A_g) > 1112 (B_{1g}) > 727 (A_g) ≈ 685 (A_g) > 486 (B_{1g}) ≈ 1086 (B_{1g}) > 799 (A_g) > 752 ≈ 1164 (A_g) > 546 (A_g). The above outlined comment to the series at 647 nm applies for this excitation as well. In addition, the behavior of the band at 1453 cm^{-1} shall be pointed out as it meets higher enhancement than in the previous instances. Overall, the EPs bear a considerable resemblance, yet are somewhat different.

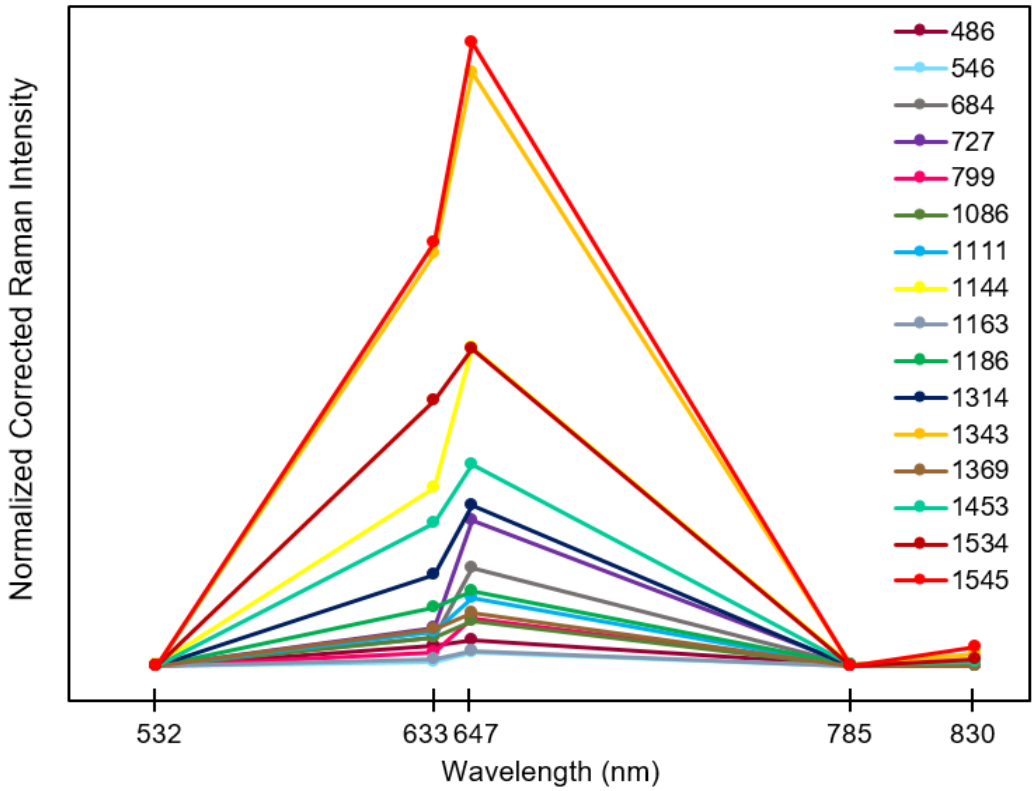

Figure 4.27: Excitation profile of glass/SLG/H_2Pc-VI Raman spectral bands.

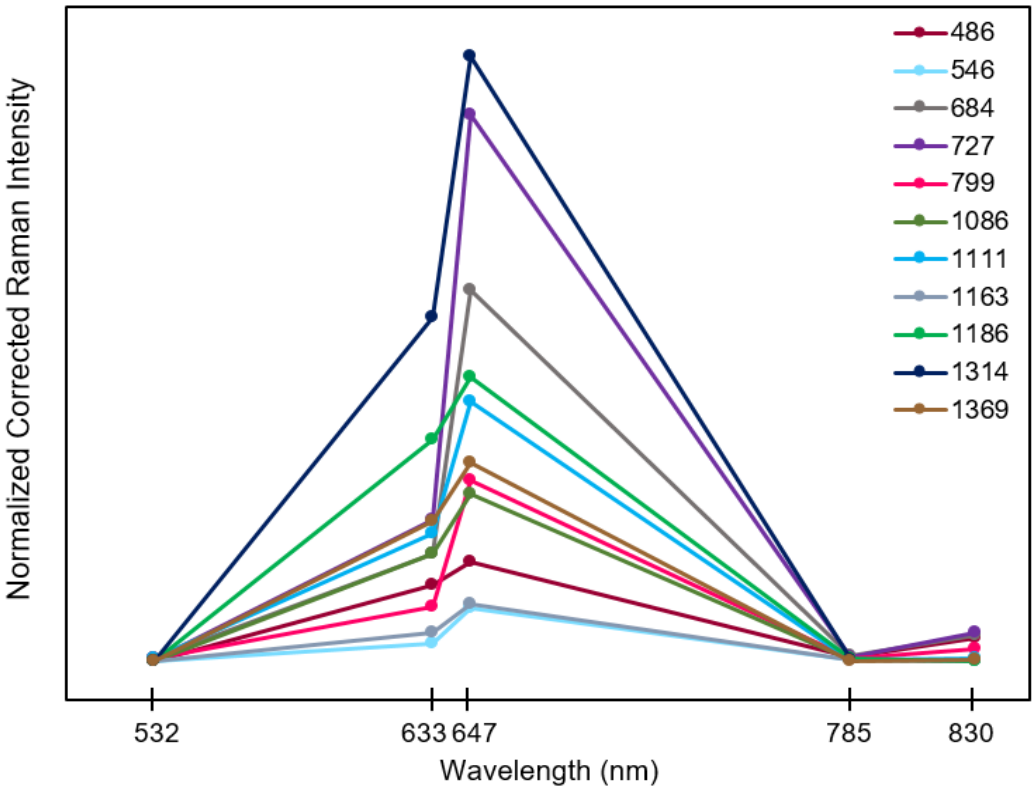

Figure 4.28: Excitation profile of glass/SLG/H_2Pc-VI Raman spectral bands - detail of less enhanced bands.

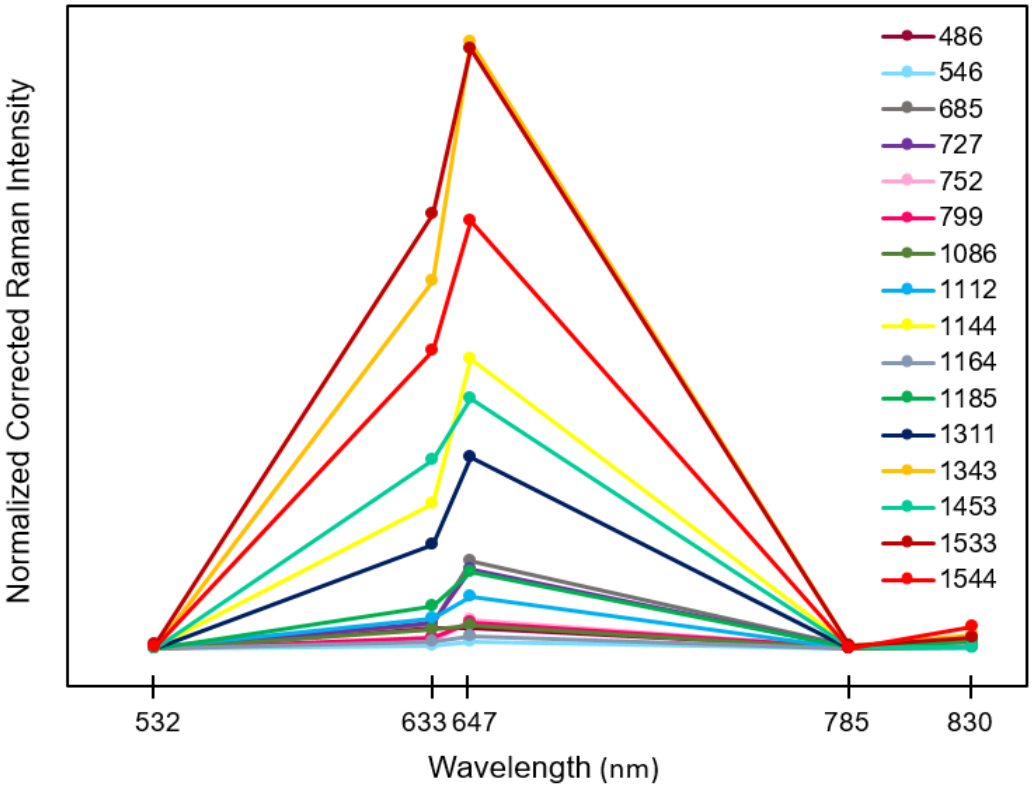

Figure 4.29: Excitation profile of glass/SLG/H_2Pc-X Raman spectral bands.

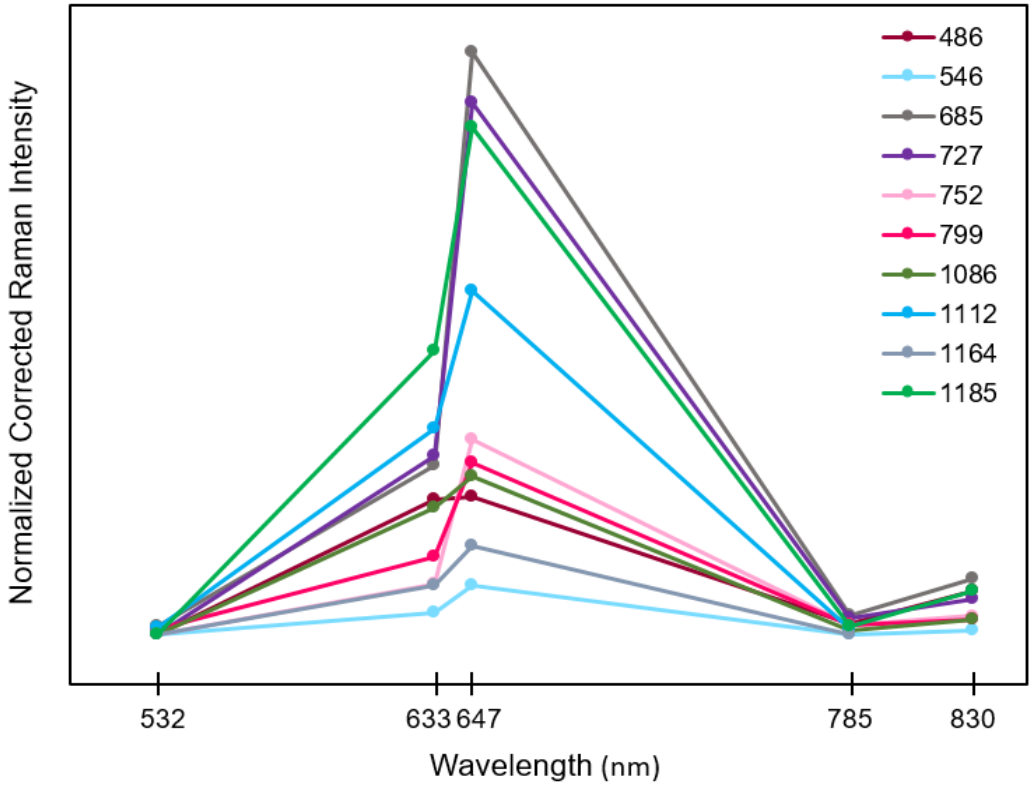

Figure 4.30: Excitation profile of glass/SLG/H_2Pc-X Raman spectral bands - detail of less enhanced bands.

Excitation Profiles in the 785 - 830 nm Region

For samples glass/SLG/H_2Pc-VI and glass/SLG/H_2Pc-X, the relative intensity of all spectral bands striking plummets at 785 nm, as depicted in Figs. 4.27 and 4.29. The majority of the bands, on the other hand, then exhibits a pronounced increase at 830 nm in case of both samples (Figs. 4.31 and 4.32). Since the glass/SLG/H_2Pc-I system features no such distinctive intensity rise, the appearance of the intensity growth may be attributed to the interaction of a monolayer of H_2Pc molecules with SLG. While the most enhanced band at 1545 cm^{-1} reaches only a slightly higher values for the system glass/SLG/H_2Pc-X than for glass/SLG/H_2Pc-VI, the sequences of relative intensities of the individual bands vary for the two samples.

The series of the glass/SLG/H_2Pc-VI system was determined as: 1545 (A_g) > 1343 (A_g) > 1144 (A_g) ≈ 727 (A_g) ≈ 684 (A_g) ≈ 1534 ≈ 486 (B_{1g}) > 1453 (A_g) > 799 (A_g) > 1111 (B_{1g}) > 1369 > 546 (A_g)

In case of the glass/SLG/H_2Pc-X sample, the order follows: 1544 (A_g) > 1343 (A_g) > 1533 ≈ 1144 (A_g) > 685 (A_g) > 486 (B_{1g}) ≈ 1185 (A_g) > 727 (A_g) > 752 > 1453 (A_g) ≈ 799 (A_g) ≈ 1086 (B_{1g}) > 546 (A_g)

Common features of the two series include the bands at 1545 and 1343 cm^{-1} being the most enhanced, as well as the totally symmetric bands at 684 and 727 cm^{-1} surprisingly together with 486 cm^{-1} of B_{1g} symmetry falling among the strongly enhanced ones. It shall be noted that all these bands belong to the macrocycle breathing and deformation modes. On the other hand, the two discussed sequences differ in many aspects. Noticeably, the relative intensity of the newly appearing band at 1534 cm^{-1} reaches markedly higher values for the glass/SLG/H_2Pc-X sample. Furthermore, while the macrocycle breathing at 684 cm^{-1} and deformation at 486 cm^{-1} exhibit virtually the same relative intensities for both samples, the relative intensity of the macrocycle deformation at 727 cm^{-1} substantially decreases for glass/SLG/H_2Pc-X. Moreover, the band at 1453 cm^{-1} grows in intensity for glass/SLG/H_2Pc-VI sample but decreases in case of glass/SLG/H_2Pc-X.

In summary, the sequences of relative band intensities of glass/SLG/H_2Pc-VI and glass/SLG/H_2Pc-X hybrid systems at 830 nm are mutually somewhat different and they do not resemble those obtained for these samples at 633 and 647 nm excitation. On the other hand, they share two common characteristics with the relative intensity sequences of glass/SLG/H_2Pc-I system at 647 and 785 nm excitation, i. e. upon excitation into the Q_x and Q_y (0-0) electronic absorption band. That is, (a) the most enhanced bands are the 1545 and 1343 cm^{-1}, and (b) the 684 and 727 cm^{-1} bands fall into the category of the strongly enhanced modes.

These observations may be tentatively interpreted as follows:

(a) The substantial and vibrational mode-selective growth of relative band intensities of the majority of spectral bands at 830 nm excitation is ascribed to generation of the photo-induced charge transfer transition from Fermi level of SLG to LUMO of H_2Pc (discussed more in detail in the Chapter 4.1.9),

(b) The differences in the realtive band intensities of some of the spectral bands between glass/SLG/H_2Pc-VI and glass/SLG/H_2Pc-X hybrid systems are attributed to reorganization of H_2Pc molecules constituting a monolayer on SLG upon repetitive soaking of the sample in toluene, which is presumed to lead to a more favorable orientation in terms of H_2Pc and SLG interaction.

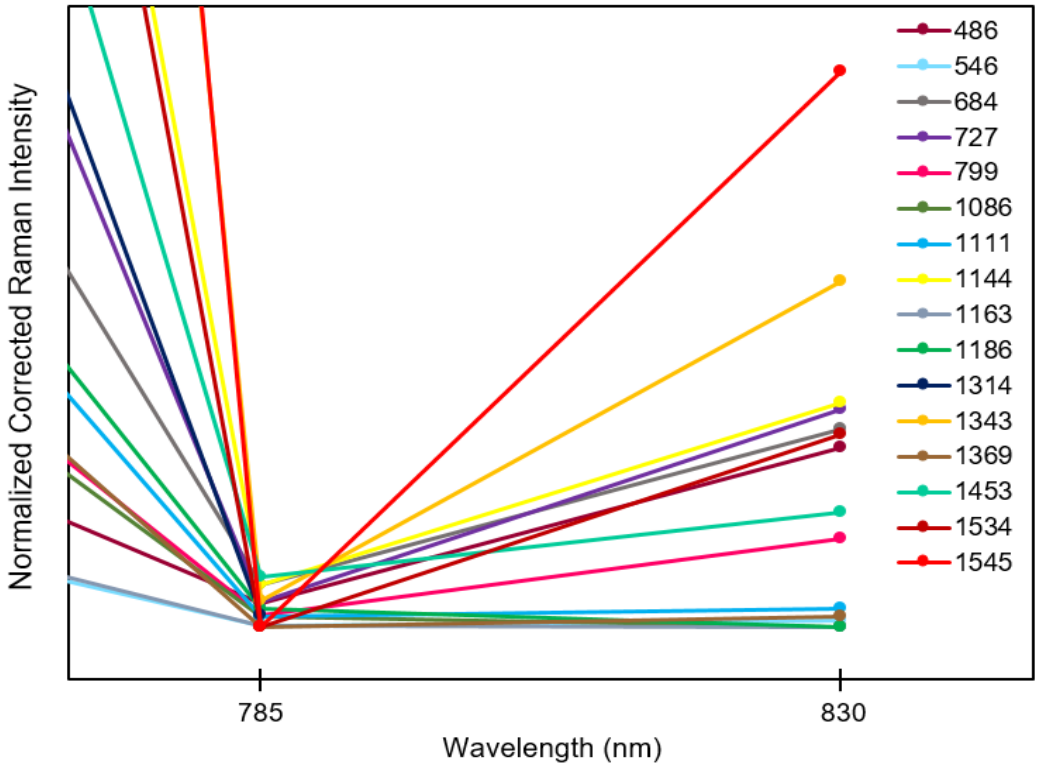

Figure 4.31: Excitation profile of glass/SLG/H_2Pc-VI Raman spectral bands - detail at 785 and 830 nm.

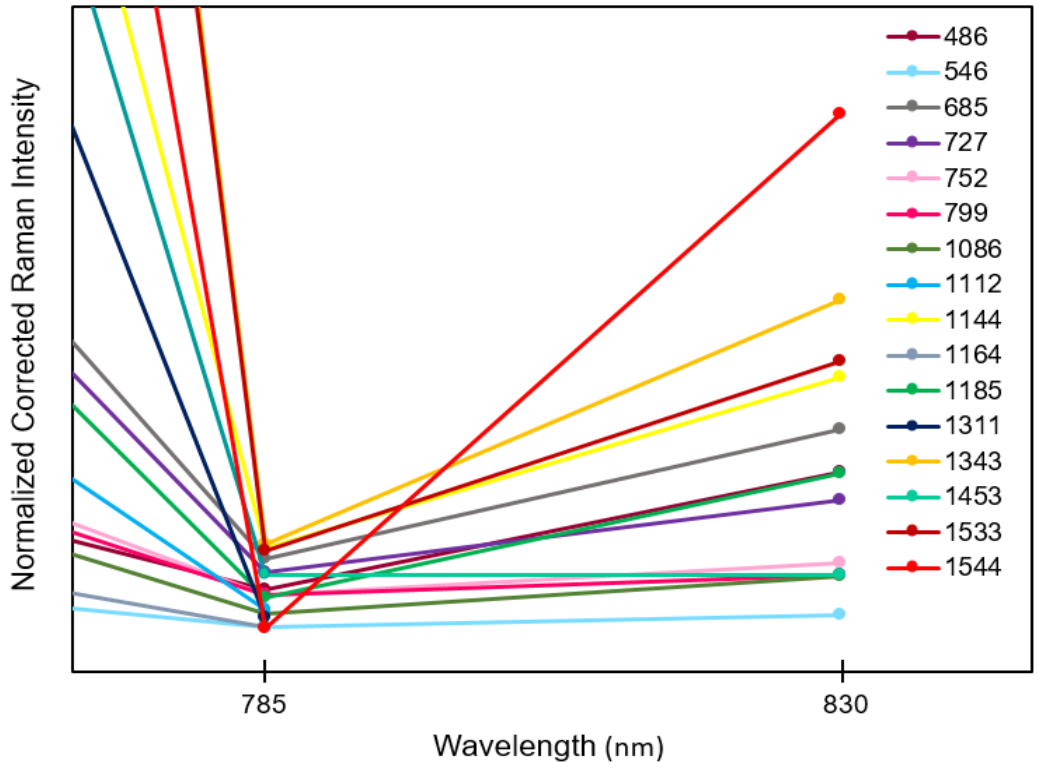

Figure 4.32: Excitation profile of glass/SLG/H_2Pc-X Raman spectral bands - detail at 785 and 830 nm.

4.2.8 Excitation-Wavelength Dependence of Raman Spectra of HOPG/H_2Pc Hybrid Reference Systems

HOPG/H_2Pc-I, HOPG/H_2Pc-VI and HOPG/H_2Pc-X reference systems were prepared the corresponding glass/SLG/H_2Pc samples alike, and their Raman spectra were obtained under identical experimental conditions (in particular with same laser powers, Tab. 3.1 in Chapter 3, and mapping procedures, Chapter 4.2.1) at five excitation wavelengths. However, detectable Raman signal of H_2Pc was obtainen only for resonance excitations, i. e. 633 and 647 nm, Figs. 4.33 and 4.34 (spectra of HOPG/H_2Pc-VI may be found in the Supplement, Figs. S11 and S12). Therefore, unlike glass/SLG/H_2Pc hybrid systems, the amount of present H_2Pc molecules could not be determined by signal in off-resonance spectra. Furthermore, intensity of H_2Pc bands increased with the amount of washing, namely up to threefold when samples HOPG/H_2Pc-I and HOPG/H_2Pc-X compared, as demonstrated for selected modes in Tab. 4.10. This behavior could be explained by progressive degradation of the stacked structure of HOPG due to prolonged soaking in toluene leading to separation of individual HOPG layers or layer groups. This explanation is supported by the previously reported study of the H_2Pc Raman signal dependence on the number of graphene layers: while no enhancement of Raman signal of H_2Pc has been observed for HOPG, the enhancement increases with decreasing number of graphene layers reaching its maxima for single and few-layer graphene [1, 4]. Therefore, while toluene appears to be an optimal solvent for removal of the second and further layers of H_2Pc (in accord with Ref. [35]), its ability to mutually separate layers of aromatic molecules brings also drawbacks in case of preparation of HOPG/H_2Pc samples.

Nevertheless, this reference system maintains its in importance since (a) it allows for calculation of minimal enhancement factors at resonance excitation wavelengths, and (b) unlike glass/SLG/H_2Pc hybrid systems, no signal of H_2Pc was observed for off-resonance excitations, and therefore the presence of those in case of the former samples arises probably from a specific interaction with SLG (and not a multilayer).

Table 4.10: Intensity ratios of selected H_2Pc bands in HOPG/H_2Pc-X to HOPG/H_2Pc-I systems at excitation wavelengths 633 and 647 nm.

Raman shift (cm^{-1})	R(633 nm)	R(647 nm)
685	2.0	2.8
1111	2.8	2.3
1145	2.5	2.5
1312	2.9	3.1
1344	2.5	2.6

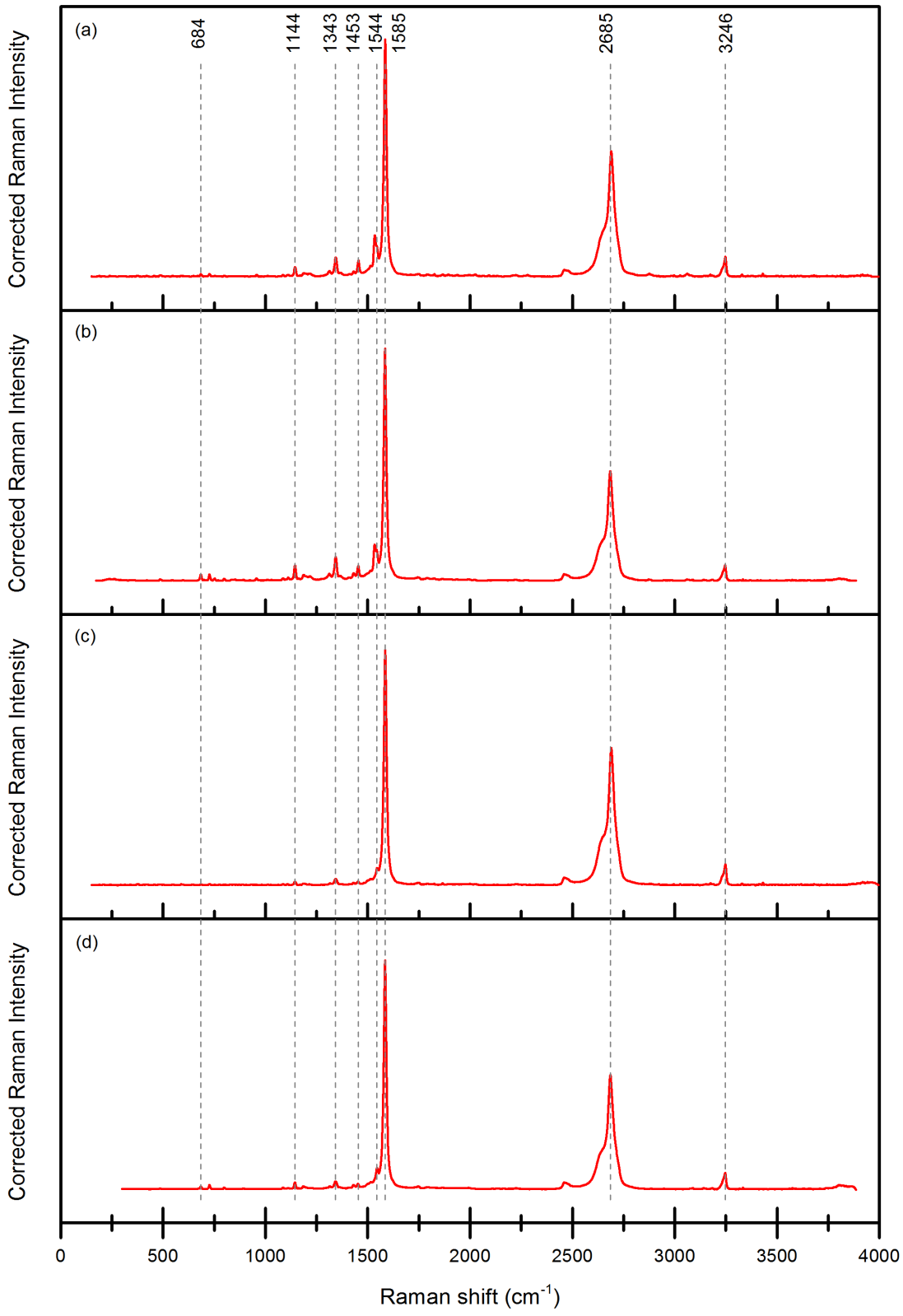

Figure 4.33: Raman spectra of HOPG/H_2Pc-X and HOPG/H_2Pc-I systems at 633 and 647 nm excitation. (a) HOPG/H_2Pc-X at 633 nm, (b) HOPG/H_2Pc-X at 647 nm, (c) HOPG/H_2Pc-I at 633 nm, and (d) HOPG/H_2Pc-I at 647 nm. (baseline corrected)

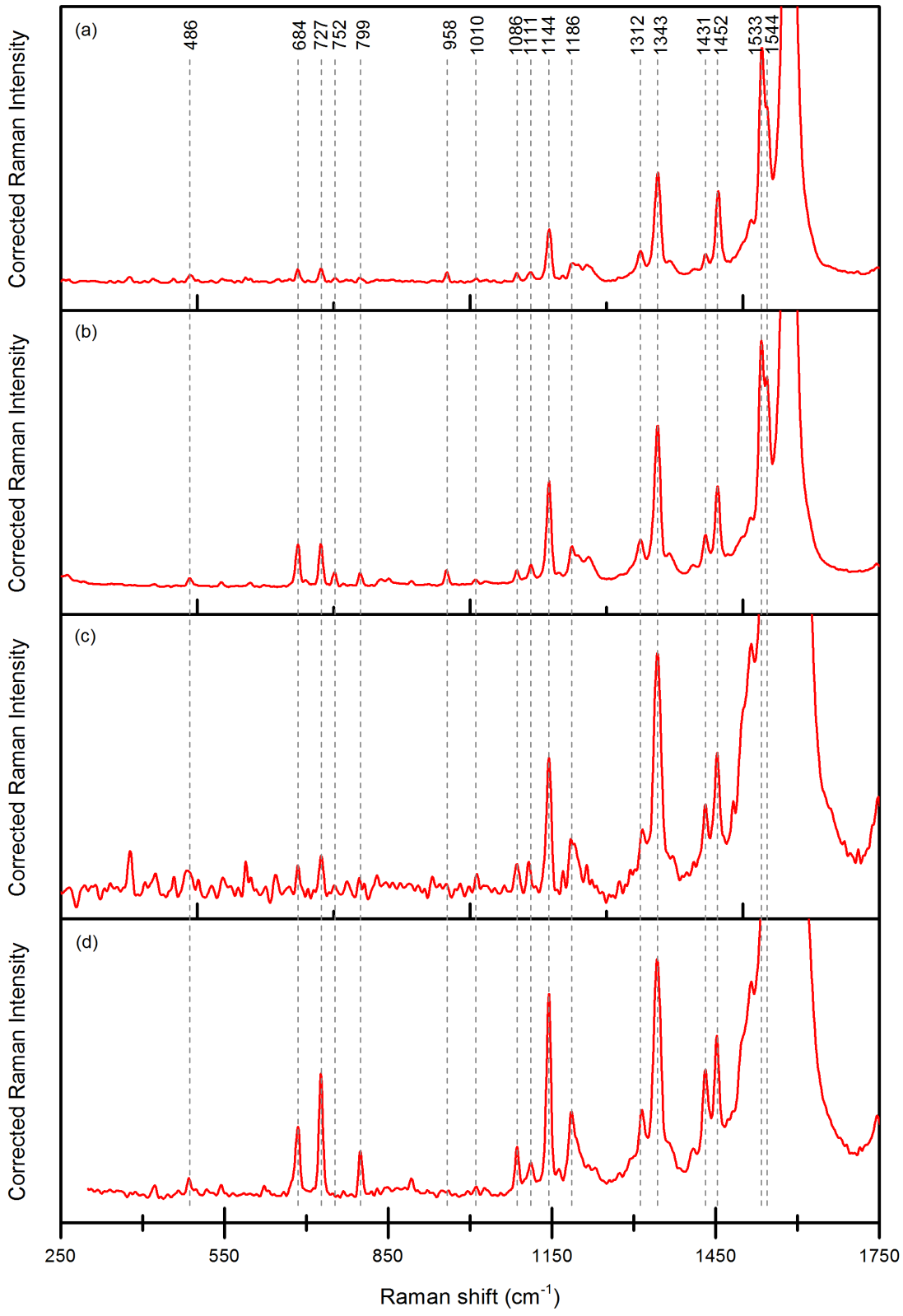

Figure 4.34: Enlarged regions of interest of Raman spectra of HOPG/H_2Pc-X and HOPG/H_2Pc-I systems at 633 and 647 nm excitation. (a) HOPG/H_2Pc-X at 633 nm, (b) HOPG/H_2Pc-X at 647 nm, (c) HOPG/H_2Pc-I at 633 nm, and (d) HOPG/H_2Pc-I at 647 nm. (baseline corrected)

4.2.9 Determination of GERS Enhancement Factor for Glass/SLG/H_2Pc-X Hybrid System

In Chapter 4.2.3, the glass/SLG/H_2Pc-VI and glass/SLG/H_2Pc samples were established to contain most probably a monolayer of H_2Pc molecules, and Raman spectra were acquired for both samples at all five excitation wavelengths. Unfortunately, HOPG eventually did not prove be as an ideal reference system as had been originally thought due to its unexpected behavior during repetitive washing with toluene, as discussed in Chapter 4.2.8Nonetheless, calculation of minimal enhancement factors remains feasible since in both cases, i. e. samples HOPG/H_2Pc-I and HOPG/H_2Pc-X, the collected spectral intensities were overestimated in comparison to the intensities of presumably a H_2Pc monolayer on HOPG.

Tab. 4.11 summarizes calculated enhancement factors of glass/SLG/H_2Pc-X to HOPG/H_2Pc-I and HOPG/H_2Pc-X systems. Intensities of H_2Pc bands in the glass/SLG/H_2Pc-X sample were corrected by factor of 1.34 due to the glass roughness [31].

Table 4.11: Minimal values of EFs for selected H_2Pc modes of glass/SLG/H_2Pc-X hybrid system with respect to the systems HOPG/H_2Pc-I and HOPG/H_2Pc-X at 633 and 647 nm excitation.

Raman shift	EF(I)		EF(X)	
(cm^{-1})	633 nm	647 nm	633 nm	647 nm
685	24	15	8	6
727	20	8	8	6
753	20	6	7	7
799	–	–	8	6
1086	13	7	8	6
1111	22	18	8	8
1145	19	18	8	7
1312	22	25	8	8
1344	19	20	7	7
1410	–	–	8	7
1454	33	27	7	8
1534	–	–	7	8
1545	–	–	7	7

4.2.10 Mechanism of GERS Enhancement of Raman Signal of H_2Pc in Glass/SLG/H_2Pc Hybrid Systems

The vibrational-mode specific relative intensity increase of the majority of Raman spectral bands of H_2Pc in glass/SLG/H_2Pc-VI and glass/SLG/H_2Pc-X hybrid systems at the excitation wavelength 830 nm was tentatively attributed to the charge-transfer resonance enhancement stemming from the excitation of the photo-induced charge transfer between Fermi level of SLG and LUMO of H_2Pc. This explanation agrees with one of the four GERS enhancement conditions formulated in Refs. [3, 7], namely Eq. 1.6d is of interest:

$$\hbar\omega_0 = E_L - E_F \quad \text{or} \quad \hbar\omega_0 = E_L - E_F - \hbar\omega_q \tag{1.6d}$$

In addition, the reasoning is supported by the actual values of SLG Fermi level energy [44, 45] and of the HOMO and LUMO energies of H_2Pc ascertained by DFT calculations [42, 46, 47]. Fig. 4.35 presents a scheme depicting the situation. Furthermore, one shall bear in mind that no Raman signal of H_2Pc was detected for any of the HOPG/H_2Pc reference systems at the excitation wavelength 830 nm. Moreover, only very weak enhancement (as illustrated by the respective EP in Fig. 4.26) was observed in case of glass/SLG/H_2Pc-I hybrid system which is assumed to comprise a multilayer (probably a bilayer) of H_2Pc. That implies the GERS enhancement to be specific for glass/SLG/H_2Pc monolayer hybrid systems.

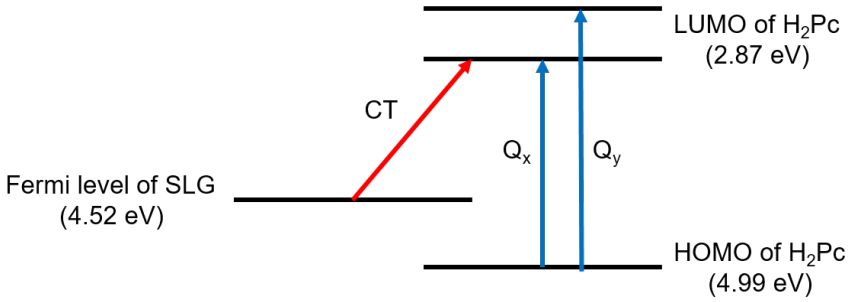

Figure 4.35: A scheme depicting the suggested charge-transfer mechanism of GERS. It features HOMO and LUMO of the H_2Pc molecule (with their energies from Ref. [46]), Fermi level of SLG (energy adopted from Ref. [45]), as well as both the Q_x and Q_y and the assumed CT transitions.

Nonetheless, one shall bear in mind that on the basis of the experimental results of this study (and predominantly due to the lack of electronic absorption spectra of glass/SLG/H_2Pc-VI and glass/SLG/H_2Pc-X hybrid systems) another explanation cannot be fully excluded. Namely of concern is the possibility that the interaction of SLG with a monolayer of H_2Pc molecules could induce such

dramatic changes into the electronic absorption spectra of H_2Pc which would result in shift of the Q_x absorption band towards much higher wavelengths. That is, its maximum would appear above 830 nm or between 785 and 830 nm, hence the excitation wavelength 785 nm would hit the minimum between the two split Q bands while the 830 nm excitation would fall into the Q_x absorption band. This alternative would likewise represent observation of GERS (for the reasons provided above, namely the lack of Raman signal of H_2Pc from HOPG/H_2Pc reference systems at 830 nm). Nevertheless, the relatively large energy difference between Fermi level of SLG and HOMO of H_2Pc, which amounts to 0.46 eV, indicates a weak (rather than a very strong) interaction of these energy levels. This fact in turn makes the previously outlined charge-transfer mechanism of GERS much more plausible.

Enhancement of Raman scattering of H_2Pc at the excitation wavelengths 647 and 633 nm in all glass/SLG/H_2Pc hybrid systems was observed, namely in comparison to HOPG/H_2Pc samples. Unfortunately, proper enhancement factors could not be determined due to reasons discussed in Chapter 4.2.8. The enhancement appears to be vibrational mode specific and values of EFs range from 6 to 27 for 647 nm and from 33 to 13 in case of 633 nm excitation, the average values equaling 16 and 21, respectively. More detailed analysis of these particular reference system as well as determination of the EFs for individual H_2Pc bands may be found in Chapters 4.2.8 and 4.2.9. The actual enhancement mechanism can most probably be related to the GERS enhancement condition (i) in Refs. [3, 7], i. e. Eq. 1.6a:

$$\hbar\omega_0 = E_L - E_H \quad \text{or} \quad \hbar\omega_0 = E_L - E_H + \hbar\omega_q \tag{1.6a}$$

This condition appears to be somewhat disconcerting as the equation in fact describes the resonance enhancement condition for chromophoric molecules, and the role of SLG itself does not seem obvious. Nevertheless, one may envisage the situation that the interaction of the chromophore with SLG shifts the electronic absorption band so as a larger resonance enhancement occurs for the particular excitation wavelength. In fact, it is quite the reverse situation to that reported Brus in Ref. [6]: the Raman cross-section of Rhodamine 6G was found to be lower in SLG/Rh6G hybrid system than in solution. Therefore, the GERS enhancement is tentatively ascribed to the increase of the resonance Raman scattering cross-section of the H_2Pc in glass/SLG/H_2Pc hybrid systems at 633 and 647 nm.

Summary

- Three types of glass/SLG/H_2Pc hybrid systems were prepared by soaking of glass/SLG system in saturated H_2Pc solution in toluene (for 24 hours) followed by soaking in pure toluene solution. The sample preparations mutually differed by the multiplicity of 10-minute exposures to pure toluene, and the samples were denoted I (1x soaking), VI (6x soaking) and X (10x soaking). Reference HOPG/H_2Pc systems were prepared by the very same procedure. The systems were investigated by the means of Raman micro-spectroscopy at five excitation wavelengths (532, 633, 647, 785 and 830 nm).

- Raman spectral mapping was employed, namely areas 25μm-by-25μm with 50-by-50 points were investigated. Each overall spectrum from the scanned area was thoroughly corrected both in terms of wavenumber and intensity calibration in the first step, and then analyzed and interpreted.

- Raman signal of H_2Pc was obtained from all three samples glass/SLG/H_2Pc. By contrast, the HOPG/H_2Pc reference systems yielded Raman signal of H_2Pc only at 633 and 647 nm.

- The sample glass/SLG/H_2Pc-I was also characterized by UV-Vis electronic absorption micro-spectroscopic measurements. The spectrum features red shift with respect to that of an isolated molecule (and several other systems), as well as decreased Q_x-Q_y splitting. The redshift of Q_x and Q_y absorption bands was attributed to bi- or multilayer of H_2Pc slipped geometry (J-dimer or aggregate).

- Additional systems were also investigated: crystalline H_2Pc and solution of H_2Pc in toluene. Both systems exhibited strong fluorescence unless the off-resonance 532 nm excitation was used, for which, unfortunately, the concentration of H_2Pc in toluene was insufficient to obtain Raman spectra. Glass/H_2Pc was also measured, but brought no results.

- Mutual comparison of SLG in glass/SLG and glass/SLG/H_2Pc systems featured no principal difference between the two systems.

- Mutual comparison of H_2Pc Raman spectral bands in the three studied SLG/H_2Pc hybrid systems showed distinctive differences. In particular, on the basis of comparison of Raman intensities at 532 nm excitation, glass/SLG/H_2Pc-I was determined to comprise most probably a bilayer of H_2Pc molecules, and the glass/SLG/H_2Pc-VI and glass/SLG/H_2Pc-X systems appear to be constituted by a monolayer. Several bands are stepping

out more distinctively in Raman spectra of especially the latter, and appear to be IR active modes, e. g. 752, 958 and 1534 cm^{-1}. This may result from a more favorable position of the H_2Pc molecules with respect to SLG, hence a more profound interaction.

- Symmetry of H_2Pc normal vibrations has been investigated by employing a solution of its derivative, namely H_2PcTS. Raman depolarization ratios obtained for H_2PcTS/water solution at 488 and 514.5 nm excitations matched DFT calculated symmetry assignment of normal vibrations bands to A_g and/or B_{1g} symmetry species presented in literature (in 19 of 22 cases).

- Raman spectral bands of H_2Pc were assigned to normal vibrations on the basis of available literature data. Overtones and combination bands were also observed (at 633 and 647 nm) and assigned.

- Excitation profiles for all three glass/SLG/H_2Pc hybrid systems were constructed on the basis of normalization of H_2Pc spectral band intensities to that of the polystyrene band 1005 cm^{-1}. Sequences of enhancement of the individual bands were determined and analyzed in terms of symmetry and localization of the corresponding vibration within the molecule.

  For glass/SLG/H_2Pc-I, sequences at 647 and 785 nm resemble each other which agrees with excitation into the Q_y and Q_x ($0 \rightarrow 0$) electronic transitions, respectively (both high and low wavenumber band are to be found among the strongly enhanced bands). The 633 nm excitation, on the other hand, falls into the vibronic sideband of Q band which leads to preferential enhancement of high wavenumber bands at around 1368 cm^{-1}.

  In case of glass/SLG/H_2Pc-VI and glass/SLG/H_2Pc-X, there are no pronounced differences in the relative band intensity sequences at 647 and 633 nm, unlike glass/SLG/H_2Pc-I. In addition, these two systems feature an apparent intensity growth from towards 830 nm after a profound drop at 785 nm, and new spectral bands appear (1534 cm^{-1}). These differences indicate changes in electronic absorption spectra, which corroborates the idea of reorganization of H_2Pc monolayer on SLG surface. The intensity increase at 830 nm in EPs of both glass/SLG/H_2Pc-VI and glass/SLG/H_2Pc-X with both low and high wavenumber bands enhanced suggests population of H_2Pc LUMO by photo-induced charge-transfer from Fermi level of SLG. That is, by the mechanism (iv) outlined by Barros and Dresselhaus [7].

- The HOPG/H_2Pc sample eventually did not serve as an ideal reference system due to its degradation upon repetitive soaking in toluene. Nevertheless,

the minimal GERS EFs were calculated for the glass/SLG/H_2Pc-X sample, namely values $13 - 33$ for 633 nm excitation and $6 - 27$ for 647 nm. GERS enhancement at these excitation wavelengths is attributed to changes in electronic absorption spectra of H_2Pc inducing a weak interaction of HOMO of H_2Pc with Fermi level of SLG, i. e. by the mechanism (i) outlined in [7].

Conclusions

H_2Pc has proved to be a very well suited molecule for the study of GERS, namely due to its planar aromatic character and D_{2h} symmetry, as well as because of the positions of its HOMO and LUMO, that is, below and above the Fermi level of SLG, respectively.

GERS of H_2Pc in glass/SLG/H_2Pc hybrid systems has been investigated with a variety of excitation wavelengths (532, 633, 647, 785 and 830 nm) which allowed for construction of excitation profiles. Especially then measurements at the two highest excitation wavelengths, i. e. 785 and 830 nm, were crucial. For chromophores with the HOMO to LUMO transition in the visible range, charge-transfer transitions from the Fermi level of SLG to LUMO or from HOMO to Fermi level of SLG may be expected to lie on the border of Vis/NIR or in NIR spectral region.

Furthermore, acquisition of electronic absorption spectra has been essential for the interpretation of excitation profiles. Collection of the spectra has been quite a difficult task due to extremely low values of absorbance of a H_2Pc monolayer (hence, for glass/SLG/H_2Pc hybrid systems, only absorption spectra for a H_2Pc bilayer were collected). Excitation profiles may, to some extent, substitute for the electronic absorption spectra. However, for a reliable reconstruction of the electronic absorption spectrum, numerous closely-spaced excitation wavelengths would be required in order to obtain more detailed EPs.

Unfortunately, a suitable reference system for accurate quantification of the GERS enhancement is yet to be found. HOPG could be such if the strategy of soaking is changed. Alternatively, a thin layer of sputtered carbon on glass may be tested for this purpose.

Due to the specific values of H_2Pc HOMO and LUMO energies with respect to the Fermi level of SLG, that is HOMO lying closer to Fermi level of SLG (0.47 eV) than LUMO (1.66 eV), manifestations of two mechanisms of GERS (outlined previously by Barros and Dresselhaus) have been observed for glass/SLG/monolayer H_2Pc hybrid system: photo-induced CT from Fermi level of SLG to LUMO of H_2Pc (at 830 nm) and a weak interaction between Fermi level of SLG and HOMO of H_2Pc which induces changes in the electronic absorption spectra of H_2Pc monolayer favorable for enhancement of resonance Raman scattering.

References

[1] Ling, X.; Xie, L.; Fang, Y.; Xu, H.; Zhang, H.; Kong, J.; Dresselhaus, M. S.; Thang, J.; Liu, Z. *Nano Letters* **2010**, *10*, 553–561.

[2] Ling, X.; Huang, S.; Mao, N.; Kong, J.; Dresselhaus, M. S.; Zhang, J. *Accounts of Chemical Research* **2015**, *48*, 1862–1870.

[3] Huang, S.; Ling, X.; Liang, L.; Song, Y.; Fang, W.; Zhang, J.; Kong, J.; Meunier, V.; Dresselhaus, M. S. *Nano Letters* **2015**, *15*, 2892–2901.

[4] Ling, X.; Wu, J.; Xie, L.; Zhang, J. *The Journal of Physical Chemistry C* **2013**, *117*, 2369–2376.

[5] Ling, X.; Moura, L. G.; Pimenta, M. A.; Zhang, J. *Journal of Physical Chemistry C* **2012**, *116*, 25112–25118.

[6] Thrall, E. S.; Crowther, A. C.; Yu, Z.; Brus, L. E. *Nano Letters* **2012**, *12*, 1571–1577.

[7] Barros, E. B.; Dresselhaus, M. S. *Physical Review B* **2014**, *90*.

[8] Clark, R. J. H.; Dines, T. J. *Angewandte Chemie International Edition* **1986**,

[9] Nakamoto, K. *Infrared and Raman Spectra of Inorganic and Coordination Compounds*, 4th ed.; John Wiley & Sons, Inc., 1986.

[10] Aroca, R.; DiLella, D. P. *Journal of Physics and Chemistry of Solids* **1982**, *43*, 707–711.

[11] Jorio, A.; Saito, R.; Dresselhaus, G.; Dresselhaus, M. S. *Raman Spectroscopy in Graphene Related Systems*; Wiley-VCH Verlag GmbH & Co. KGaA: Weinheim, Germany, 2011.

[12] Ferrari, A. C.; Basko, D. M. *Nature Nanotechnology* **2013**, *8*, 235 – 245.

[13] Ochsner, M. *Journal of Photochemistry and Photobiology B: Biology* **1996**, *39*, 1–18.

[14] Menaa, B.; Takahashi, M.; Tokuda, Y.; Yoko, T. *Journal of Photochemistry and Photobiology A: Chemistry* **2007**, 362 – 366.

[15] Kaya, E. N.; Basova, T.; Polyakov, M.; Durmus, M.; Kadem, B.; Hassan, A. *RSC Advances* **2015**, *5*, 91855–91862.

[16] Brotman, A.; Burstein, E. *Physica Scripta* **1985**, *32*, 385–390.

[17] Heutz, S.; Salvan, G.; Silaghi, S. D.; Jones, T. S.; Zahn, D. R. T. *Journal of Physical Chemistry B* **2003**, *107*, 3782–3788.

[18] Murray, C.; Dozova, N.; McCaffrey, J. G.; FitzGerald, S. *Physical Chemistry Chemical Physics* **2010**, *12*, 10406–10422.

[19] Aroca, R.; Loutfy, R. O. *Journal of Raman Spectroscopy* **1982**, *12*, 262–265.

[20] Marshell, J. *Material Science Research India* **2010**, *7*, 221–224.

[21] Kalbáč, M.; Frank, O.; Kavan, L. *Carbon* **2012**, *50*, 3682–3687.

[22] Taran, M. N.; Rossman, G. R. *American Mineralogist* **2001**, *86*, 973–980.

[23] NIST: Atomic Spectra Database Line Forms. `http://physics.nist.gov/PhysRefData/ASD/lines_form.html`.

[24] Plant, A. L.; Watters, R. L. Standard Reference Material 2242: Relative Intensity Correction Standard for Raman Spectroscopy: 532 nm Excitation. 2013; `https://www-s.nist.gov/srmors/certificates/2242.pdf`.

[25] Choquette, S. J.; Watters, R. L. Standard Reference Material 2245: Relative Intensity Correction Standard for Raman Spectroscopy: 633 nm Excitation. 2015; `https://www-s.nist.gov/srmors/certificates/2245.pdf`.

[26] Choquette, S. J.; Watters, R. L. Standard Reference Material 2241: Relative Intensity Correction Standard for Raman Spectroscopy: 785 nm Excitation. 2015; `https://www-s.nist.gov/srmors/certificates/2241.pdf`.

[27] Choquette, S. J.; Watters, R. L. Standard Reference Material 2246: Relative Intensity Correction Standard for Raman Spectroscopy: 830 nm Excitation. 2015; `https://www-s.nist.gov/srmors/certificates/2246.pdf`.

[28] Fitch, P. A. H.; Haynam, C. A.; Levy, D. H. *Journal of Chemical Physics* **1980**, *73*, 1064–1072.

[29] Murray, C.; Dozova, N.; McCaffrey, J. G.; Shafizadeh, N.; Chin, W.; Broquier, M.; Crépin, C. *Physical Chemistry Chemical Physics* **2011**, *13*, 17543–17554.

[30] Loutfy, R. O. *Canadian Journal of Chemistry* **1981**, *59*, 549–554.

[31] Henke, L.; Nagy, N.; Krull, U. J. *Biosensors and Bioelectronics* **2002**, *17*, 547–555.

[32] Bayliss, S. M.; Heutz, S.; Jones, T. S. *Physical Chemistry Chemical Physics* **1999**, *1*, 3673–3676.

[33] Cook, M.; Chambrier, I. In *The Porphyrin Handbook, Volume 17: Phthalocyanines: Properties and Materials*; Kadish, K., Guilard, R., Smith, K. M., Eds.; Academic Press, 2003; Chapter Phthalocyanine Thin Films: Deposition and Structural Studies, pp 37–128.

[34] Nilson, K.; Ahlund, J.; Brena, B.; Göthelid, E.; Schiessling, J.; Martensson, N.; Puglia, C. *Journal of Chemical Physics* **2007**, *127*.

[35] Hunter, C. A.; Sanders, J. K. M. *Journal of American Chemical Society* **1990**, *112*, 5525–5534.

[36] Prince, B. J.; Williamson, B. E.; Reeves, R. J. *Journal of Luminescence* **2001**, *93*, 293–301.

[37] Pinto, H.; Markevich, A. *Beilstein Journal of Nanotechnology* **2014**, *5*, 1842–1848.

[38] Dissanayake, D. M. N. M.; Ashraf, A.; Dwyer, D.; Kisslinger, K.; Zhang, L.; Pang, Y.; Efstathiadis, H.; Eisman, M. D. *Scientific Reports* **2016**, *6*, 21070.

[39] Melendres, C. A.; Maroni, V. A. *Journal of Raman Spectroscopy* **1984**, *15*, 319–326.

[40] Tackley, D. R.; Dent, G.; Smith, W. E. *Physical Chemistry Chemical Physics* **2001**, *3*, 1419–1426.

[41] Shurvell, H. F.; Pinzuti, L. *Canadian Journal of Chemistry* **1966**, *44*.

[42] Zhang, X.; Zhang, Y.; Jiang, J. *Vibrational Spectroscopy* **2003**, *33*, 153–161.

[43] Šloufová, I.; Vlčková, B.; Procházka, M.; Svoboda, J.; Vohlídal, J. *Journal of Raman Spectroscopy* **2014**, *45*, 338–348.

[44] Giangregorio, M. M.; Jiao, W.; Bianco, G. V.; Capezzuto, P.; Brown, A. S.; Bruno, G.; Losurdo, M. *Nanoscale* **2015**, *7*, 12868.

[45] Das, S.; Sudhagar, P.; Ito, E.; Lee, D.; Nagarajan, S.; Lee, S. Y.; Knag, Y. S.; Choi, W. *Journal of Materials Chemistry* **2012**, *22*, 20490–20497.

[46] Komeda, T.; Isshiki, H.; Liu, J. *Science and Technology of Advanced Materials* **2011**, *11*.

[47] Zheng-Lin, S.; Fu-Shi, Z.; Xi-Qiao, C.; Fu-Qun, Z. *Acta Physico-Chimica Sinica* **2003**, *19*, 130–133.

List of Figures

List of Tables

List of Abbreviations

CCD	Charge-coupled device
CT	Charge-transfer
DFT	Density functional theory
dp	Depolarized
EF	Enhancement factor
EP	Excitation profile
FePc	Iron phthalocyanine
GERS	Graphene-enhanced Raman scattering
glass/H_2Pc	H_2Pc on a glass substrate
glass/SLG	SLG deposited on glass
glass/SLG/H_2Pc	H_2Pc adsorbed on SLG on glass
H_2Pc	29,31H-Phthalocyanine
H_2PcTS	29,31H-Phthalocyanine-C,C,C,C-tetrasulfonate hydrate
HOMO	Highest occupied molecular orbital
HOPG	Highly-ordered pyrolitic graphite
HOPG/H_2Pc	H_2Pc adsorbed on HOPG
IR	Infra-red
LUMO	Lowest unoccupied molecular orbital
LWD	Long-working distance
MO LCAO	Molecular orbitals linear combination of atomic orbitals
NCA	Normal coordinate analysis
NIR	Near infra-red
NIST	National Institute of Standards and Technology
p	Polarized
Rh6G	Rhodamine 6G
RRS	Resonance Raman scattering
RS	Raman scattering
SERRS	Surface-enhanced resonance Raman scattering
SERS	Surface-enhanced Raman scattering
SLG	Single-layer graphene
UV	Ultraviolet
Vis	Visible

Supplement

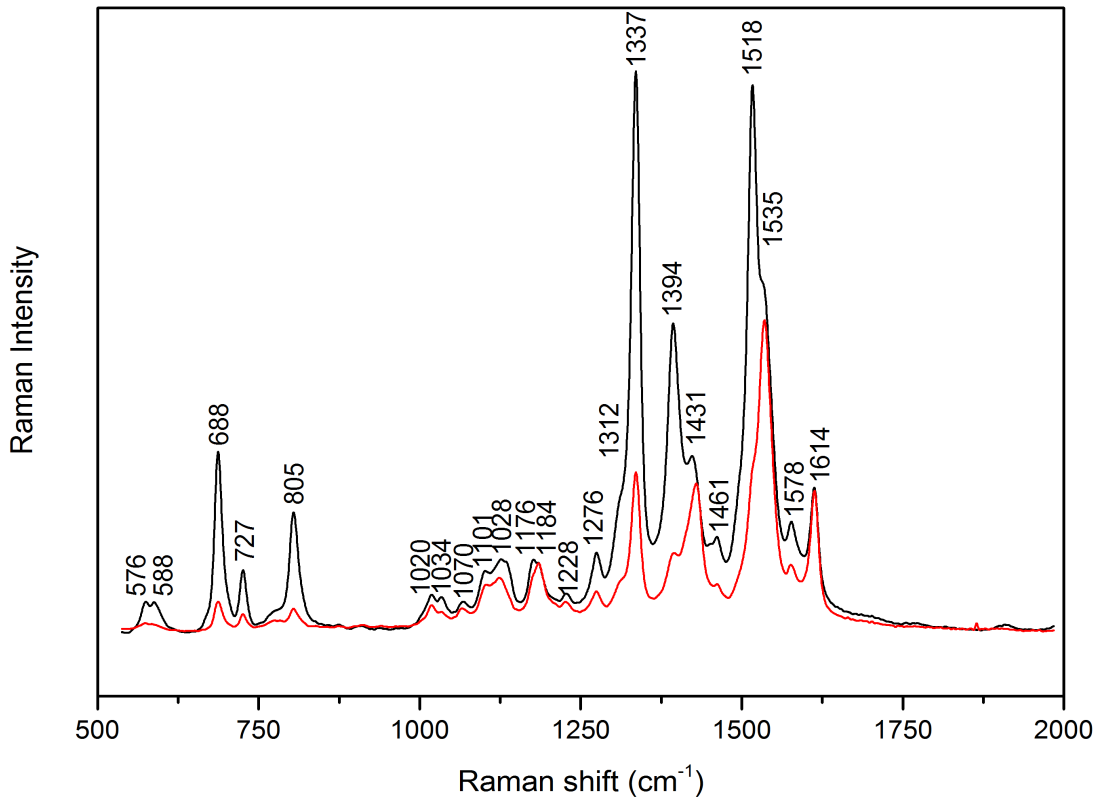

Figure S1: Raman spectra of $1.0 \cdot 10^{-2}$ M H_2PcTS in water at 514.5 nm excitation with parallel (black) and perpendicular (red) polarization with respect to the incident radiation. (baseline corrected)

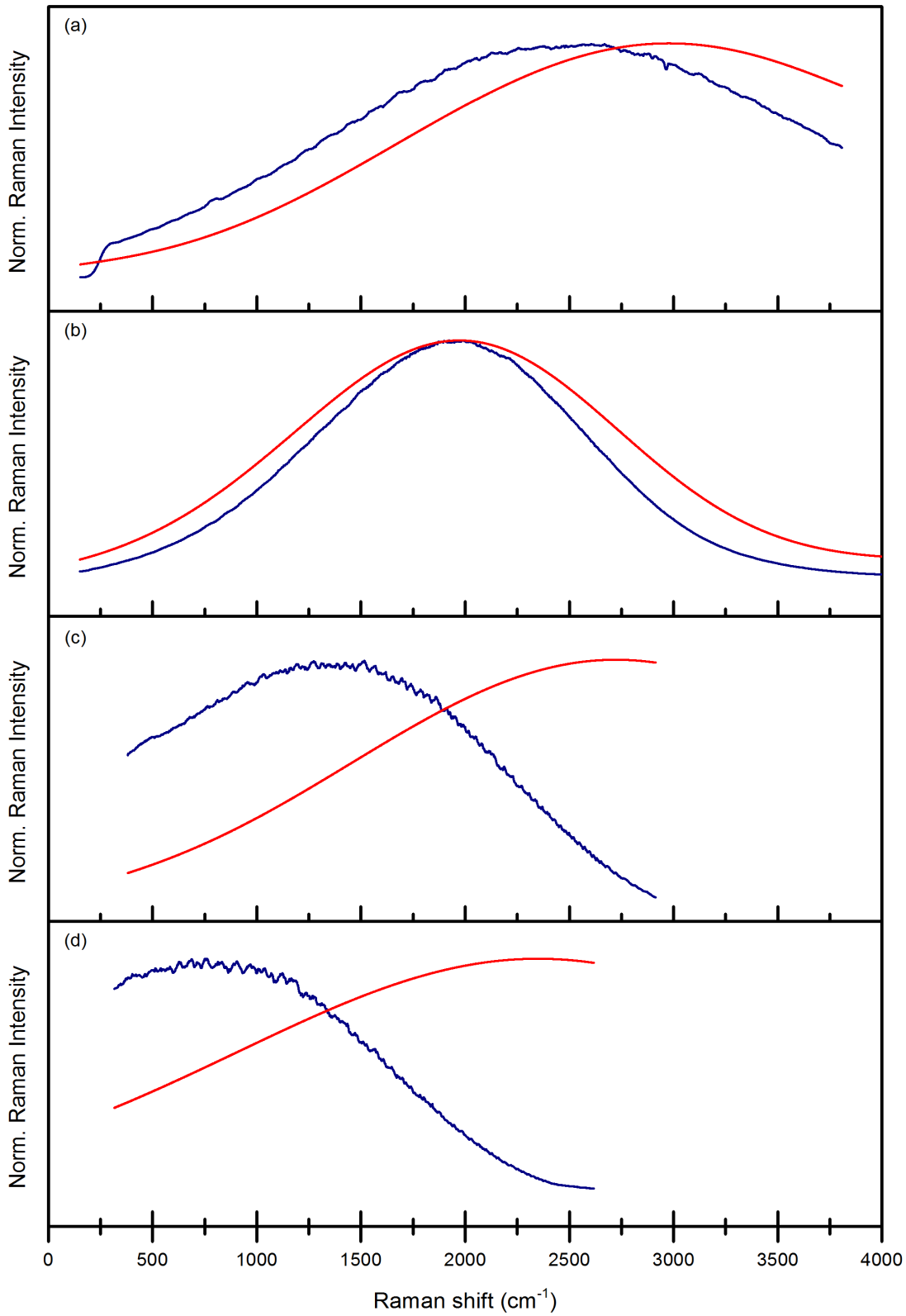

Figure S2: Acquired (blue) and theoretical (red) emission spectra of available certified fluorescence standards for four excitation wavelengths. Spectra are normalized to unity at their respective maxima. (a) 532, (b) 633, (c) 785 and (d) 830 nm.

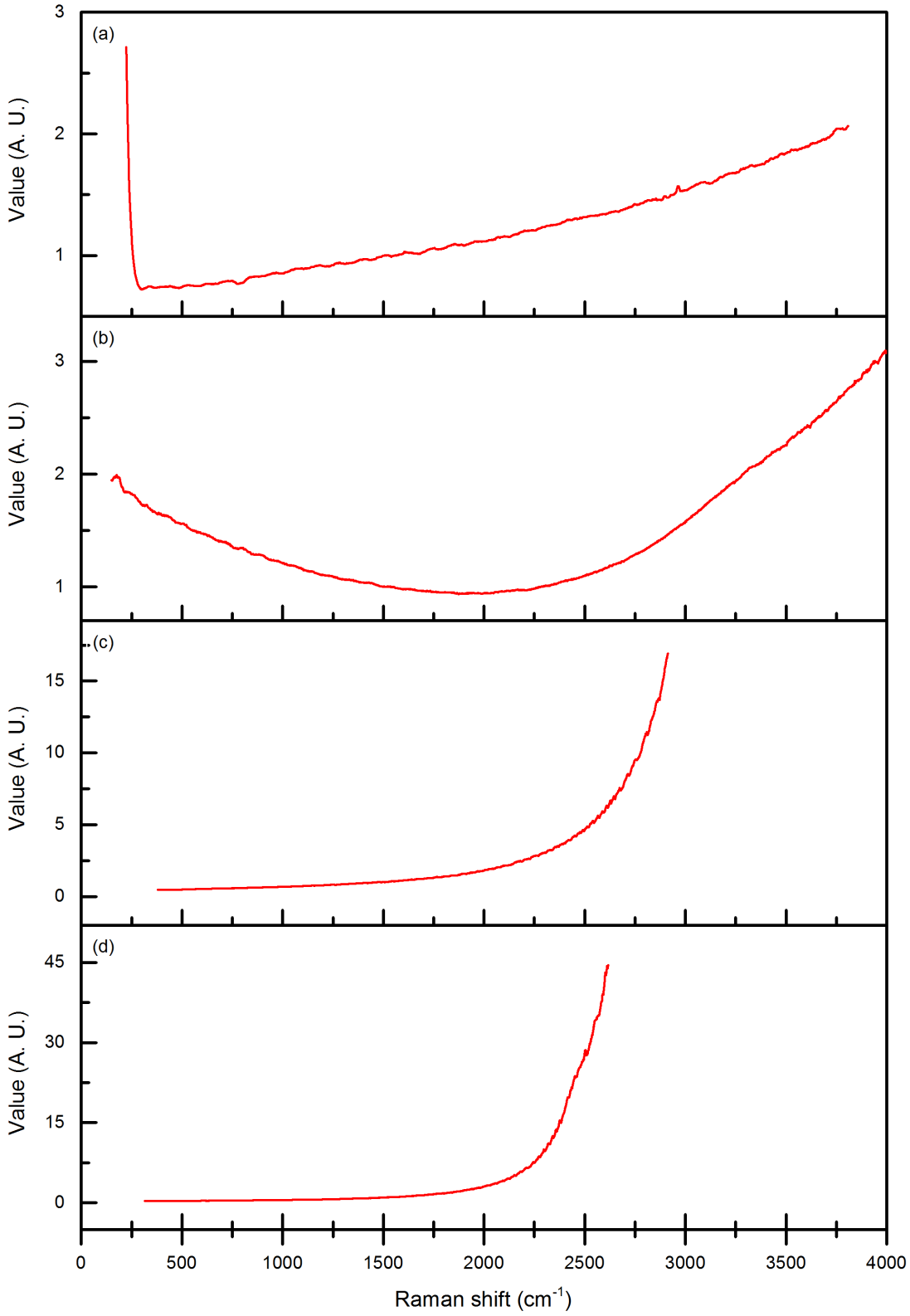

Figure S3: Intensity correction functions based on the available certified fluorescence standards. Functions are normalized to unity at 1500 cm^{-1}. (a) 532, (b) 633, (c) 785 and (d) 830 nm.

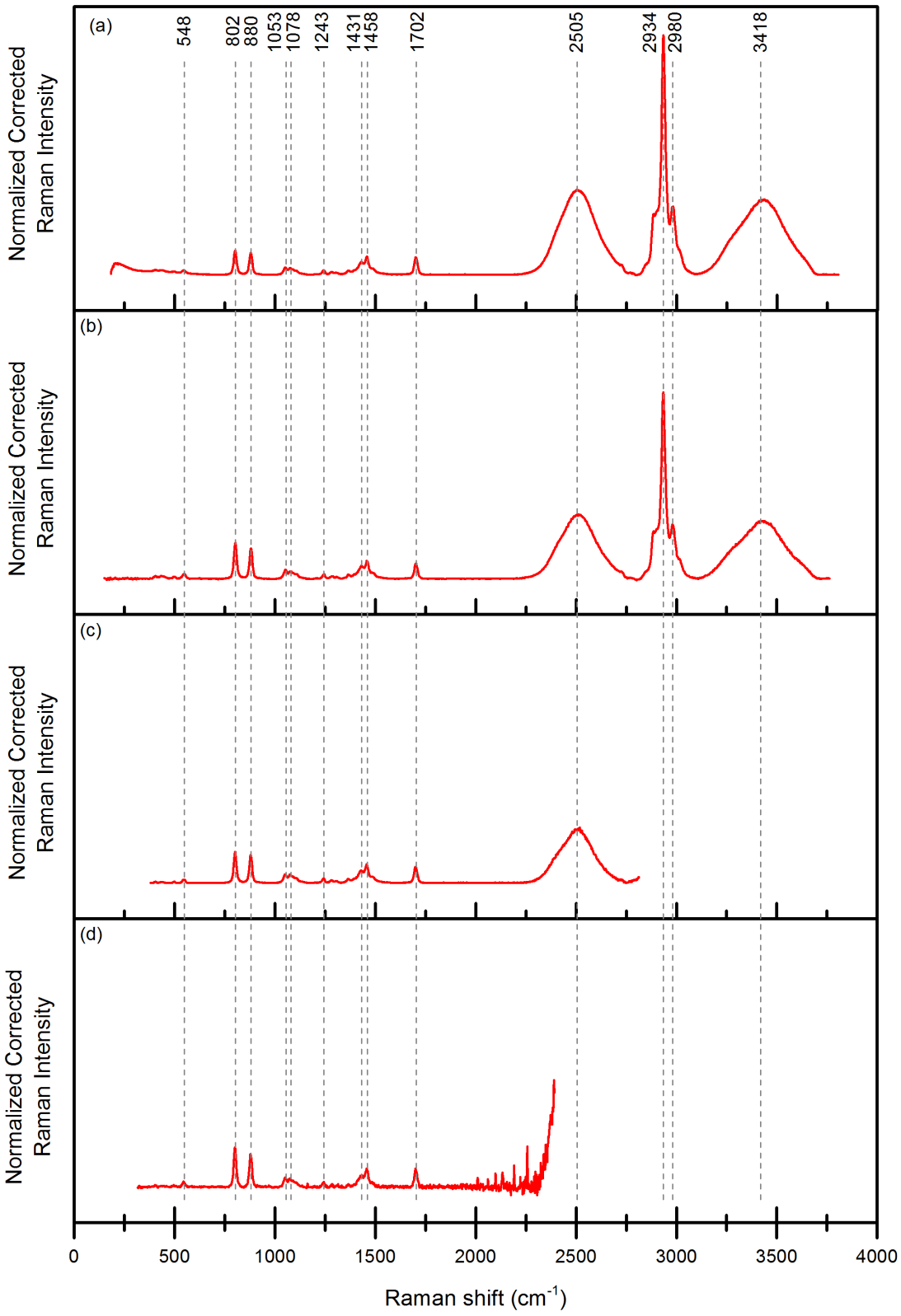

Figure S4: Raman spectra of the calibration mixture after correction based on the certified standards. Normalized to unity at 1458 cm^{-1}. (a) 532, (b) 633, (c) 785 and (d) 830 nm. (baseline corrected)

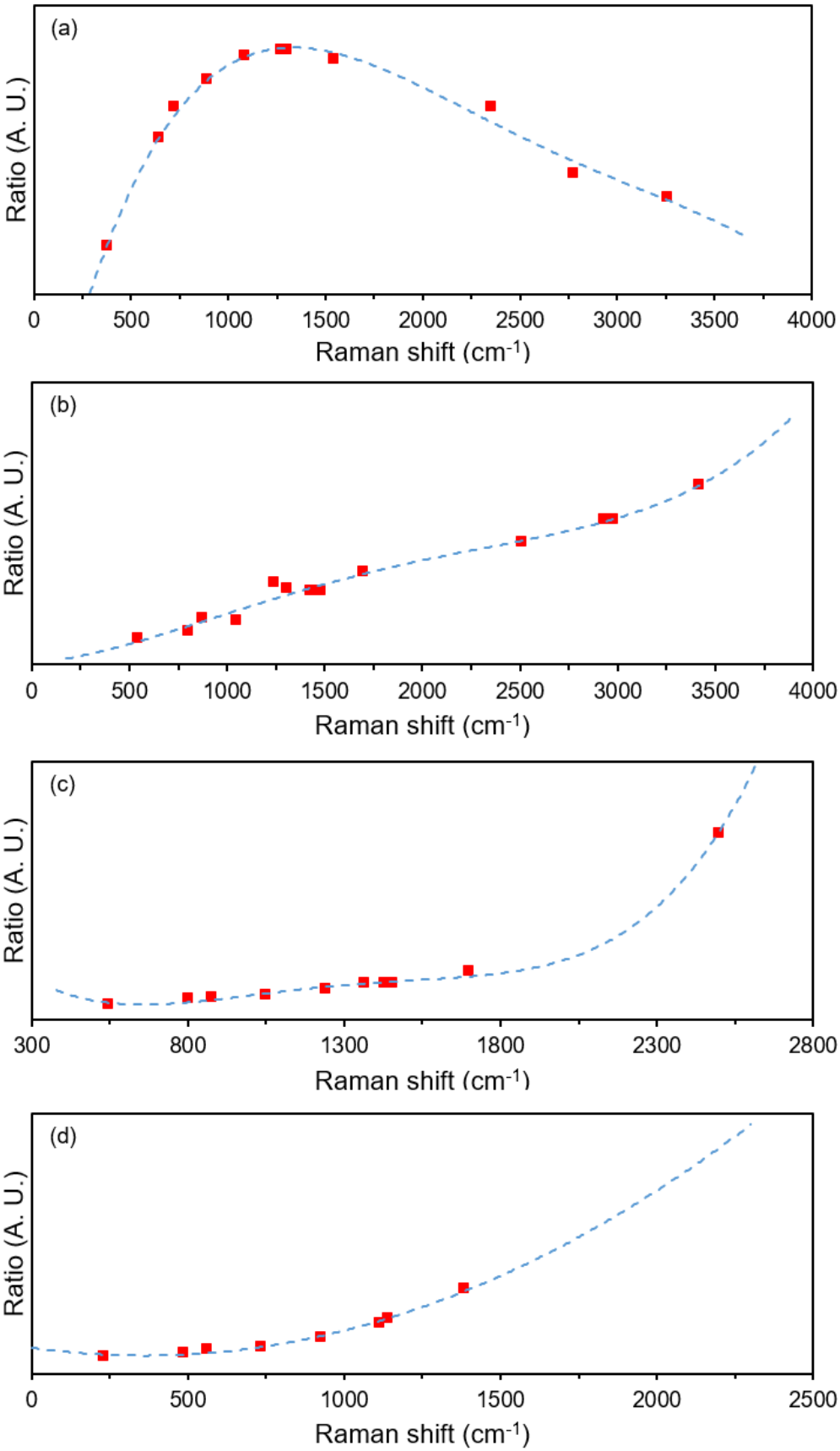

Figure S5: Selected points and their intensity ratios to those at 633 nm excitation and the fitting functions. (a) 532, (b) 647, (c) 785 and (d) 830 nm.

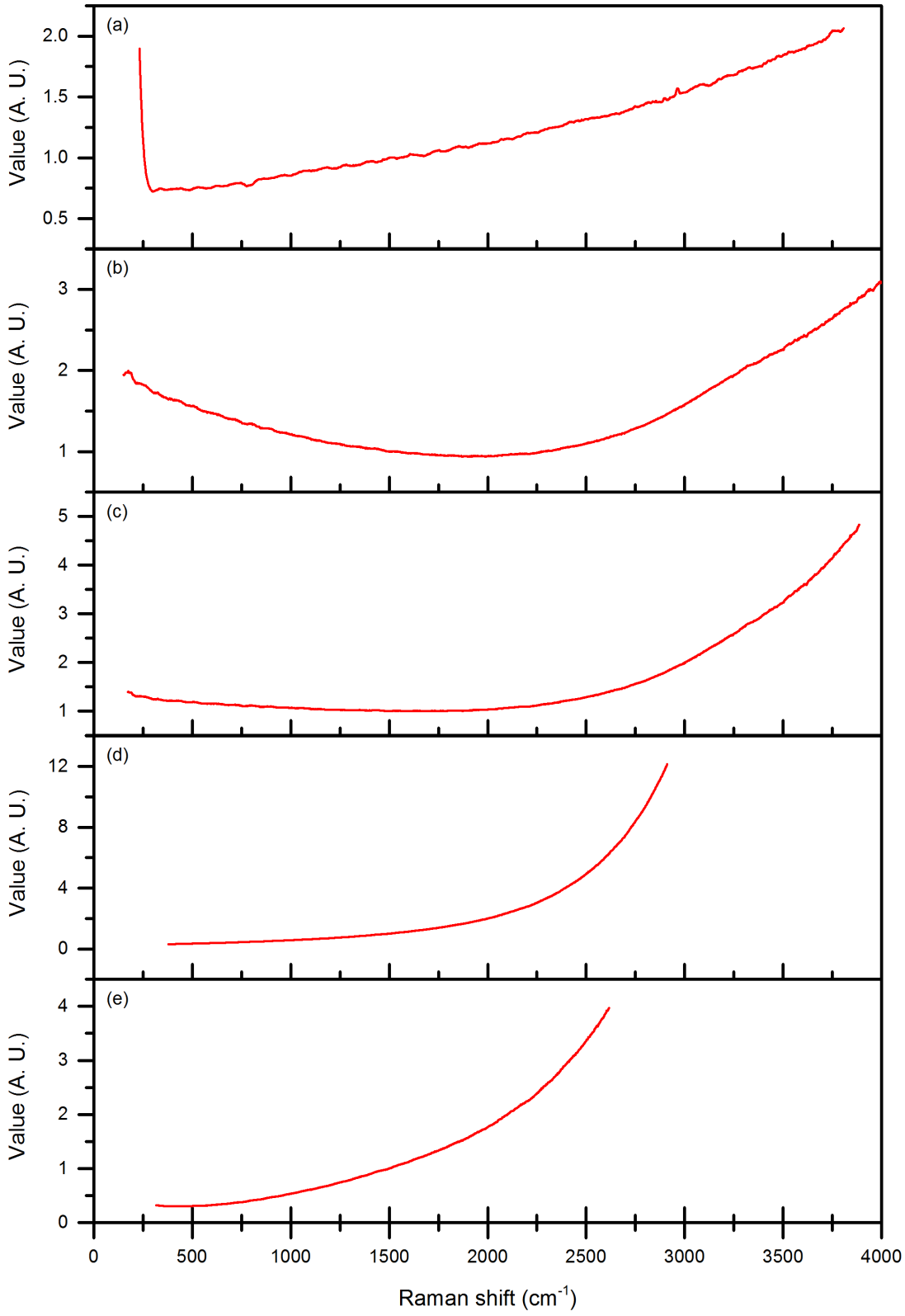

Figure S6: Final intensity correction functions for individual excitation wavelengths: (a) 532, (b) 633, (c) 647, (d) 785 and (e) 830 nm. These correction functions were applied to all discussed spectra acquired at WITec alpha300. Functions are normalized to unity at 1500 cm^{-1}.

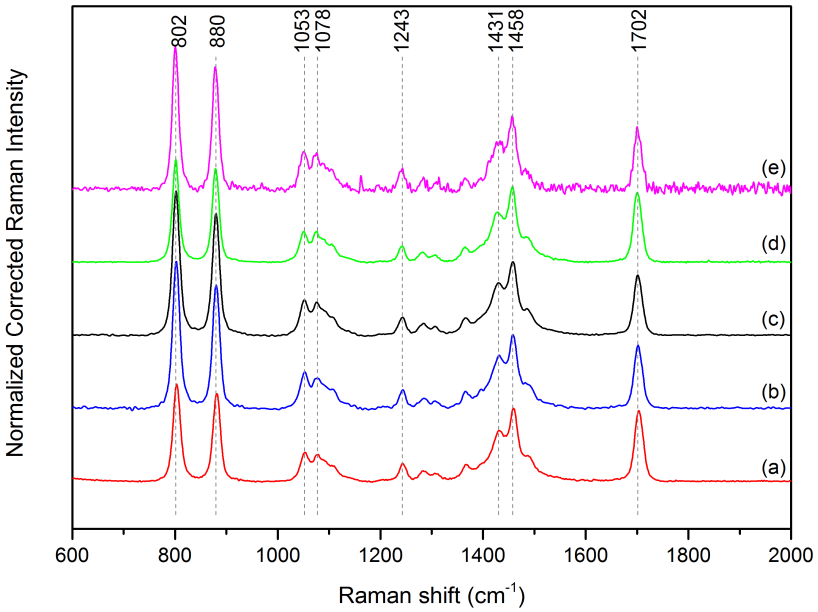

Figure S7: Raman spectra of the calibration mixture after final employed intensity correction, spectral region $600 - 2000$ cm^{-1} in detail. Normalized to unity at 1458 cm^{-1} and baseline corrected. (a) 532, (b) 633, (c) 647, (d) 785 and (e) 830 nm. Although the intensity of the lower wavenumber bands in spectra at 532 and 785 nm reaches slightly lower values than for the other three excitation wavelengths, the correction functions overall balance very well the plummeting CCD detector response.

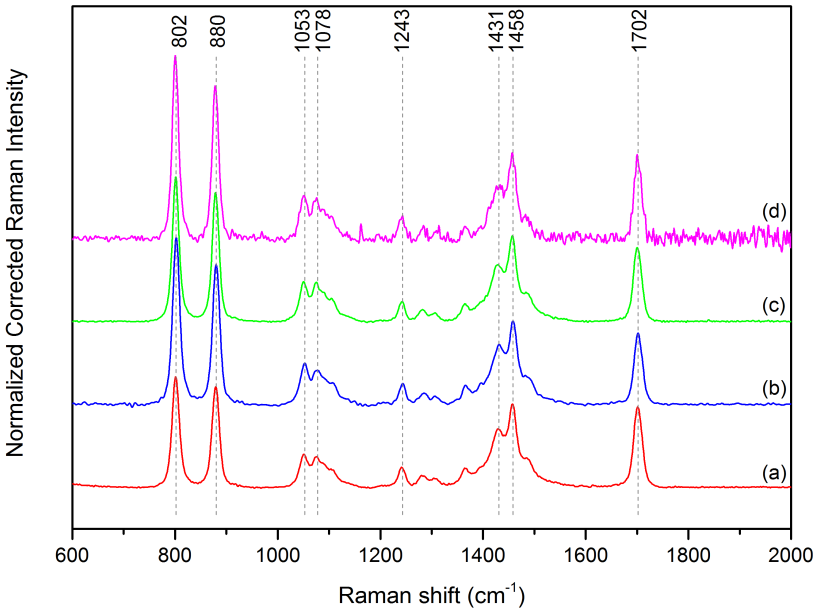

Figure S8: Raman spectra of the calibration mixture after intensity correction based on the certified standards, spectral region $600 - 2000$ cm^{-1} in detail. Normalized to unity at 1458 cm^{-1} and baseline corrected. (a) 532, (b) 633, (c) 785 and (d) 830 nm. While the spectra for higher excitation wavelengths match each other well, the correction for 532 nm excitation appears to slightly differ at lower wavenumbers, and further investigation is in place to resolve this minor discrepancy. Nevertheless, the correction functions overall compensate very well for the decreasing CCD detector response.

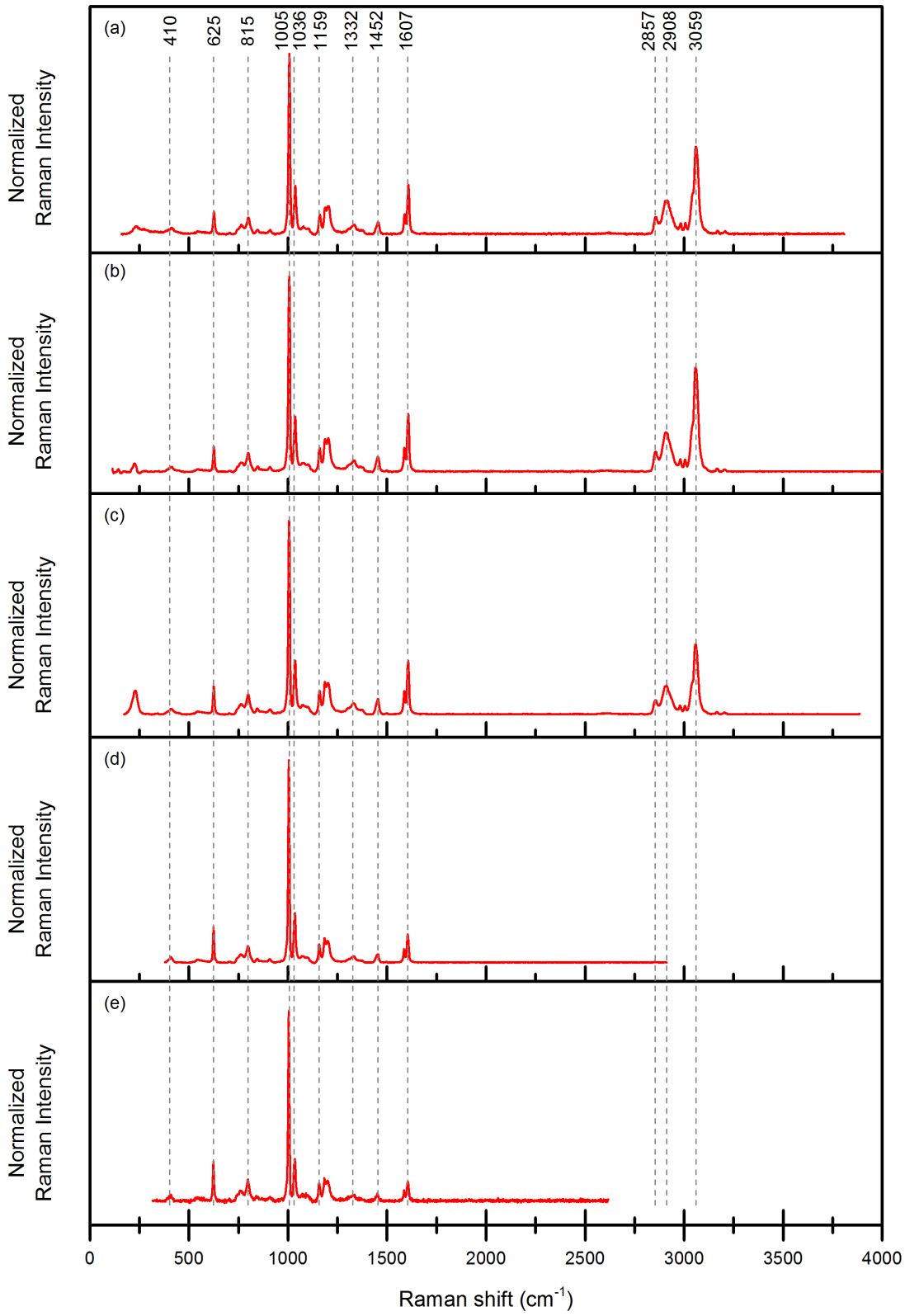

Figure S9: Raman spectra of polystyrene at five excitation wavelengths prior to intensity correction. Spectra are normalized to their respective maxima. (a) 532, (b) 633, (c) 647, (d) 785 and (e) 830 nm.

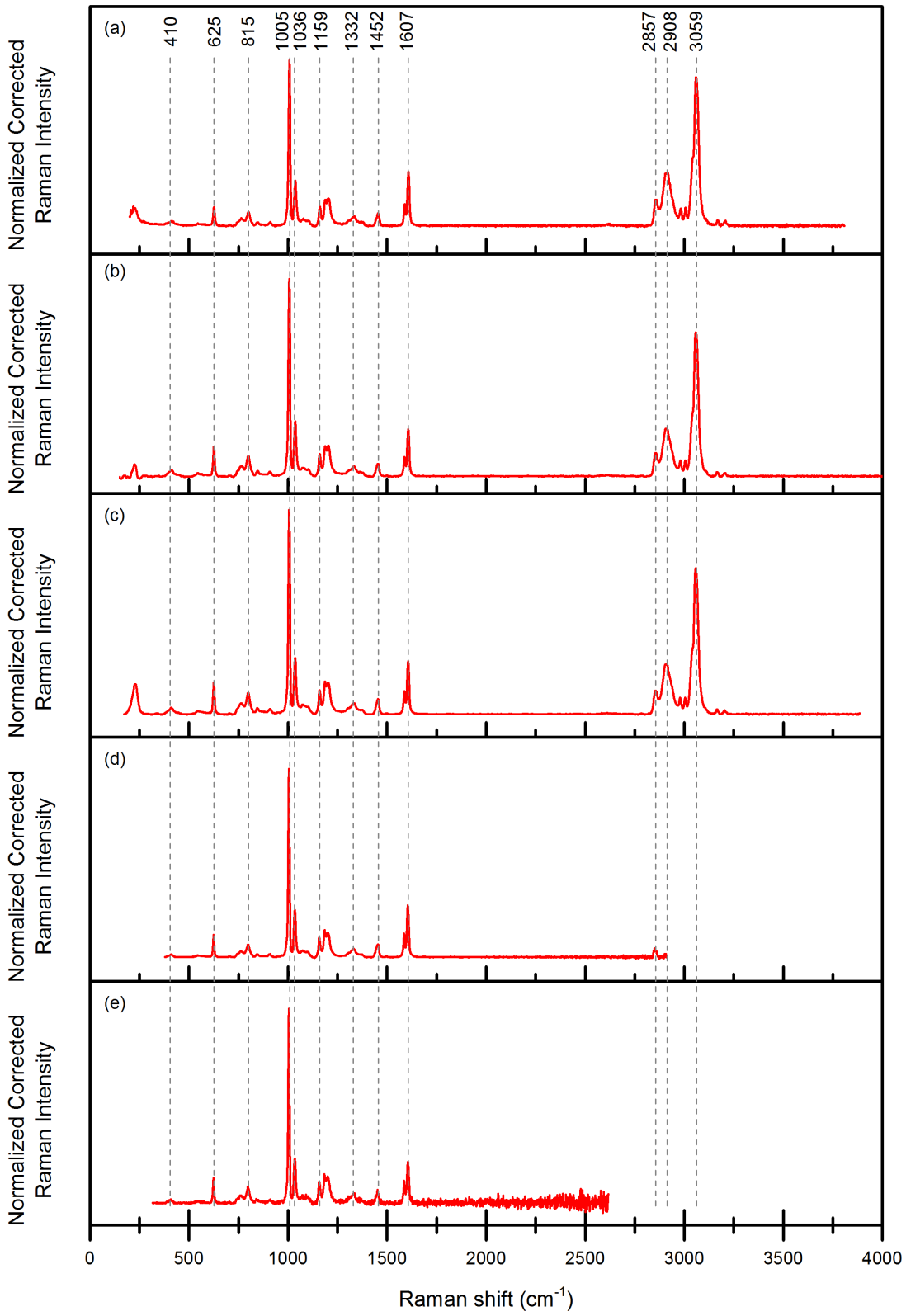

Figure S10: Raman spectra of polystyrene at five excitation wavelengths after intensity correction. Spectra are normalized to their respective maxima. (a) 532, (b) 633, (c) 647, (d) 785 and (e) 830 nm.

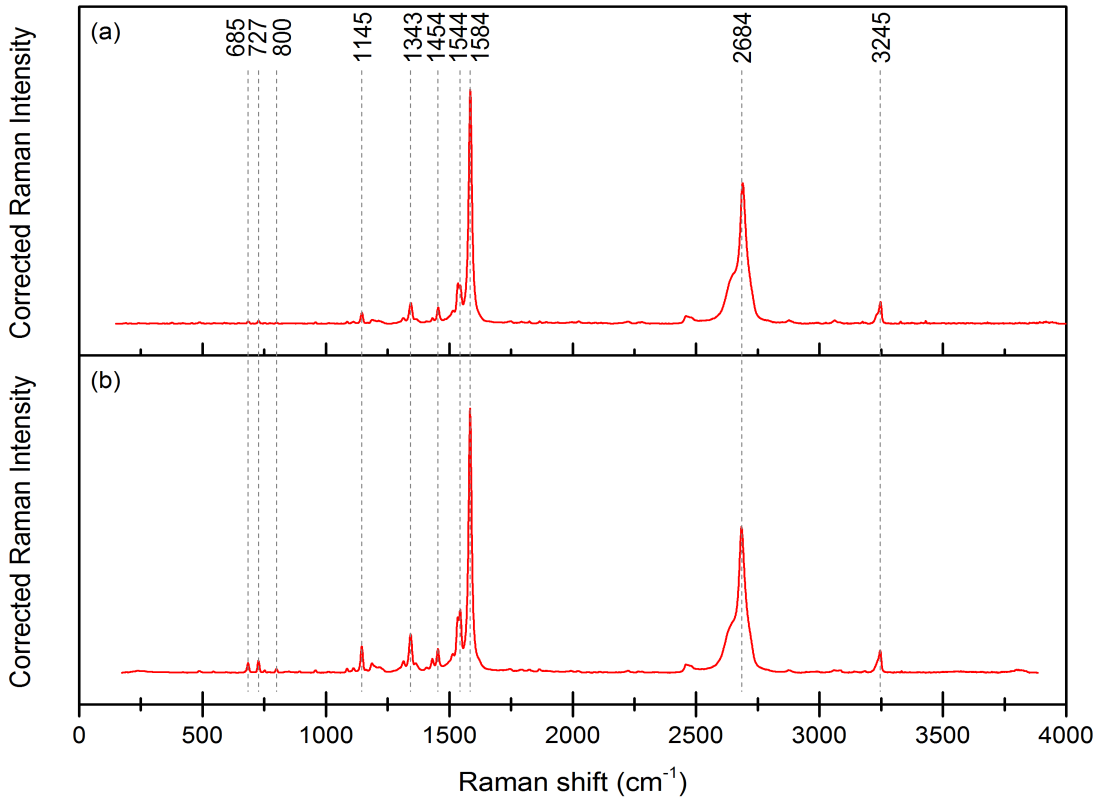

Figure S11: Raman spectra of HOPG/H_2Pc-VI system at excitation wavelengths (a) 633 and (b) 647 nm.

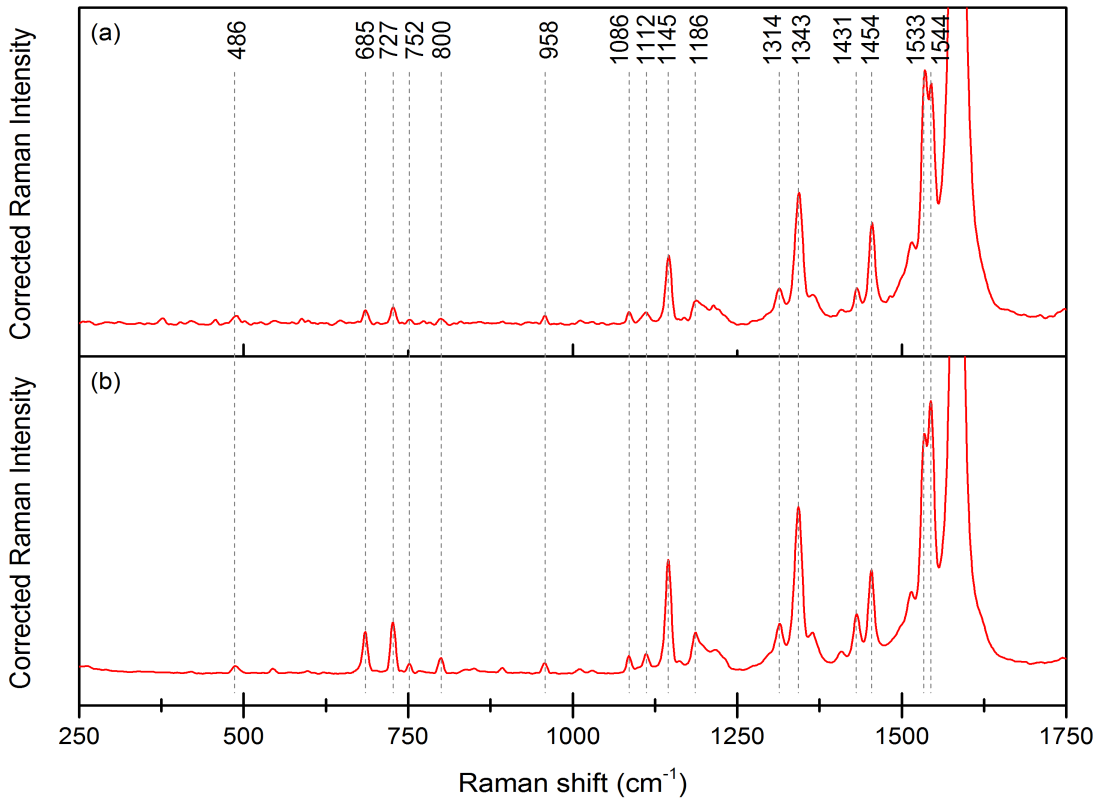

Figure S12: Enlarged region of Raman spectra of HOPG/H_2Pc-VI system at excitation wavelengths (a) 633 and (b) 647 nm.